Material Deformation Mechanisms during Machining of Superalloys

by

ALBIN HAGBERG
PETER MALM

Diploma work No. 28/2010
at Department of Materials and Manufacturing Technology
CHALMERS UNIVERSITY OF TECHNOLOGY
Gothenburg, Sweden

Diploma work in the Master programme Advanced Engineering Materials

Performed at: Volvo Aero Corporation

Supervisor: Stefan Cedergren
Department of Materials and Manufacturing Technology
Chalmers University of Technology
SE-412 96 Gothenburg

Examiner: Adjunct Professor Göran Sjöberg
Department of Materials and Manufacturing Technology
Chalmers University of Technology
SE-412 96 Gothenburg

Material Deformation Mechanisms during Machining of Superalloys
ALBIN HAGBERG
PETER MALM

Diploma work no 28/2010
Department of Materials and Manufacturing Technology
Chalmers University of Technology
SE-412 96 Gothenburg
Sweden
Telephone + 46 (0)31-772 1000

Cover:
A micrograph showing a shear localized chip produced by turning at 480 m/min in a small grained aged Inconel 718 material.

Chalmers Reproservice
Gothenburg, Sweden 2010

Abstract

In this work, deformation mechanisms in chips produced from orthogonal turning of the superalloy Inconel 718 was studied. The cutting speeds used were in an interval ranging from 30 m/min to 480 m/min while all other cutting parameters were kept constant. The material selection consisted of large grained and small grained material both in a hardened and non-hardened state. During the turning experiments, forces were recorded and the chips produced were collected. Longitudinal cross sections of the chips were investigated in an optical microscope. A stereomicroscope was used to investigate the chip macrostructure as well as the contact length between tool and chip.

The investigation showed that large grained materials are deformed in an irregular way producing serrated chips at all cutting speeds while small grained materials produce continuous chips at low cutting speeds (30 and 60 m/min) and segmented chips at high cutting speeds (120 to 480 m/min). Segmented chips showed nearly undeformed microstructures separated by highly localized shear zones. The localized shear zone was shown to decrease in width as the cutting speed was increased as well as being smaller in the hardened than in the non-hardened condition.

Cutting force measurements showed a general decrease in cutting force at higher cutting speeds. The small grained material required higher cutting force in the non-hardened state than in the hardened state. Higher cutting speeds also showed shorter contact lengths between chip and tool.

Keywords: Inconel 718, turning, deformation mechanisms, shear bands, chip microstructure

Preface

This diploma work was done in the spring of 2010 in a joint project between Chalmers University of Technology in Gothenburg and Volvo Aero Corporation in Trollhättan. It was supervised by Stefan Cedergren and adjunct professor Göran Sjöberg both representing Volvo Aero Corporation and Chalmers University of Technology, Göran Sjöberg also serving as the examiner of the diploma work.

Turning tests were performed at Chalmers University of Technology at the Materials and Manufacturing Department at campus Lindholmen. Microscopic evaluations and sample preparation was done mainly at Chalmers University of Technology campus Johanneberg but also at Volvo Aero Corporation in Trollhättan.

Contents

1 Introduction

In almost all manufacturing of metallic components the process that gives the component its final shape is a machining operation. The aerospace industry is no exception and a lot of machining is performed in the making of components to be used in aircraft engines. As the materials used in such applications have to withstand high temperatures and still retain high strength, machining of these alloys is very hard. As a consequence a lot of resources are put into the research of this problem.

There is also a strong driving force for modeling and simulations of the cutting processes in the industry. At Volvo Aero there is a vision that in the not too distant future, all cutting processes will be simulated before a single chip is cut. To be able to perform simulations that are accurate enough, a lot of work needs to be done, not only at the simulation and modeling level but also at the material level to better understand the basic material behavior and to develop testing methodologies that can provide relevant data to be used in the modeling.

1.1 Background

When the machinability of a low pressure turbine casing made of Inconel 718 suddenly changed at Volvo Aero causing tool failures in a way not before seen an investigation was launched. As the change occurred after a change of material supplier it was suspected that the reason had to be related to the work material. Maria Krook [1] conducted a study where she compared the tool wear of the tools used in producing these components to material samples of the materials being machined. She found that variations in chemical composition, microstructure and strength influenced the machinability.

She then went on to test this in materials tailored to contain larger variations and verified that these variations indeed had a large influence on the machinability of these materials.

The work of Krook was later expanded by Stefan Olovsjö [2] who, in a systematic way, investigated the influence of grain size and hardening on the machinability of Alloy 718 and Waspaloy. He found big differences in the tool wear and burr formation depending on the heat treatment. In his work all cutting parameters were fixed and only the material and heat treatments of the materials were varied.

Olovsjö, together with Geraldiné Puyoo [3], also investigated the chip microstructure and deformation in the different materials and found that the chip morphology varied between the small grained and large grained materials, the former produced continuous chips and the latter serrated chips.

The work done by Krook, Olovsjö and Puyoo was then further extended by Peter Hjärtstam [4] who in his diploma work investigated the influence of feed on tool wear and chip formation. He found that the feed to grain size ratio was important for tool wear and chip morphology.

1.2 This project

This project builds on and extends the work done earlier as explained in the previous section by investigating the influence of cutting speed on chip formation. It is also a part of a larger effort to build a solid base which will serve as a reference for development and evaluation of test methods later to be used to validate and verify simulations and modeling of the turning process which is illustrated in figure 1.

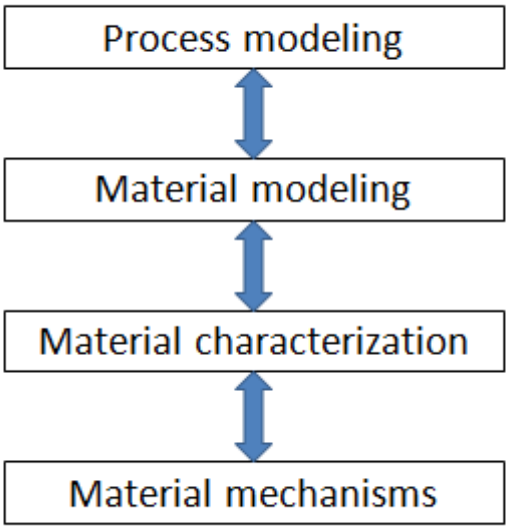

Figure 1: The philosophy behind the Optima project where it is emphasized that an understanding of the basic material mechanisms is key in order to know how to characterize the material and build a material model to be used in the actual process modeling.

This effort is in turn part of a larger research project called “Optima”. Optima is a joint operation between Volvo Aero Corporation and Chalmers University of Technology among others, aiming to reduce machining problems stemming from material variations.

This work contributes to this effort by giving an overview of the deformation taking place during chip formation and its relation to the cutting speed used in the process. This is done for one material (Inconel 718) but in four different conditions due to different heat treatments making it possible to see the effect of hardening and grain size as well as the cutting speed.

In contrast to the previous work, no extensive investigation of tool wear will be performed.

2 Superalloys

2.1 Historical perspective

In the early years of the jet engine, austenitic stainless steels where used for the turbine blades [5]. These materials soon proved to be limiting the development of the turbines, as improving turbine efficiency meant increasing operating temperatures. This called for a new type of material, one which would be more tailored to meet the need for better mechanical properties at high temperatures. This demand led to the development of a class of materials known today as the superalloys [6].

The development of these materials continues to this day with optimization of chemical composition and production methods, because these materials have to work in, what is described in the journal *Flight* [7] from 1948 as "…the most arduous instances of high-temperature operation." Something that is still (and possibly more than ever) true in this age of environmental awareness and subsequent demands for increased fuel efficiency.

In order to do this successfully superalloys are required to have a broad spectrum of properties such as high temperature strength and high resistance to creep, oxidation and fatigue just to name a few. These extraordinary properties require extraordinary materials, something that is reflected in the prefix "super" in superalloys and which will be explained deeper in the following sections.

2.2 Alloy 718

The alloy used in the tests performed in this diploma work is Alloy 718 which is often referred to as Inconel 718 (which is a registered trademark of Special Metals Corporation) and this section will describe the chemical composition, strengthening mechanisms and phases present in this alloy specifically and nickel-based superalloys in general and address how these give the alloys their mechanical properties.

Alloy 718 is a nickel-iron based superalloy containing roughly 20 wt% of iron (complete chemical composition in table 1). The main difference between 718 and other nickel based superalloys is that iron will make it possible to form γ'' precipitates if the material is aged and give the alloy a high strength up to temperatures of roughly 650 ˚C [8].

Table 1: Chemical composition (in wt%) of Alloy 718 [9].

Ni + Co	Co	Cr	Fe	C	Mo	Al	Ti
50.00-55.00	1.00 max	17.00-21.00	Bal.	0.08 max	2.80-3.30	0.20-0.80	0.65-1.15
Nb + Ta	B	Mn	Si	Cu	S	P	
4.75-5.50	0.006 max	0.35 max	0.35 max	0.30 max	0.015 max	0.015 max	

Alloy 718 is by far the most used superalloy, often used in discs holding the blades in turbine engines as the temperature is comparably low and the strength requirements are comparably high which fits the profile of Alloy 718 like a glove. The alloy is also known for its weldability which is excellent as far as superalloys are concerned [10].

2.2.1 Strengthening mechanisms

Nickel based and nickel-iron based superalloys are primarily strengthened in two ways; precipitation hardening and solid solution hardening. For temperatures below $0.5T_m$ grain size hardening according to Petch-Hall is also effective, however at higher temperatures larger grains is to be preferred as they give better creep resistance by reducing the amount of grain boundaries in the material.

Solid solution strengthening

Chromium and Molybdenum are added to give solid solution strengthening. The mechanisms working to strengthen the material is atomic size mismatch, elastic modulus mismatch and short distance order which all increase the stress needed to deform the material [8].

Precipitation strengthening

The main strengthening mechanism in nickel based superalloys is precipitation hardening. The hardening effect comes from the fact that dislocation movements through precipitates are hindered by the ordered structure of the precipitates. For a dislocation to pass through the precipitate the order of the atoms must be broken which means that a thermodynamically less attractive state is achieved by the creation of APB (anti phase boundary) which means that more energy is needed to move a dislocation through the precipitate. To restore order dislocations have to travel in pairs, referred to as superdislocations, where the first dislocation destroys the order and the second restores it. In some cases it is not even enough for two dislocations to cooperate but even more have to move together [10].

Another way in which precipitates increase the strength of the material is through the strain field created by the precipitate in the matrix due to the size mismatch of the crystal structures. This works in principle in the same way as for solid solution strengthening but in this case the strain field is much larger [8].

To achieve optimum strength the size and distribution of precipitates is important as well as the degree of mismatch between the precipitate and the matrix. It is also important that the precipitate is coherent with the matrix as most of the strength is lost in the event of precipitates becoming incoherent with the matrix [6].

2.2.2 Phases

Several phases are present in superalloys. Properties and characteristics of the most important are discussed below.

Gamma (γ)

The continuous matrix in nickel based superalloys is an FCC (face centered cubic) phase (γ) containing nickel and in the case of nickel-iron based superalloys also iron. Alloying elements added for solid solution hardening effects like chromium and molybdenum are also found in the γ phase [8].

Gamma prime (γ')

The γ' phase is formed from aluminum and titanium together with nickel as $Ni_3(Ti, Al)$. Other elements that can go into the γ' phase are niobium, tantalum and chromium. The γ' phase forms ordered FCC precipitates that are coherent with the matrix. The main strengthening mechanism of this phase is not from coherency strain, as the lattice mismatch is low, but from APB and the subsequent need for superdislocations to shear the precipitate. At high temperatures the γ' precipitates give nickel based superalloys most of their strength [8].

Gamma double prime (γ'')

If iron is present in the alloy, as in the case of in Alloy 718, nickel and niobium form an ordered BCT (body centered tetragonal) phase (γ'') as Ni_3Nb that is coherent with the matrix but with rather large mismatch strains (≈2.9%). In addition to the strain field formed around the precipitates the amount of dislocations needed in a superdislocation to shear γ'' and restore order in the crystal is higher than in γ' precipitates leading to a larger strengthening effect compared to γ' hardenable alloys. The γ'' precipitates are stable at temperatures up to roughly 650°C. Above this temperature γ'' precipitates are no longer stable and are dissolved into the matrix [6].

Delta (δ)

The δ-phase is a thermodynamically stable form of the Ni_3Nb that also made up the γ'' and is formed at the expense of γ''. The δ-phase is of an orthorhombic structure and is incoherent with the matrix meaning that it will not work to strengthen the material. It is possible to use δ-phase to control and refine the grain size as it nucleates at grain boundaries preventing grain growth [10].

Carbides and Borides

A number of carbide species can be found in superalloys including MC, $M_{23}C_6$, M_6C, and M_7C_3. Borides appear in superalloys in the form of M_3B_2. Carbides serve three functions in superalloys. The first function is to strengthen the grain boundary and prevent grain boundary sliding. The second function is precipitation strengthening of the matrix. The third is to bind elements that could cause phase instability during service [6].

2.2.3 Processing

A thorough overview of the processing of Inconel 718 is provided by Krook [1] and following below is a short summary.

As superalloys are used in critical parts it is very important that the material is homogenous and free of defects. To achieve this, the material processing is very important and consists of three steps; melting, forging and heat treatment.

To avoid segregations and other defects the material is melted and remelted in several steps using techniques such as vacuum induction melting, vacuum arc remelting and electroslag remelting. The techniques focuses on composition control and making sure that no contaminants enter into the melt as well as homogenous solidification.

The forging step serves the purpose of reducing the grain size and further increase homogeneity as well as forming the general shape of the product later to be finalized in machining processes.

The heat treatment step is the step determining the strength and final microstructure of the material. The heat treatment is done in two steps, a solution heat treatment and an aging (hardening) heat treatment. The solution heat treatment serves the purpose of dissolving any precipitates present and to fully recrystallize the material and is in the case of Alloy 718 often performed at about 950 °C which is above the solvus temperature of the γ’ and γ’’ phases but below the solvus temperature of the delta phase. The delta phase pins the grain boundaries and prevents unwanted grain growth.

The aging heat treatment is performed at about 750 °C. The purpose is to allow for precipitation of γ’ and γ’’ in the matrix to give the material its final strength.

3 Machining

By virtue of its flexibility, machining is used to form almost all metallic materials into geometries useful for engineering, ranging in scale from micrometers to several tens of meters. Machining spans several processes that all have one thing in common; the material is removed from the pre-shaped starting material called the *workpiece* by cutting in the form of chips. Some commonly known and widely used processes fitting this description is turning, milling and drilling [11].

This work concerns turning and therefore the following topics will describe this process in a more elaborate manner.

3.1 Turning

In turning the workpiece is rotated while a rigid tool removes material from the external surfaces by following a path along the rotational axis, creating a rotational symmetric geometry.

3.1.1 Principles

The principles behind turning and machining processes in general are the two motions usually called *cutting motion* and *feed motion*. The cutting motion is the motion that creates a difference in velocity between the tool and the workpiece and the feed motion presses the tool against the workpiece [12]. In the case of turning, the cutting motion is generated by fixation of the workpiece in for example a chuck or on a table, which in turn is connected via a gearbox to an electric motor. This setup makes it possible to rotate the workpiece within a range of rotational speeds.

The feed motion, usually just called *feed*, has two possible directions; parallel or perpendicular to the rotational axis (see figure 3). Feed along the longitudinal or axial direction creates a cylindrical surface and is called *turning* or *straight turning.* If on the other hand feed is in the radial direction, it is called *facing* or *parting of* depending on if the purpose is to create a face or a shoulder perpendicular to the axis of rotation (facing) or to cut off a piece from the parent work material (parting). Movement in the two directions can be combined and allows a more complex profile to be created [12].

In turning there is essentially three force components involved, called the cutting force (F_C), the feed force (F_f) and the radial or passive force (F_p) (see figure 2).

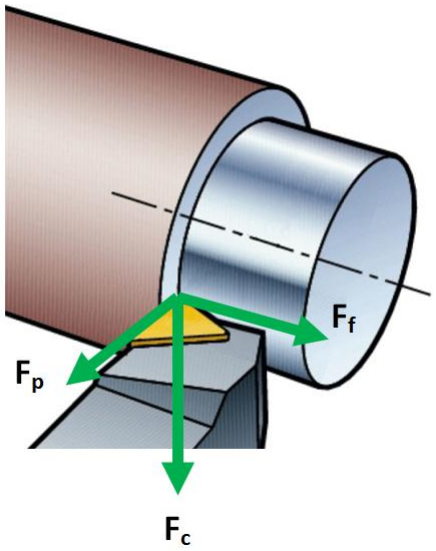

Figure 2: The force components involved during turning. Modified, original from Sandvik Technical Guide [13].

3.1.2 Cutting parameters

In dealing with turning, there are several parameters that control the process and affect the tool life, surface finish and the material removal rate. The optimum selection of the processing parameters is therefore a combination that results in the best possible compromise between the three previously mentioned variables depending on the demands placed upon the part being produced [14]. Below is a listing of the essential parameters with a short description of their definition and the units that will be used throughout this work.

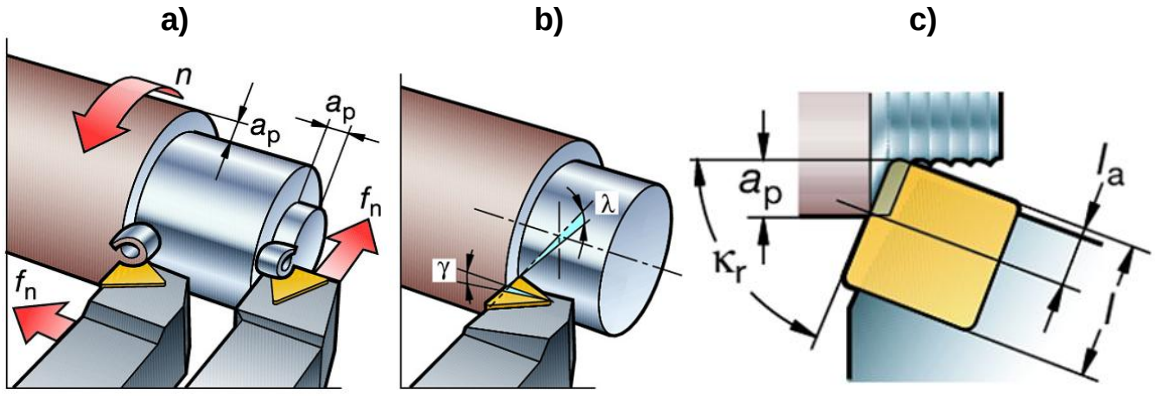

Figure 3: a) Definition of feed (here called f_n to clarify that it is in mm per revolution (= n)) and cutting depth (a_p) for longitudinal turning (left tool) and facing (right tool). b) Definition of rake angle (γ) and inclination angle (λ) in longitudinal turning. c) Definition of entering angle (κ_r), cutting depth (a_p), total cutting edge length (l) and effective cutting edge length (l_a). [13].

Cutting speed (V_c)– The relative speed between the workpiece surface and the tool. Depends on spindle rotational speed and diameter of the workpiece and is usually given in the unit m/min.

Feed (*f*) – The movement of the tool per revolution often presented in millimeters per revolution.

Depth of cut (a_p) –The distance (measured in mm) between the uncut and the cut surfaces measured perpendicular to the feed direction.

The following parameters are tool dependent parameters and are a result of the combination of the tool holder and the cutting insert.

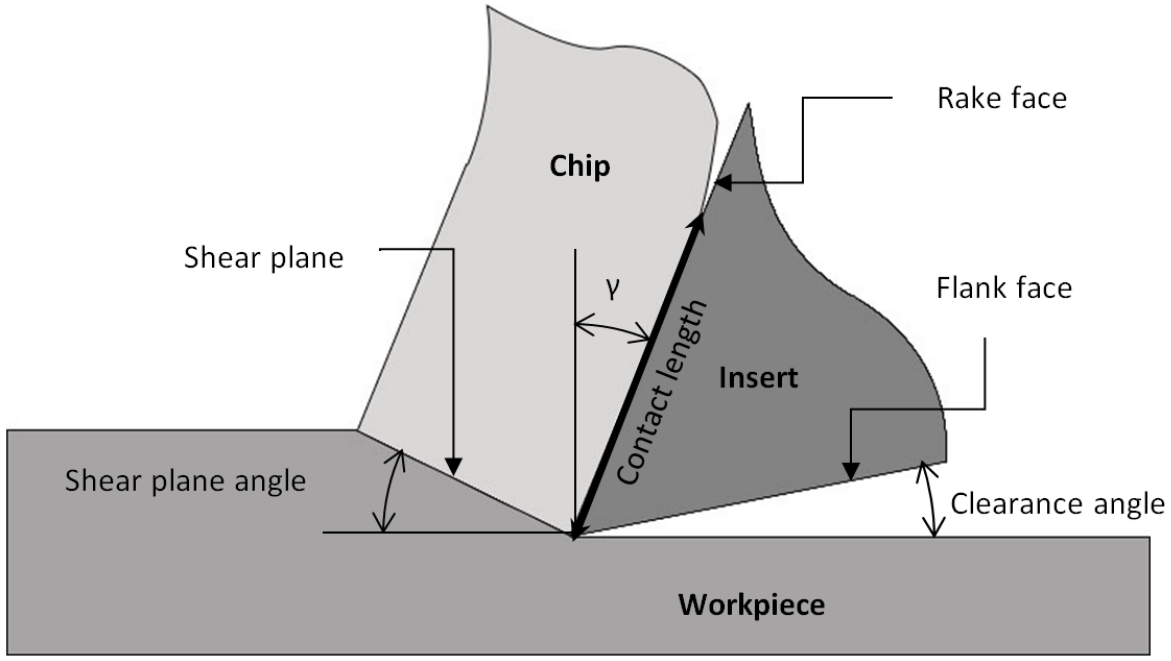

Figure 4: Schematic illustration of the cutting process, showing basic definitions and important angles and faces. Worth noticing is that the rake angle (γ) shown is positive.

Rake angle (γ) – The angle between a line parallel to the workpiece rotational axis and the rake face of the cutting insert, see figure 3b and figure 4. A negative rake angle provides a stronger cutting edge but also leads to higher cutting forces [11].

Inclination angle (λ) – The angle at which the cutting insert is mounted in the tool holder (see figure 3b) [13].

Entering angle (κ_r) – The entering angle is defined as the angle between the cutting edge and the feed direction (see figure 3c). The entering angle controls the length of the cutting edge and also affects the cutting forces. A small entering angle gives a large cutting edge length for a given depth of cut and thereby increases the passive (or radial) force component.

A small entering angle promotes longer tool life in a number of ways [13]:

- A gradual buildup of forces as the cutting edge length is increased gradually.
- Initial contact with the workpiece is made further from the relatively weaker tip of the insert.
- The surface layer, which often is harder, perhaps by scales from the previous forming process, heat treatment or work-hardening from the previous cutting pass, is spread over a larger length of the cutting edge. This reduces notch wear.
- The greater contact length promotes better heat conduction into the workpiece and more even heat distribution in the cutting insert.

Clearance angle – The angle between the tangent to the workpiece surface and the flank face of the insert (see figure 4 and figure 5). The clearance angle is often on the order of 6-10˚ to avoid rubbing the flank face against the workpiece [11].

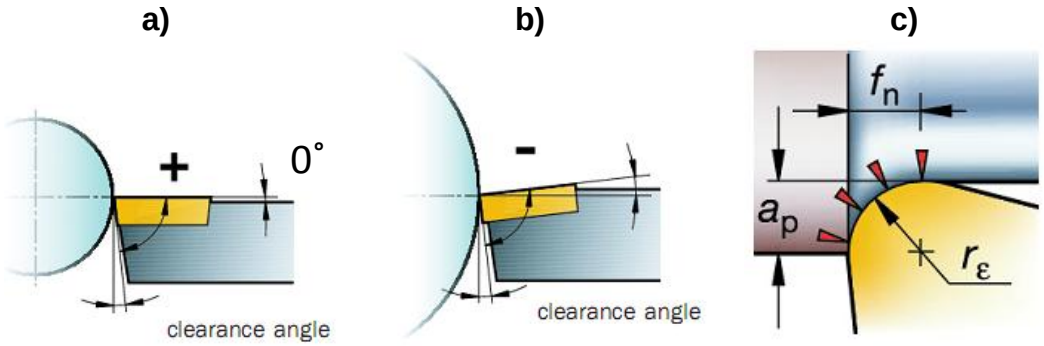

Figure 5: Clearance angle for a a) positive insert b) negative insert. Note that the negative insert by itself has no clearance angle. In this case it is provided by the tool holder, which also introduces a negative rake angle. c) Schematic drawing of the nose radius (r_ε), feed (f_n) and cutting depth (a_p). [13].

Nose radius (r_ε) – The purpose of the nose radius is to provide strength to the tip (nose) of the insert and it is essential in determining the surface finish. A small nose radius is useful for small cutting depths and reduces vibrations but suffers from lower strength while a larger nose radius is desirable for higher depths of cut and feed rates, as this result in higher forces, demanding a stronger cutting edge [13].

A special case of turning is orthogonal cutting. In orthogonal cutting a straight tool edge is used and it is normal to both the direction of cutting and to the feed. This can be achieved by cutting in tubes or flanges, where flanges have the advantage of having a constant cutting speed over the cutting edge. The disadvantage is that the rotational speed has to be increased gradually as the diameter decreases in order to have a constant cutting speed [11].

In order to have a purely orthogonal setup, the nose radius of the tool should not be used for cutting; otherwise the condition is known as “semi-orthogonal” cutting [11].

3.1.3 Inserts

Cutting inserts (here after called inserts) are the components that are in contact with and cut away material from the workpiece to produce the desired component geometry within specified tolerances. This imposes requirements on dimensional stability and this dictates the characteristics of the insert regarding both its geometry and material.

Another aspect is that of economy. In order to increase productivity, the volume of material removed (see equation (1)) per unit time should be maximized.

(1)

At the same time, there is the need for the machining operation to run continuously without interruption. So ideally an insert should allow for increased material removal rate (which is also dependent on the lathe’s power and stability) and at the same time have longer lifetime.

These demands have made way for a quite rapid evolution of tool materials, from carbon steels, via high speed steels (HSS) and cemented carbides to ceramic, polycrystalline boron nitride (PCBN) and diamond (PCD). The reason for this can be explained by studying the material properties that govern the above mentioned dimensional stability and lifetime such as hot hardness, toughness and wear resistance [12].

Hot hardness measures how well a material retains hardness at elevated temperatures (see figure 6). A higher hot hardness allows for higher cutting speeds, and as seen in equation (1), increases the material removal rate and therefore also productivity.

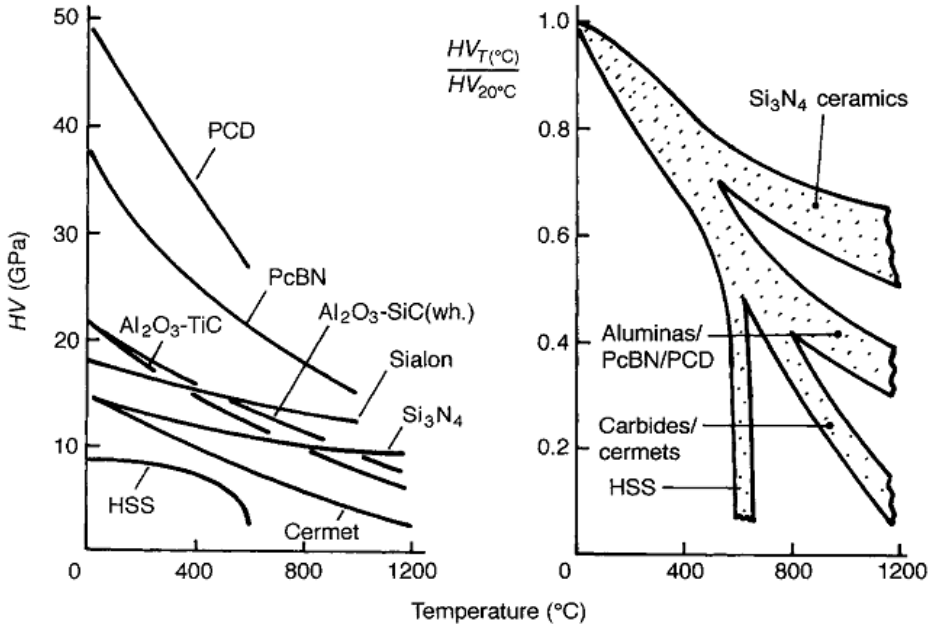

Figure 6: Hardness of tool materials plotted against temperature. The left graph shows absolute hardness values and the right hardness relative to room temperature hardness. [15]

Toughness is a measure of how much energy a material can absorb before it fractures. A high toughness is preferred as it means there is less risk of tool failure from impact loads such as when the insert enters the material. Both tensile rupture strength (TRS) and K_{IC} are measures of toughness in the form of fracture resistance and can be seen for a selection of common tool materials in figure 7.

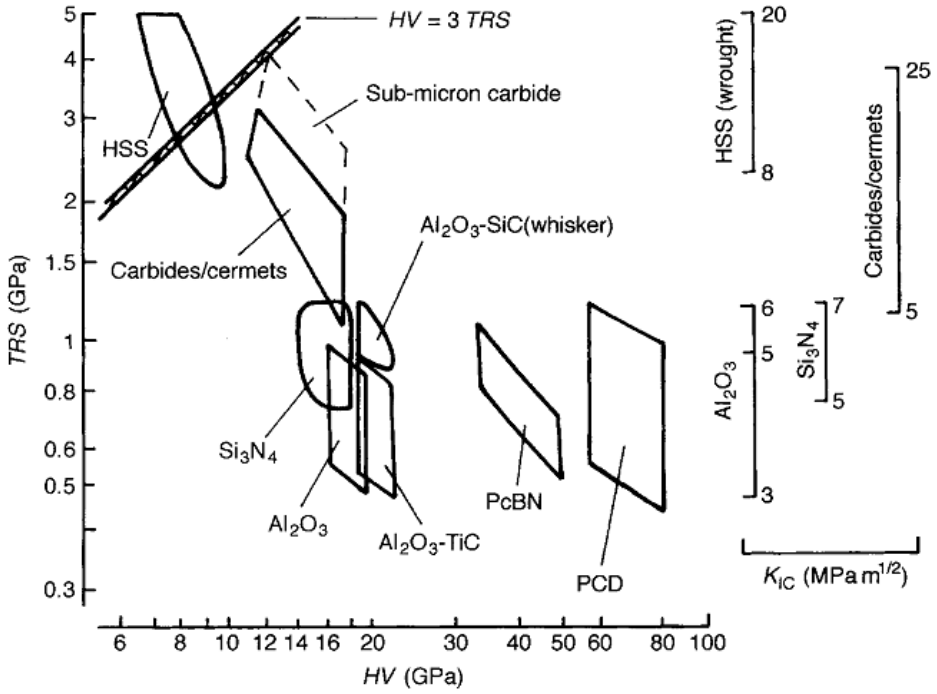

Figure 7: The mechanical properties of different tool materials (uncoated) at room temperature. TRS stands for Tensile Rupture Strength. The line "HV = 3 TRS" in the top left corner shows the relation between hardness and tensile yield stress. Materials below the line are expected to fail in a brittle (elastic fracture) manner as opposed to failure with some plastic deformation (yielding) for those above the line. [15]

Wear resistance is the inserts ability to resist wear caused by different mechanisms such as abrasion, adhesion, diffusion and oxidation. This will be discussed more thoroughly under the topic "wear mechanisms".

Today a plethora of different insert materials and geometries are available and the correct insert depends on the type of operation and the material to be cut. Short descriptions of the most common types follow below.

Cemented carbide

Cemented carbide inserts features hard carbides (Usually WC, TiC, TaC or combinations of those three) in a ductile matrix which often consists of cobalt. The amount of cobalt binder can be varied to tailor the properties as increased cobalt content increases toughness but decreases strength and hardness. Insert materials for machining of metals usually contain between 4-12 wt% cobalt binder phase and a carbide grain size varying between 0.5 µm to 10 µm [11].

Coatings such as TiN, TiC, Ti(C,N) (titanium carbonitride), HfN or alumina are commonly applied to cemented carbide inserts by means of PVD or CVD. These coatings give the insert a harder and more abrasion resistant surface, but the most important effect seems to be that they act as a diffusion barrier. Coatings are proven to allow an increase in cutting speed by 25-50% or extended tool life by a factor of 2 or 3 [11].

Ceramics

Ceramic materials used for cutting inserts are mainly alumina (Al_2O_3) and silicon nitride (Si_3N_4) and composites based on those. These materials offer a high hot hardness and high compressive strengths but lack toughness (see figure 6 and figure 7) which is why they are often reinforced. These

reinforcements can be in the form of whiskers, such as SiC whiskers or an addition of ZrO_2 or TiC in the case of alumina or additions of aluminum and oxygen to silicon nitride to form SiAlON (Si-Al-O-N).

The reason for using ceramic inserts is that they allow for higher cutting speeds compared to cemented carbide inserts. This goes well with the fact that higher cutting speeds lead to lower cutting forces and that cutting fluids largely become ineffective at high cutting speeds [16].

CBN and PCD

Cubic Boron Nitride (CBN) and Polycrystalline Diamond (PCD) are both synthetic materials that show exceptional hardness (see figure 6). An advantage of CBN is that it has higher temperature stability in contact with ferrous metals compared to diamond. Diamond tools are less useful for machining high melting point materials such as superalloys where high interface temperatures are generated at the workpiece – tool interface. In contact with iron diamond starts to transform into graphite at about 730˚C. PCD is therefore used to machine non-ferrous, low melting point metals such as aluminum and copper alloys and non-metallic materials at high speeds and with excellent tool life [11].

3.1.4 Cutting fluids

Cutting fluids are often employed in metal cutting operations to reduce cutting forces by providing lubrication and to reduce tool, workpiece and machine temperatures. This increases tool life and improves surface finish and the use of the correct cutting fluid is sometimes even necessary in order to have an efficient cutting operation [11]. Other notable effects include flushing away chips from the cutting zone and to protect the workpiece from corrosion [16].

However, cutting fluids also have drawbacks, such as higher machining costs, stemming from both the cost of acquisition and subsequent disposal of the fluid and the cleaning of the finished component. This can account for more than four times the cost of the cutting inserts in the case of aeronautical materials [16].

Thus economic incentives combined with growing environmental concerns and demands for higher productivity (often leading down the high speed machining route) has increased the interest of manufactures of aeronautical components towards reduction (such as Minimum Quantity Lubrication - MQL) of cutting fluid use and dry machining [16].

Research on the effects of cutting fluids in high speed machining using ceramic inserts has shown that they have little or no effect [17], [16], further reinforcing the movement towards dry cutting.

3.1.5 Wear and wear mechanisms

When discussing wear mechanisms it is important to keep in mind that the factors controlling wear depend on a multitude of properties, regarding not only the tool material, but also the work material, the process, the process parameters and the resulting temperatures and forces. Trent et al [11] summarizes this well:

”Wear resistance is not a unique property of a tool material which can be determined by one simple laboratory test, or correlated with one simple property such as hardness.”

Abrasion

Abrasion is the wear on a surface in sliding contact with another surface. Harder materials scratch less hard materials and if a material contains hard particles such as carbides or nitrides, these can

have a higher hardness than the tool material, which leads to abrasive wear of the tool [18]. This is one of the reasons for the development and use of harder tool materials and the use of coatings, especially when cutting materials with high hardness or with hard particles or inclusions.

Adhesion and diffusion

In metal cutting the conditions for metal bonding of the workpiece material to the tool is particularly favorable. The newly cut metal is shielded from the external atmosphere which prevents oxidization and the high temperatures combined with high contact forces helps to weld the two materials together [11]. This adhesion of the work material to the tool can be in the form of a built-up edge (BUE) or as small particles or layers. These deposits of work material are often rejoined to or pushed on by the chip flowing past them and in the process of breaking off they might peel off some of the tool material resulting in adhesive wear of the tool [19].

A mechanism working in synergy with adhesion is that of diffusion. Solid state diffusion between the material adhering to the tool and the tool material replaces the atoms of the tool material with that of the work material, which weakens the tool [19]. The flow of work material over the tool also carries the tool material atoms away and restricts build-up of a concentration gradient [11].

Both these mechanisms are dependent on the reactivity between the work material and tool [19]. This is the reason why diamond tools aren't used to cut ferrous metals for example and is the mechanism responsible for crater wear (see figure 8) when cutting steels with WC-inserts [11].

Wear geometry

The previously discussed wear mechanisms manifest themselves as areas of wear on the insert as it is used for cutting the work material (for definitions, see figure 8). Depending on tool and workpiece material and the cutting conditions, certain types of wear dominate and therefore dictates tool lifetime [20].

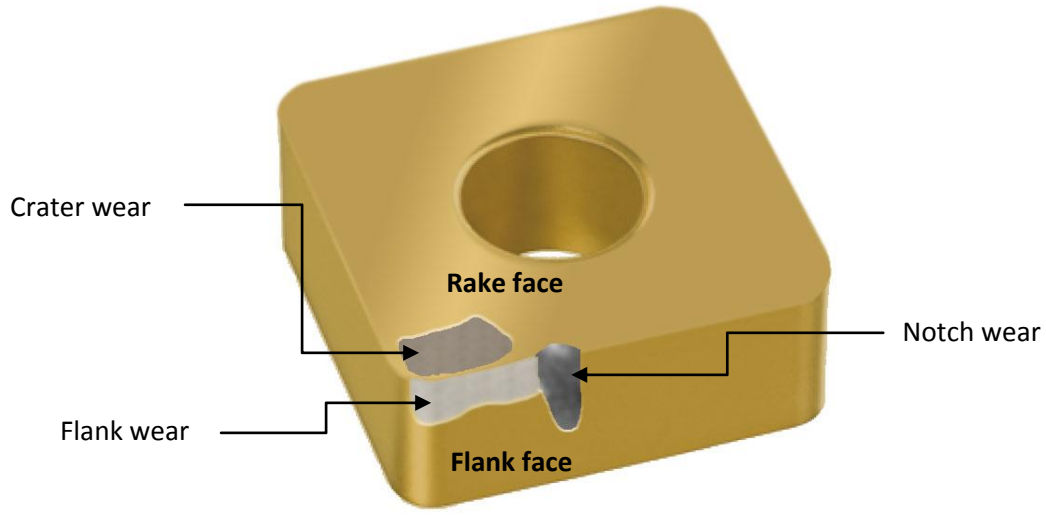

Figure 8: Schematic illustration of different kinds of wear.

Following below is a short description of three commonly seen wear types, but as this work does not investigate wear the reader more interested in this topic is encouraged to read the works of Olovsjö [2], Krook [1] and Hjärtstam [4].

Crater wear

Crater wear occurs on the rake face of the tool and is due to the high temperatures in this region, allowing diffusion between the work material and the tool. The high temperatures also affect the tool material yield strength, and for high cutting speeds it is possible that the tool is sheared. This produces a rapid crater wear and is often followed by tool fracture. This type of shearing crater wear is more common for high strength, high melting point materials such as superalloys [11].

Flank wear

Flank wear is the wear occurring at the flank face, below the cutting edge of the tool [19]. The cause for this is the tool rubbing against the work material, and this sliding contact produces wear by abrasion and adhesion [11].

Notch wear

Notch wear is a localized form of wear at the depth of cut line. This type of wear is common for work hardening materials such as superalloys and austenitic steels and is thought to be caused by oxidation of the tool material as well as contact with the previously cut surface, which is harder and may include oxides and burr [20], [19].

3.2 Deformation

From the general description of the machining process it can be understood that in order to form chips with a tool severe plastic deformation of the material is required. This section will describe how and where this deformation takes place and by which deformation mechanisms the material is deformed.

3.2.1 Models for chip formation

In classical chip formation theory all deformation of the material being machined into a chip takes place in one plane. This shear plane is seen as extending from the tip of the tool to the surface of the workpiece (see figure 4). One also specifies the shear plane angle as the angle between the shear plane and the surface of the workpiece. From this it is possible to calculate the chip velocity which will be different from the cutting speed as the feed and chip thickness is not the same as long as the shear plane angle is not 45° [11].

The shear plane model is very simple and easy to use but it has been shown to be inadequate to describe the intricacies of chip formation to any greater detail [21]. There are also many different modes of chip formation. Examples of chip morphologies as presented by Trent and Wright [11] can be seen in figure 9.

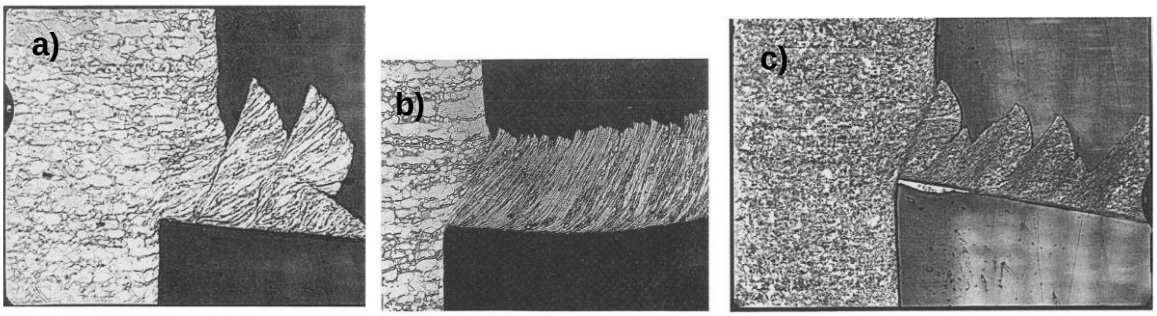

Figure 9: Chip morphologies. a) discontinuous chip produced at low speeds b) continuous chip c) segmented chip [11].

Discontinuous chips produced at low speeds are commonly explained by the stick-slip model which uses friction between the chip being formed and the cutting tool. As the chip slides against the tool the friction force will grow as the surface increases leading to a point where the chip will stick to the tool. The material will then be pushed up along the shear plane making the chip thicker. However this will increase the force on the chip which will overcome the friction force holding it back and the chip will slip away. At this point the thickness of the chip will decrease thanks to the increased speed of the chip. As this cycle repeats itself a serrated chip will be formed [11].

3.2.2 Deformation zones

In studies of chip formation three zones of particular interest have been found; the primary, secondary and tertiary shear zones. The primary shear zone extends from the tip of the tool to the surface of the workpiece, the secondary zone is at the interface between tool and chip as it slides on the tool and the third is at the tool tip extending into the workpiece figure 10.

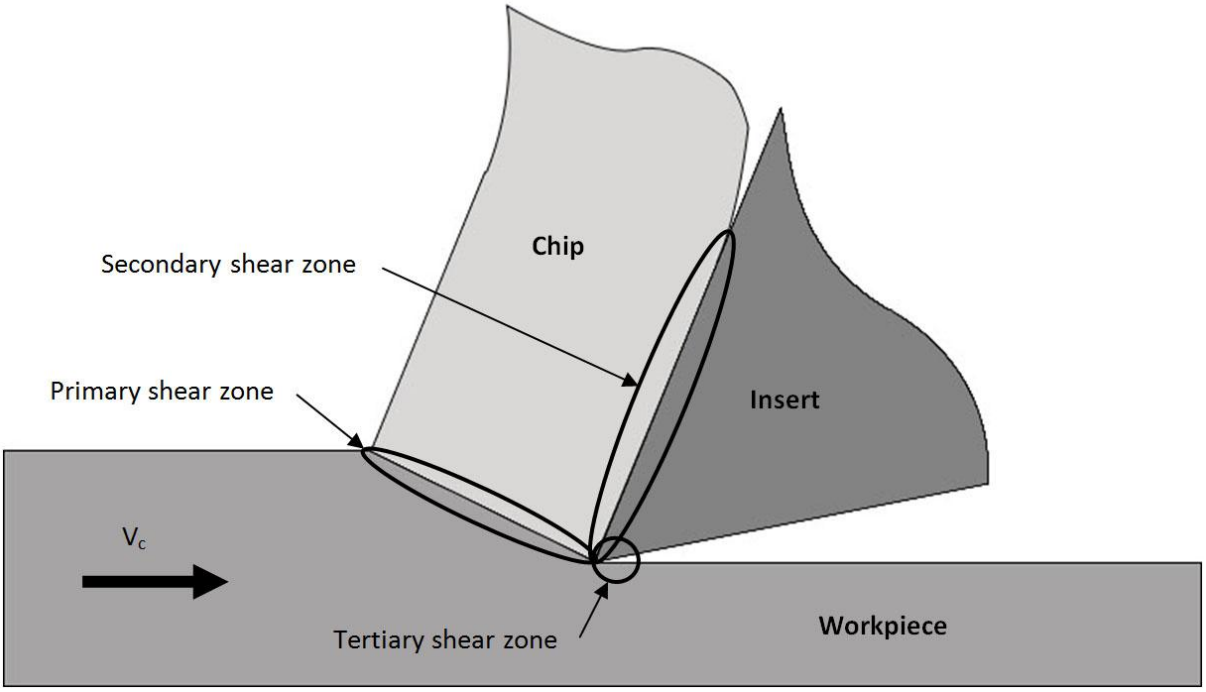

Figure 10: Definition of shear zones during chip formation.

The impact of these shear zones can be seen in figure 11. The influence of the different shear zones on the chip formation is dependent on many things. Among them are material, tool material, tool geometry and cooling.

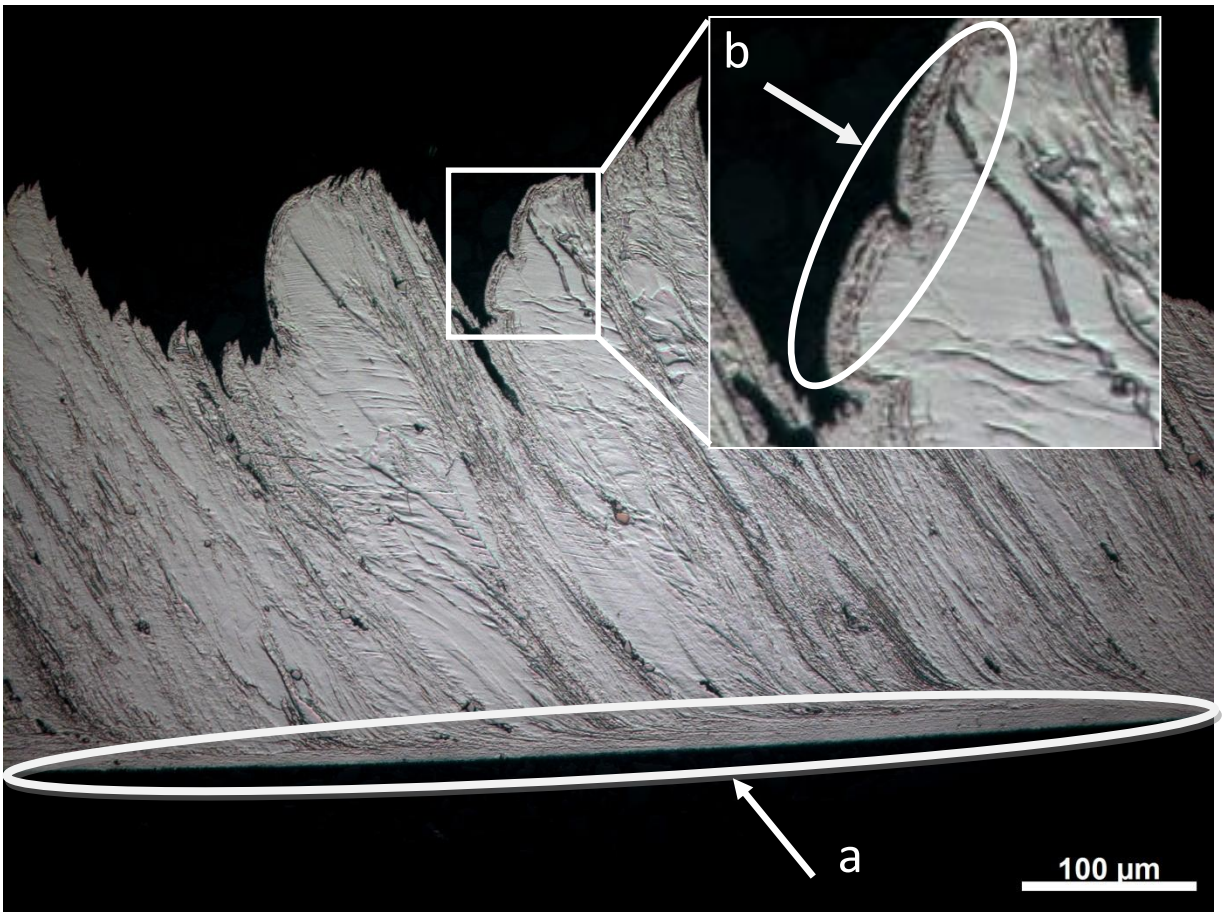

Figure 11: Impact of secondary (a) and tertiary (b) shear zones.

3.2.3 Slip

The deformation taking place in the shear zones is mainly due to dislocation movements or slip. This is the main plastic deformation mechanism in all metallic materials. Dislocation movement takes place in specific planes and in specific directions for crystalline materials like metals. The combination of a plane and a direction is called a slip system. In single crystal materials the orientation of these slip systems in relation to the direction of the force being applied is important to how easy it is to deform the material whereas in polycrystalline materials these orientation differences tends to even out as many grains are deformed at once [22].

3.2.4 Twinning

In certain materials another plastic deformation mechanism can be active, twinning. Twinning means that the deformation takes place without any dislocation movement but instead the entire crystal structure is sheared in such a manner that a mirror plane forms in the crystal (see figure 12). The amount of deformation due to twinning is often not that large but it can make it possible in crystals with an unfavorable orientation for slip to be reoriented making normal slip deformation possible again [22].

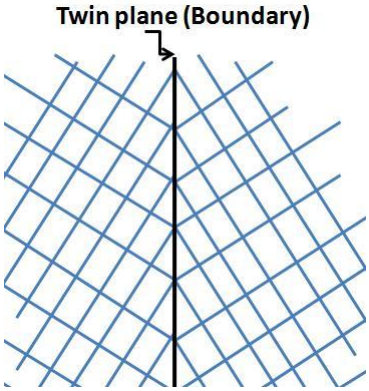

Figure 12: Twin grain boundary. Atoms are positioned where the lines intersect. [4]

3.2.5 Shear bands – shear localization

Shear localization means that almost all deformation is localized into bands in the material and that the surrounding material is more or less undeformed, at least compared to the amount of deformation in the shear band. A simple way of explaining this was presented already in 1943 by Zener and Hollomon [23] as

"When the material undergoes an element of strain, dE, adiabatically, the stress is raised by the strain hardening and lowered by the associated rise in temperature".

In other words this means that as the material is deformed it gets stronger due to work hardening but weaker due to the temperature rise associated with the work done. If locally the temperature effect is stronger than the work hardening effect, the materials ability to resist strain will locally be lower leading to a situation where all strain will be concentrated to this band. This leads to an even higher temperature and lower strength as the work done in the band increases rapidly.

Even though the above explanation still is considered to be the correct explanation to how shear bands are formed most of the details about them are still debated and uncertain. Which properties are important for the formation of shear bands? How can one predict the organization of shear bands? How and why do they nucleate? These are all questions without clear answers yet and much research is taking place in the area.

Some suspects have been identified as properties influencing the formation of shear bands for example strain hardening, strain rate hardening, geometrical factors, thermal softening and heat conduction properties of the material all play a role but the relative importance is not clear [24], [25].

The relevance of shear bands to machining is that most if not all metals will at sufficiently high cutting speeds start to form chips that are segmented instead of continuous due to the fact that shear bands will form. The speed at which this will happen is highly material dependent [11].

3.3 Machinability of Superalloys

Superalloys are well known as difficult-to-cut materials and this of course applies to Alloy 718 as well. The reasons behind the difficulty in cutting superalloys are rather easily grasped by recalling what they were designed to do. As previously mentioned they are high-temperature, high strength materials, retaining their already high strength up to high homologous temperatures (the ratio between operating temperature and melting temperature) [10]. This is but one of the reasons and following below is a list [16] of the properties that make Alloy 718, and nickel-based superalloys in general, some of the most difficult to cut materials in existence:

- FCC γ matrix which imparts high work hardening and high strain rate sensitivity
- High strength leading to high cutting forces which readily induces vibrations
- High content of hard particles (carbides and nitrides) promotes abrasive wear
- Low thermal conductivity leads to high temperatures in the workpiece-tool interface, promoting wear by diffusion
- Chemical affinity for common tool materials, coupled with the above mentioned high temperatures worsens the diffusion wear
- Adhesion or welding to the tool materials (like the forming of a BUE) leads to pull-out of the tool material

The combination of all these properties boils down to short tool life and poor surface quality.

4 Experimental techniques

This section will cover the experimental techniques used in the project including the work material used, design of turning experiments and actual test setup.

4.1 Work material

The work material used in this project was the same material used by Olovsjö [2] and Hjärtstam [4] meaning that the material was already heat treated and ready to be used.

4.1.1 Heat treatment

The heat treatments used by Olovsjö are summarized in table 2. Hjärtstam modified this heat treatment for the large grained and aged (hardened) material which is also seen in table 2.

Table 2: Heat treatments performed on materials.

Material	Solution heat treatment	Aging heat treatment (hardening)
Small grains not hardened	954 °C (2 h)	None
Small grains hardened	954 °C (2 h)	718 °C (8 h) + 622 °C (10h)
Large grains not hardened	954 °C (2 h) + 1050 °C (3 h)	None
Large grains hardened (Olovsjö)	954 °C (2 h) + 1050 °C (3 h)	718 °C (8 h) + 622 °C (10h)
Large grains hardened (Hjärtstam)	1050 °C (3 h) + 954 °C (2 h)	718 °C (8 h) + 622 °C (10h)

The solution heat treatment is designed to first dissolve γ’ and γ’’ into the matrix, this takes place at 954 ˚C which is below the δ solvus temperature but above the γ’ and γ’’ solvus temperatures. When large grains are wanted a higher temperature is needed as the δ phase hinders grain growth. For this purpose the large grained materials are heated to 1050 ˚C which is above the δ solvus temperature.

The reversal of the steps in Hjärtstams material means that γ’, γ’’ and δ all are dissolved in the first stage. The result is almost the same material as the one Olovsjö produced in two steps, a large grained material with no γ’, γ’’ or δ. After this Hjärtstam lowered the temperature to 954 ˚C which means that he re-precipitates some δ phase in the grain boundaries. In this work, for the large grained hardened material, the material used was heat treated by Hjärtstam meaning that delta phase was present in the grain boundaries.

After all finished solution heat treatments the materials were quenched in water to avoid growth of γ’ and γ’’ during cooling.

The aging heat treatment is a standard two stage heat treatment widely used to precipitate γ’ and γ’’.

4.1.2 Properties of materials

The grain size and hardness of the materials as measured by Olovsjö can be seen in table 3.

Table 3: Grain size and hardness of materials used.

Material	Grain size [ASTM]	Average diameter [μm]	Hardness [HV]
Small grains not hardened	9	16	250
Small grains hardened	9	16	445
Large grains not hardened	3	127	170
Large grains hardened	3	127	430

The properties measured are in accordance with the fact that the main hardening mechanism in Alloy 718 is precipitation hardening from γ'' and that the effect of grains size hardening is not that important.

4.2 Turning experiments

In order to characterize the interrelationship between material properties, deformation mechanisms and deformation rate in turning of Inconel 718 a series of tests were performed to evaluate possible experimental setups. This section deals with the reasoning underpinning the choice of experimental methods (Design of experiment) and their subsequent practical implementation (Test setup).

4.2.1 Design of experiment

As this work builds on previous work done by Olovsjö [2], Puyoo [3] and Hjärtstam [4] the intention was to use the same test setup as far as possible but let the cutting speed be the variable. The test setup used by Olovsjö, Puyoo and Hjärtstam was facing of discs with constant cutting parameters apart from varying feed rate in the experiments performed by Hjärtstam. As all previous work contained tool wear measurements the cutting time was quite long. It should also be noted that they used cemented carbide cutting tools and cutting fluid for all experiments.

To evaluate the possibility to use similar parameters and setup tests were performed where the cutting speed was varied between 30 m/min to 240 m/min and all other parameters kept the same as in the old setup. It was found that the tool wear at cutting speeds over 120 m/min was too rapid to allow the process to stabilize. This was seen in cutting force measurements and studies of the tool inserts in optical microscope. As the aim of the work was to vary the cutting speed in quite large intervals it was deemed unsatisfactory not to be able to exceed 60 m/min which was the last tested cutting speed with stable cutting forces.

To be able to reach higher cutting speeds while still keeping the test setup as close as possible to the one used by Olovsjö, Puyoo and Hjärtstam, tests were performed with a facing operation in the same way as before but with ceramic inserts instead of cemented carbide inserts. It should be noted that the geometry of the ceramic inserts available was not the same as the cemented carbide ones used before. After evaluating the cutting forces for the same cutting speeds as before, it was found that the passive component of the cutting force was significant and unstable. This was also deemed unsatisfactory as it would be impossible to say to which extent the passive force component would affect the deformation behavior.

For the final test setup it was decided that the passive force would be eliminated by cutting in flanges in an orthogonal manner. In this way the effect of the nose radius as well as the effect on the tool wear created by rubbing against the previously cut material was eliminated. As discussed earlier, cutting fluids show little or no effect at high cutting speeds with ceramic inserts and there is a movement towards dry machining. On this basis it was decided that no cutting fluid would be used for the experiments. The downside of using this test setup however was the fact that it was not quite as close to the setup used previously by Olofsjö, Puyoo and Hjärtstam making it harder to compare results.

4.2.2 Test setup

All turning experiments were carried out at Chalmers Lindholmen in a SOMAB Optimab 400 CNC lathe under orthogonal, dry, cutting conditions using ceramic inserts (see table 4) in a Sandvik Coromant LF150.23-3244M-0635C tool holder also (partly) seen in figure 13.

Table 4: General information about the inserts from Greenleaf which were used in the experiments. WG-300 is an Alumina-SiC whiskers reinforced material.

Part nr.	Material	Length [mm]	Width [mm]	Thickness [mm]	Corner radius [mm]	Clearance angle
WG-6218-2A	WG-300	19.05	5.54	6.35	0.79	11°
WG-6250-2A	WG-300	19.05	6.35	6.35	0.79	11°

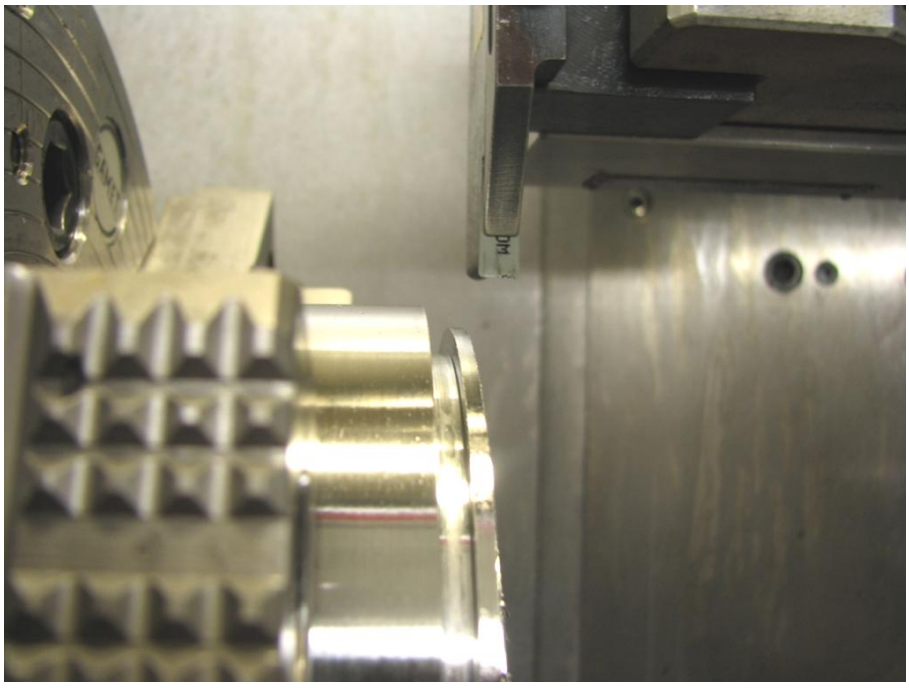

Figure 13: Experimental setup showing the insert and the workpiece with flange.

Care was taken in order to not have any nose radius effects by machining out a 2 mm wide flange (see figure 13) and making sure that the flange was placed on the tool edge a distance from the nose radius (see figure 14). The feed was kept constant at 0.1 mm/rev for all tests.

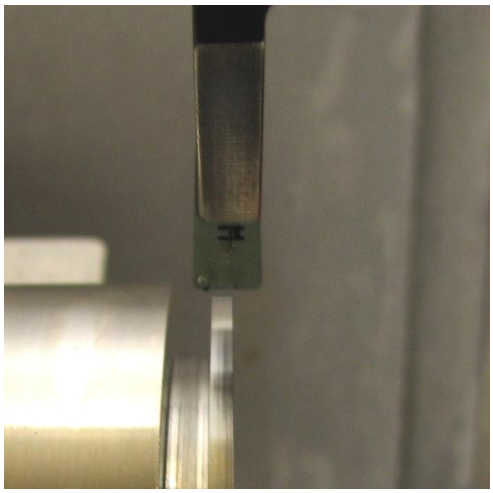

Figure 14: Placement of the flange on the tool edge.

Forces were recorded for each test using a Kistler Type 9121 3-component tool holder dynamometer and Kistler multichannel charge amplifier Type 5019A (see figure 15) connected to a computer running DASYLab software to record the forces in order to evaluate if stable cutting conditions were achieved.

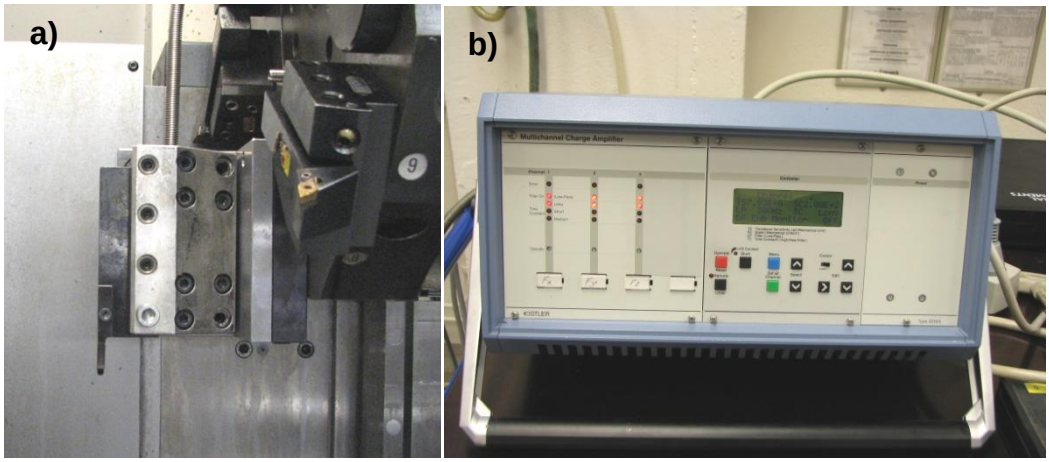

Figure 15: a) Tool mounted in the Kistler dynamometer. b) The charge amplifier used for the experiments.

To get reliable results, the experiments were carried out in a random order with respect to cutting speed. For each cutting speed two repetitions (also randomized) were carried out for each of the four materials tested (see table 5) and the chips were collected by placing a plastic tray inside the lathe, below the workpiece.

Table 5: Test variables for the turning experiments

Material	Cutting speeds [m/min]	Depth of cut [mm]	Feed [mm/rev]	Number of runs per cutting speed	Total number of runs
Large grains, not hardened	30, 60, 120, 240 and 480	2	0.1	3	15
Large grains, hardened	30, 60, 120, 240 and 480	2	0.1	3	15
Small grains, not hardened	30, 60, 120, 240 and 480	2	0.1	3	15
Small grains, hardened	30, 60, 120, 240 and 480	2	0.1	3	15

Between each test, the flange was machined down ("clean-up cut") using separate inserts and a constant cutting speed. This was made to make sure that each test would have similar entry conditions when cutting into the material and to minimize the effect of the differences in the deformed layer produced by the previous machining pass as much as possible, considering that the previous cutting speed was random.

When creating the program for this experiment, care was taken to have a quick exiting (G0) of the material at the end of the cut to avoid affecting the later contact length measurements. The "clean-up" step was also added where a certain thickness of material was removed from the flange and a preset hold time at the end of cut diameter made sure that subsequent experimental runs would have a gradual entry into the material.

The experimental procedure can be summarized as following (in chronological order):

1. Choose a material, place it in the chuck of the lathe and machine out a 2 mm flange with a separate grooving insert.
2. Switch tool holder to the one selected for the experiment.
3. Perform a "Clean-up cut" using separate insert.
4. Change to an unused cutting edge.
5. Insert cutting parameters (cutting speed) into the program and also the start and finish diameter.
6. Reset the charge amplifier and start recording.
7. Start program.
8. When program has finished – stop recording, collect chips, take overview photographs, bag and tag chips and insert.
9. Repeat from step 3, without releasing the workpiece from the chuck, until all tests are done for the chosen material.

5 Analysis methods

The methods used in the analysis of the experiments will be discussed below. The main part of the analysis was a metallographic investigation of the chips produced in the turning experiments. This was done in order to be able to map the differences in deformation behavior over a range of cutting speeds and for different material states.

The inserts used in the turning experiments were investigated in a stereomicroscope to complement the metallographic investigation of the chips. Macroscopic images of the chips and workpieces were also taken.

5.1 Metallographic investigation of chips

After each turning experiment the chips produced were collected, placed in plastic bags that were marked with material, cutting speed, test number and which insert that had been used. Chips from one out of the three tests performed for every material and cutting speed was selected for metallographic investigation. These chips were then mounted in plastic, ground, polished and etched to reveal the microstructure of the chips.

5.1.1 Mounting

The chips were cut with pliers into roughly 1 cm long pieces. The pieces were cut from the chip close to the end but still a distance from the very end to avoid getting chip samples from a part of the chip where non-stable cutting conditions could be expected due to the quick removal of the insert at the end of the cutting cycle (see the section on the test setup for more details on the cutting cycle).

The cut pieces were cleaned in an ultrasonic cleaner in a bath of ethanol to remove any residue and promote good adhesion to the mounting plastic. After they were cleaned the pieces were put into plastic clips as seen in figure 16a. Care was taken to mount the chip in the clip so that the surface that would be revealed after the grinding and polishing steps would be a true longitudinal cross section and not a cross section at an angle. It should be noted that an absolute precision in this technique is impossible but that due to the length of the chip piece and thanks to the nearly straight chip formed using orthogonal cutting, the cross sections produced are very close to longitudinal cross sections.

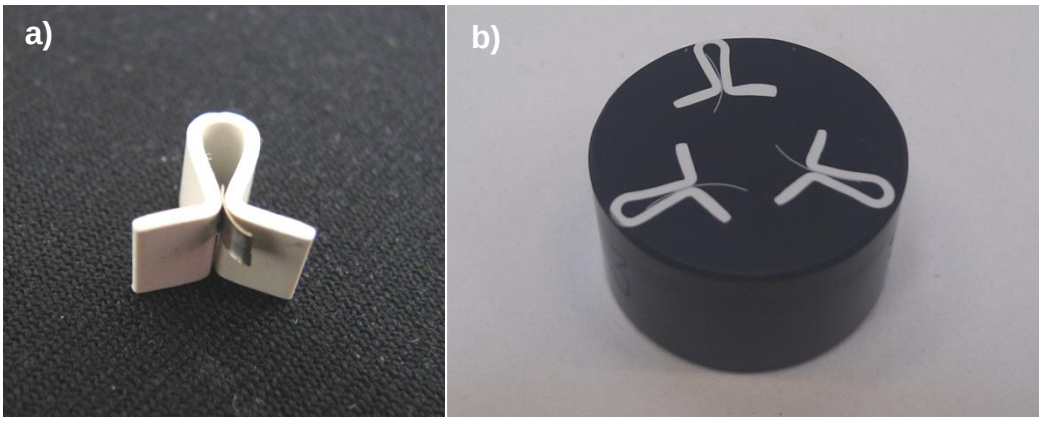

Figure 16: a) Chip in plastic clip. b) Three clips in a mount.

Three plastic clips, each holding a chip piece were then put into a Struers CitoPress-20 hot mounting machine and mounted in Struers DuroFast mounting material (epoxy with mineral filler). The resulting mounts can be seen in figure 16b. The parameters used in the mounting process are summarized in table 6. The mounts produced were measured with a caliper rule after mounting and every subsequent grinding step to make it possible to produce cross sections approximately in the middle of the samples and avoid getting to close to the chip edges.

Table 6: Mounting parameters used.

Material	Struers Durofast (Epoxy + Mineral filler)
Temperature	180 °C
Heating time	7 min
Cooling time	3 min
Pressure	350 bar
Amount of resin	Fine powder to cover the samples + 15 ml of coarser material

5.1.2 Grinding and polishing

The mounts produced were ground and polished in six steps, three grinding steps and three polishing steps. The steps, along with the approximate thickness removed from the mounts in every step, are summarized in table 7 and table 8. The machine used to grind and polish the mounts was a Struers TegraPol-31 with a Struers TegraForce-5 sample mover. After every step the mounts were cleaned in a soap solution to remove particles from previous steps. Before and after the polishing steps an ultrasonic cleaning in ethanol was added after the soap solution to make completely sure no residue was left from the previous step.

Table 7: Grinding parameters used in the sample preparation. All grinding papers used SiC abrasives.

Grit	Time	Force	Rotation	Removed thickness
240	60 s	25 N	300/150 rpm	Ca 0.5 mm
600	60 s	25 N	300/150 rpm	Ca 0.2 mm
1000	60 s	25 N	300/150 rpm	Ca 0.1 mm

Table 8: Polishing parameters used in the sample preparation. Cloths are all brands of Struers A/S.

Particle size	Time	Force	Rotation	Cloth
9 µm	3 min	30 N	150/150 rpm	Allegro
3 µm	2 min	20 N	150/150 rpm	Mol
1 µm	1 min	15 N	150/150 rpm	Nap

The described grinding and polishing process produced surfaces free of scratches.

5.1.3 Etching

A couple of different etchants were tested to find how to best reveal the microstructure in general and the deformation pattern in the chip cross sections. Similar samples have previously been etched in an electrolytic etching process with an etchant containing 50% Methanol and 50% HCl with a voltage of 3V for a couple of seconds [3], [4]. In this work however it was found that a waterless Kalling's etchant that was swabbed on the surfaces gave a better result with less variation as the etching times used were longer. The contents of the waterless Kalling's etchant were 87 ml HCL (37%), 100 ml ethanol and 5 g $CuCl_2$.

Because the different materials did not all etch in the same way, different times had to be used for the four material states to achieve good results. A summary of the times used for the different material states can be seen in table 9. No time or concentration variation was used between different cutting speed samples.

Table 9: Etching times used for different materials.

Large grains, not hardened	45 s
Large grains, hardened	15 s
Small grains, not hardened	20 s
Small grains, hardened	15 s

The etching procedure was performed on one chip only in every mount by selective swabbing with a stick with a small cotton tip. This was done in order to be able to use other etchants in the future in case deemed necessary or in case of bad etching results that could imply that a shorter or longer etching time should be used.

It should be noted that not too much time should pass between the last polishing step, the etching and the examination in the microscope as oxidation of the material makes the finer details blurry and also gives a discoloration of the surface after etching.

5.1.4 Microscopic evaluation of longitudinal cross sections

In order to observe and photograph the deformed microstructure of the chips, light optical microscopy (LOM) was used throughout this work. Images of the chips longitudinal cross sections were captured with a Leica Leitz DMRX microscope using the Carl Zeiss Axiovision software and a Zeiss AxioCam MRc 5 camera.

Three objectives (see table 10) with magnifications 20, 50 and 100 times where used in order to provide both an overview of a longer section of the chips and a more detailed view of the microstructure and deformation patterns.

Table 10: Objectives used during the microscopic evaluation.

Manufacturer	Magnification	Type	Numerical aperture
Leitz Wetzlar Germany	20x	Pl Fluotar	0.45
Leitz Wetzlar Germany	50x	Pl Fluotar	0.85
Leitz Wetzlar Germany	100x	Pl Fluotar	0.90

Bright field (BF) as well as Dark field (DF) and Interference Contrast (ICR) techniques where evaluated and led to the selection of BF as the main method to be used, as the other techniques either provided no additional information (DF) or distorted color reproduction (ICR), making identification of carbides, nitrides and δ-phase more difficult (see figure 17).

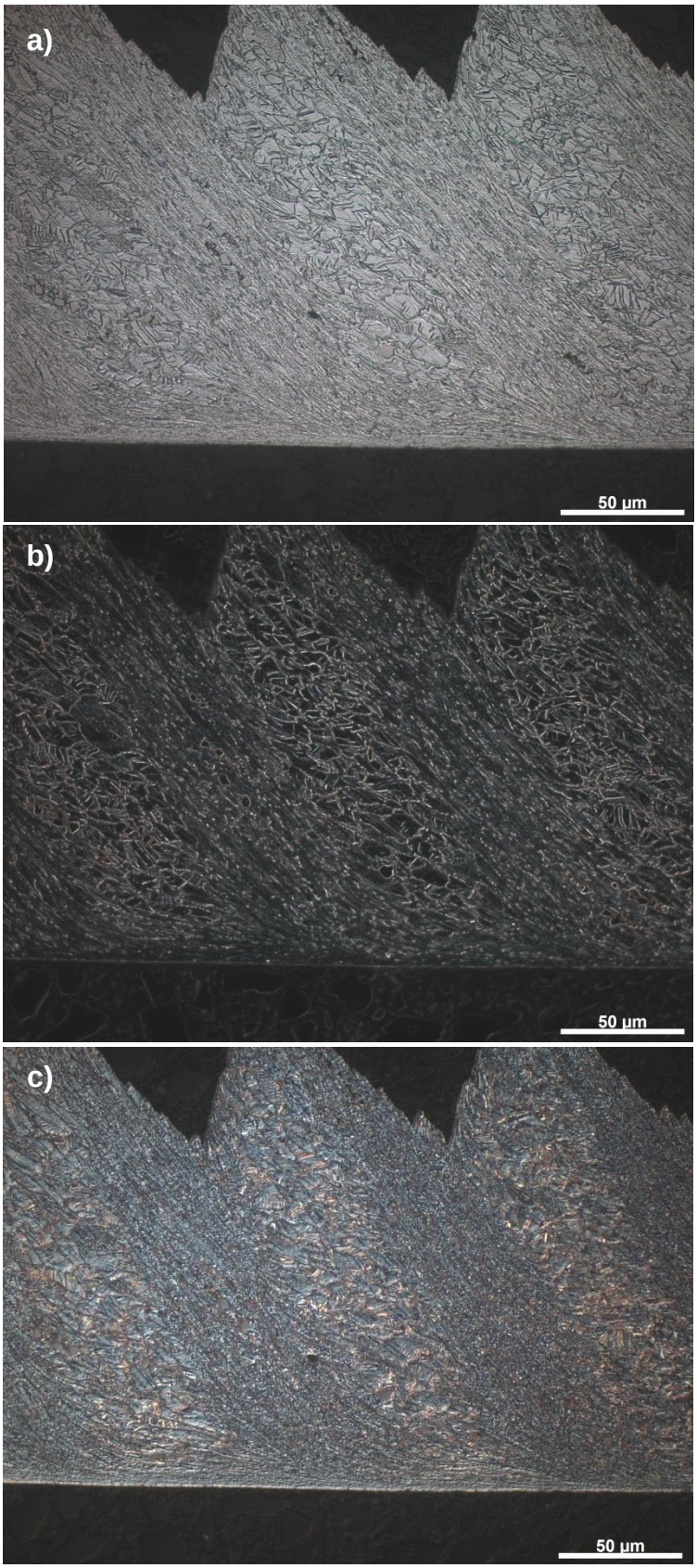

Figure 17: Example of differences between microscopy techniques. a) Bright field b) Dark field c) Polarized light (ICR).

In order to reveal the grains better, the aperture was deliberately put out of alignment to produce a relief effect which also made it easier to spot localized deformation areas as these where perceived as a height difference.

5.1.5 Chip dimension measurements

The focus in this work has been on getting a broad visual overview of the deformation patterns formed in chips and as a consequence less work has been put into statistical measurements of chip dimensions. The measurements taken are to be seen as rough estimates to see trends more than an extensive quantification of the chip dimensions produced. Because of this, if it is clear from the micrographs that the variation of some dimension is large it has not been measured at all.

With this said some chip dimensions have been measured in the micrographs in the software AxioVision by Carl Zeiss and the methodology will be explained below.

Segment width

Segment width was measured for the small grained materials for cutting speeds from 120 m/min to 480 m/min. The large grained materials showed too high variation to be accurately measured easily while the chips produced at lower speeds showed no segmentation. Figure 18 shows an example of how the measurements were taken. An average was calculated and the difference between the average and the highest and lowest value was recorded.

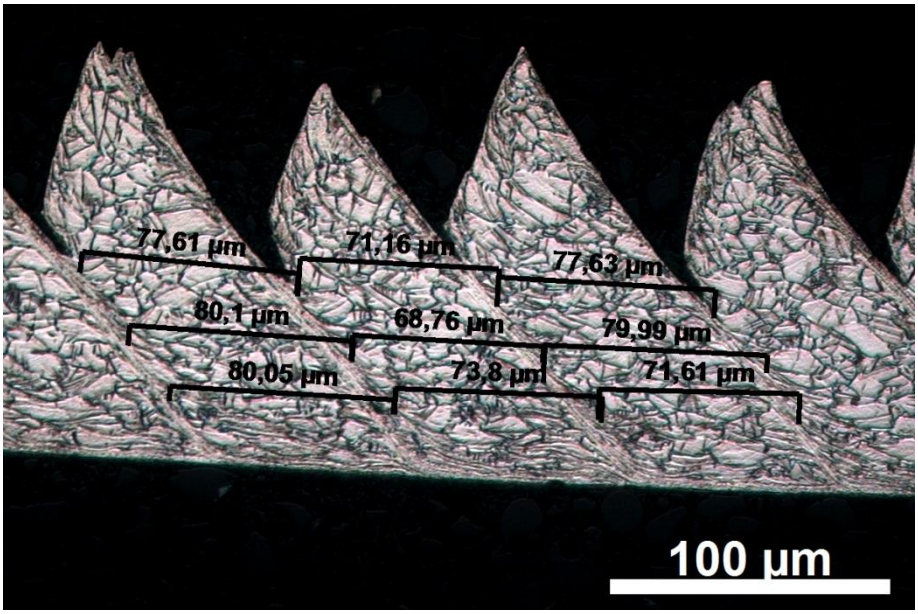

Figure 18: Segment width measurements.

Localized shear zone

The width of the localized shear zone was measured in chips from the small grained materials at speeds between 120 m/min and 480 m/min. No segmentation was shown at lower speeds. Large grained materials showed a highly irregular localization pattern making it impossible to measure band width in an easy way. Figure 19 shows how the band width was measured. An average was calculated and the difference between the average and the highest and lowest value was recorded.

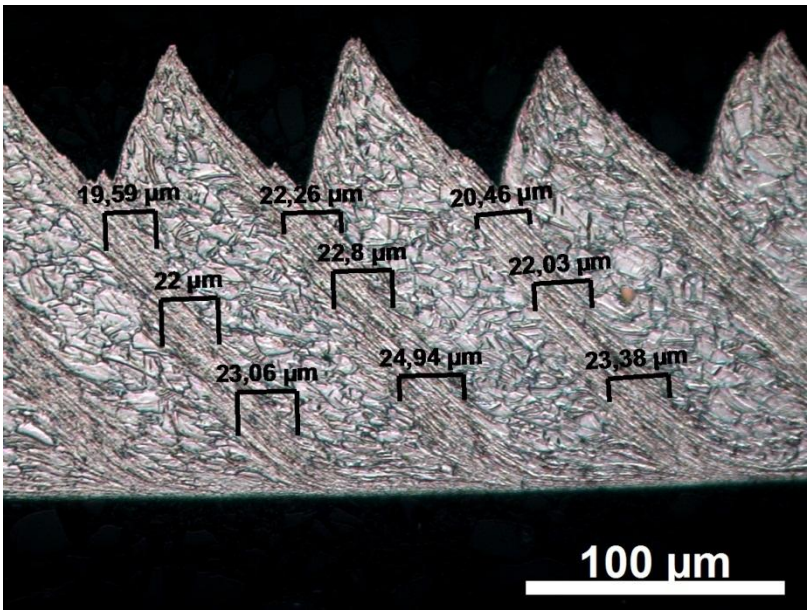

Figure 19: Localized shear zone width measurements.

Chip thickness

Chip thickness was measured for all speeds in the small grained materials. The large grained materials showed too much variation for an accurate average to be measured. The chip thickness was measured in six points taken at random in case of continuous chips and as three peaks and three valleys for segmented chips. In all cases an average was calculated. Figure 20 shows how the thickness was measured in a segmented chip.

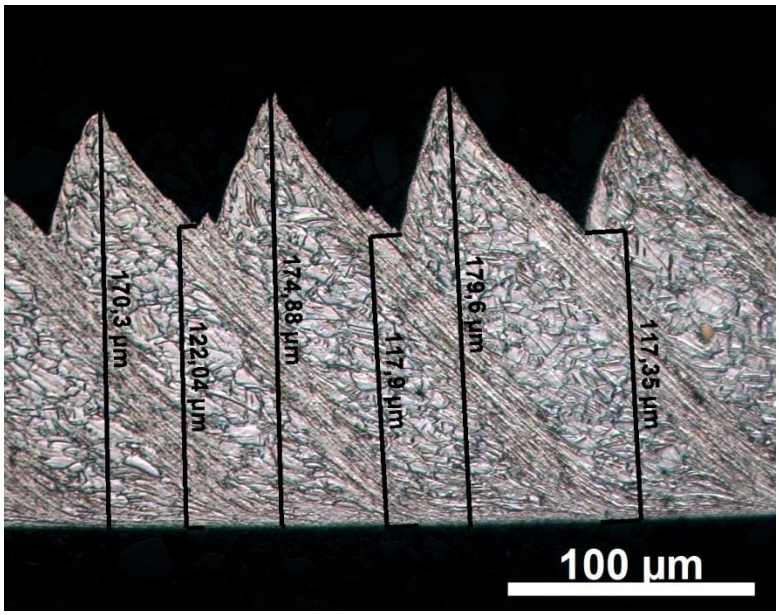

Figure 20: Chip thickness measurements.

Chip width

Chip width was measured from chip macrographs taken in a stereomicroscope (see 5.2.2 Stereomicroscopic investigation of chips). As the chip macrostructure in large grained materials varied too much to be even remotely accurately quantified with three width measurements (see figure 21) it was not measured at all.

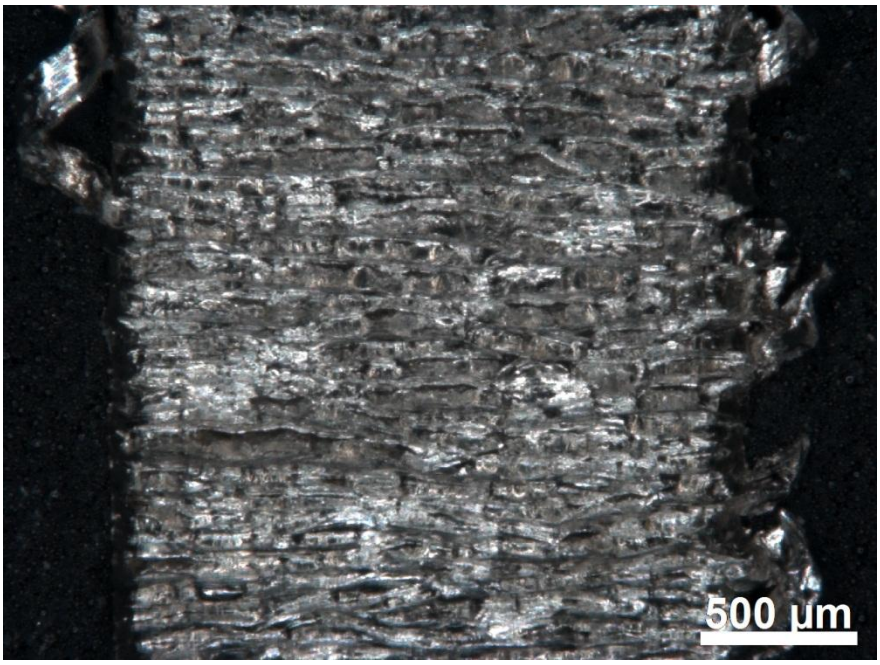

Figure 21: Large variation in chip widening in large grained hardened material.

Figure 22 shows how the measurements were taken. Average values as well as the highest and lowest value for each speed were recorded and the initial width of 2000 µm was subtracted from all values to get the chip widening.

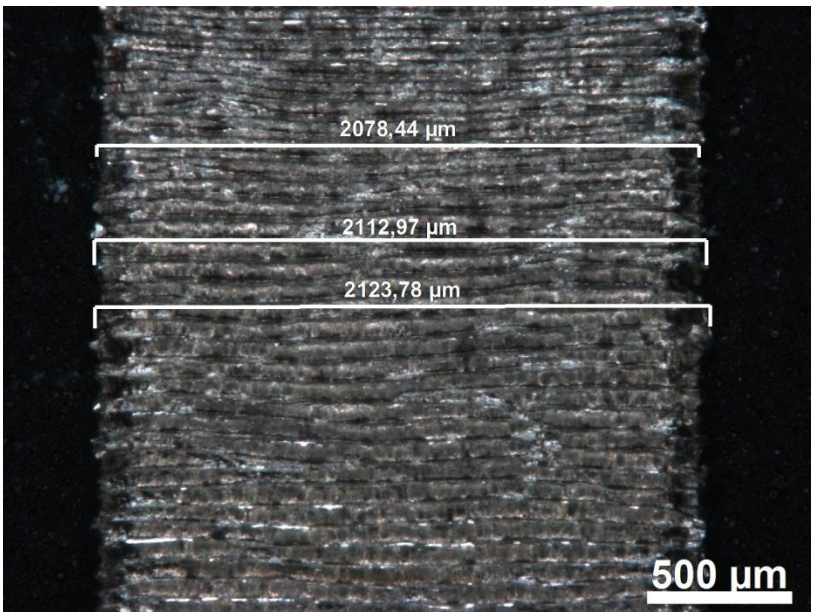

Figure 22: Chip width measurements.

5.2 Macroscopic evaluation of chips

The macroscopic examination of the chips was performed by ordinary photography of the chips and stereomicroscopic inspection of cut chip samples as described below.

5.2.1 Overview photographs

All chips were photographed with a Canon Powershot S3 IS that was mounted on a stand to make it possible to reduce vibrations and give constant distances between camera and chip. This was done to be able to document the general shape of the chips to find macroscopic discrepancies between different tests with the same material and speed.

5.2.2 Stereomicroscopic investigation of chips

Pieces similar to the ones mounted for the metallographic investigation were also studied in a stereomicroscope to reveal patterns on a macroscopic scale regarding segmentation and also the final chip width. The rough side of a piece of the same chip used in the metallographic investigation was documented in this way for every material and cutting speed used in a Zeiss Discovery V.20 stereomicroscope. Two magnifications were used, one to show the complete chip width and a larger one to make it easier to see the segmentation pattern.

5.3 Tool wear evaluation

The aim of this work is not to evaluate tool wear and the experiments are not designed for that purpose. It is however interesting to evaluate the tool wear to see if the wear is similar between tests in the same material and speed. It is also interesting to see the contact lengths in order to relate contact length and cutting force.

To evaluate tool wear the rake face of all inserts used in the turning experiments were investigated in a Zeiss Discovery V.20 stereomicroscope. The contact lengths were measured with the help of the AxioVision software. Three measurements were done in the left, in the center and in right part of the contact width and the mean values were recorded. This was done by two persons giving six datapoints in total. In some cases the contact length showed a dark and a light zone in which case both zones were measured giving a total of twelve datapoints. Figure 23 shows an example of measurements taken by one person for both a single zone contact length and a two zone contact length.

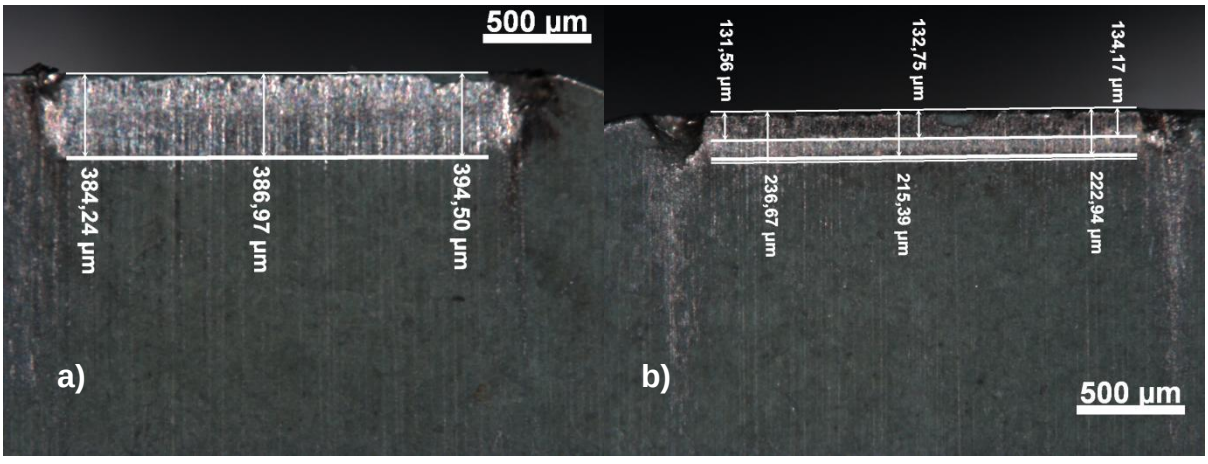

Figure 23: Examples of measurements of contact lengths. a) Only one zone visible b) Two distinct zones.

5.4 Force evaluation

The cutting force measurements taken during the turning tests were analyzed in a software called DASYLab in which it was possible to define an interval and get the average value in that interval. An interval at the end of each test where stable cutting forces could be seen was selected by three persons giving a total of nine data points for every cutting speed and material combination. A mean value was calculated from these data points as well as the difference between the mean value and the largest/smallest data point. This was done for both the main force component and for the feed component.

6 Results

This section presents the results of the experiments as explained in chapter 5 Analysis methods. No interpretations are given but interesting results are highlighted and further discussed in chapter 7. Some of the results have been moved to appendices and can be found at the end of the report.

6.1 Chip microstructures

Figure 24, figure 25 and figure 26 show the chip microstructures in increasing magnification. All figures have increasing cutting speed in columns (30, 60, 120, 240 and 480 m/min) and the different material conditions in the rows starting with large grains not hardened (LGS) in the first row, large grains hardened (LGH) in the second row, small grains not hardened (SGS) in the third row and small grains hardened (SGH) in the last row.

The micrographs in figure 24, figure 25 and figure 26 can be seen in a larger format in appendix A.

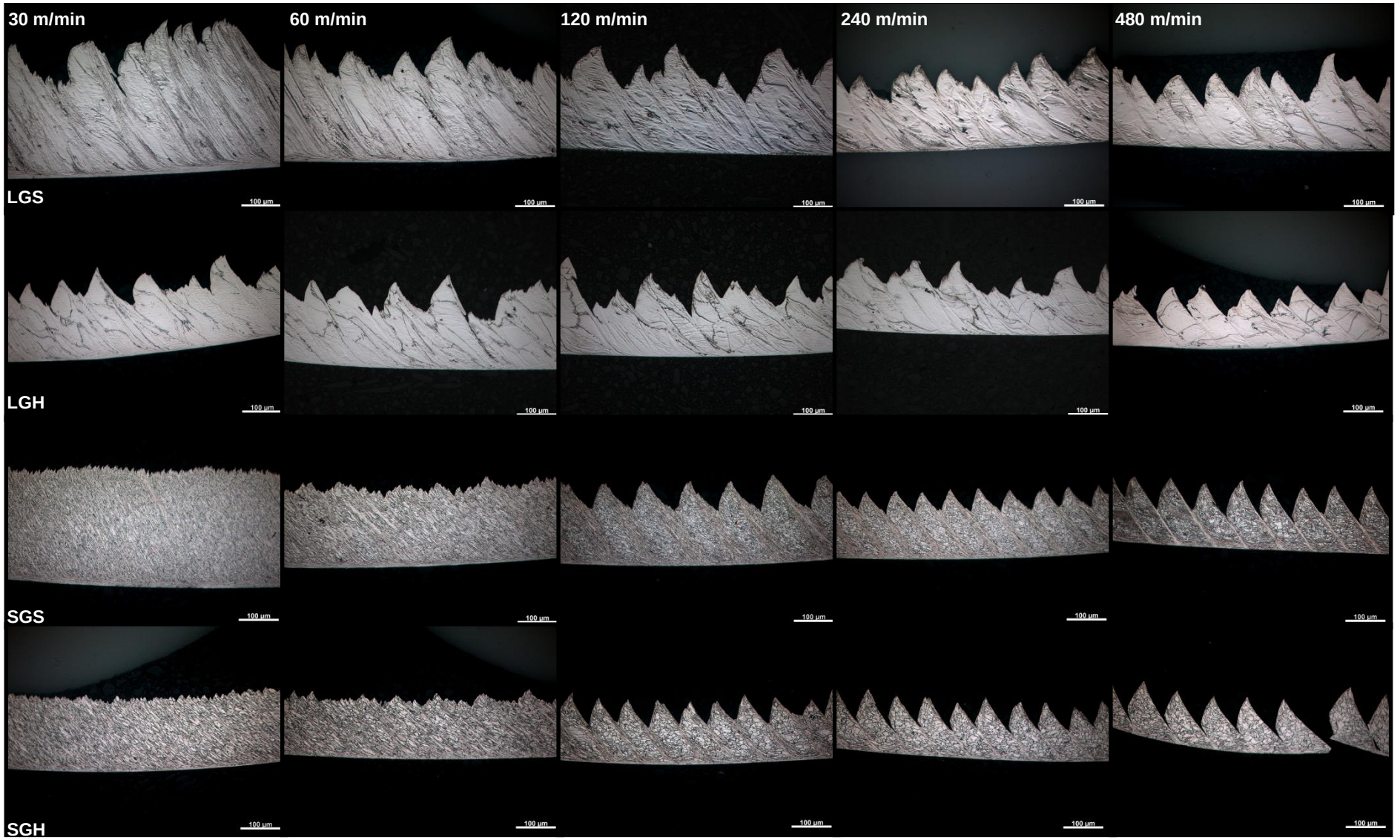

Figure 24: Low magnification of chip microstructures. Rows are from top to bottom: Large grains not hardened, Large grains hardened, Small grains not hardened, Small grains hardened. Columns are from left to right: V_c = 30 m/min, 60 m/min, 120 m/min, 240 m/min and 480 m/min. Scale bars are 100 µm.

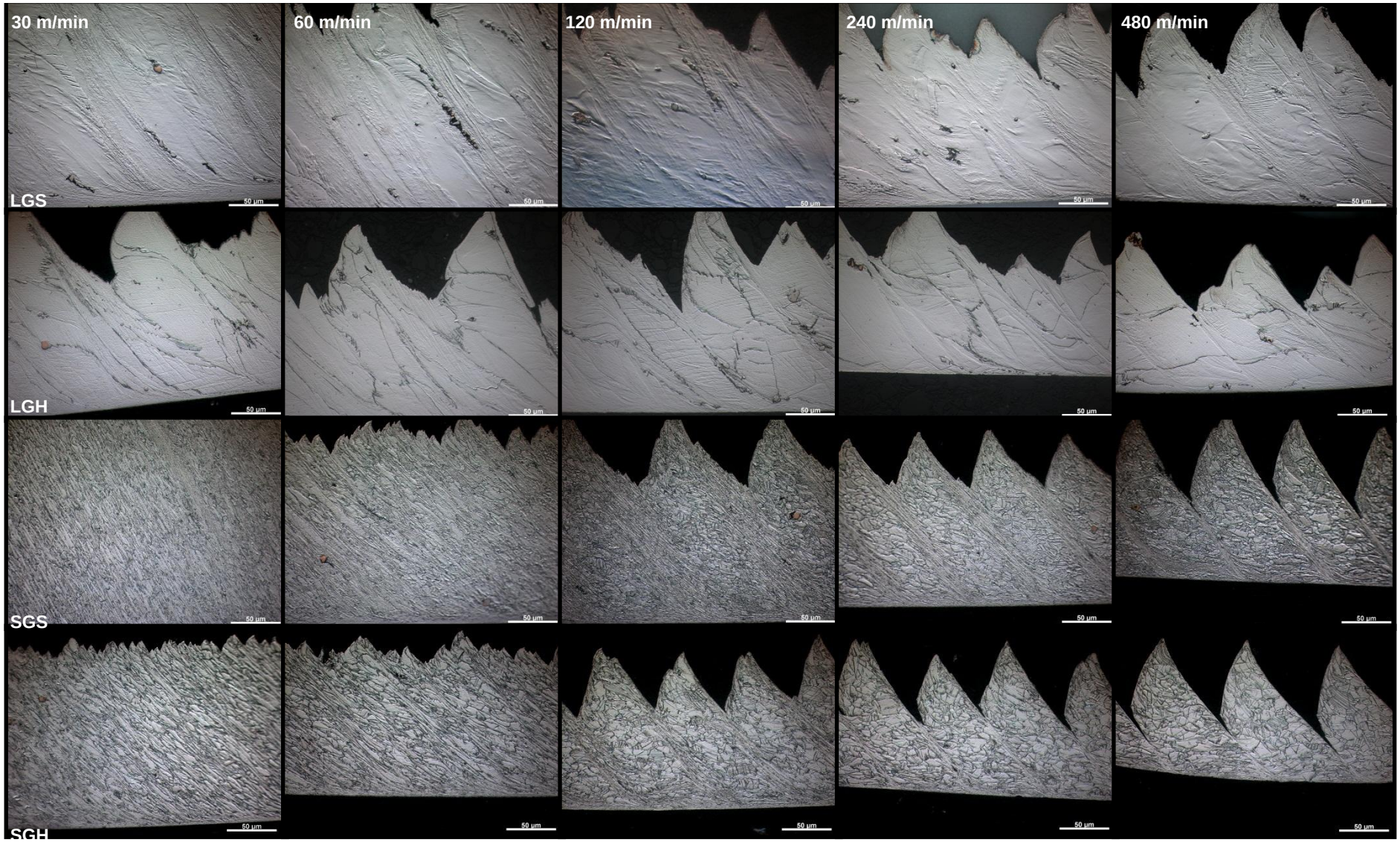

Figure 25: Medium magnification of chip microstructures. Rows are from top to bottom: Large grains not hardened, Large grains hardened, Small grains not hardened, Small grains hardened. Columns are from left to right: V_c = 30 m/min, 60 m/min, 120 m/min, 240 m/min and 480 m/min. Scale bars are 50 µm.

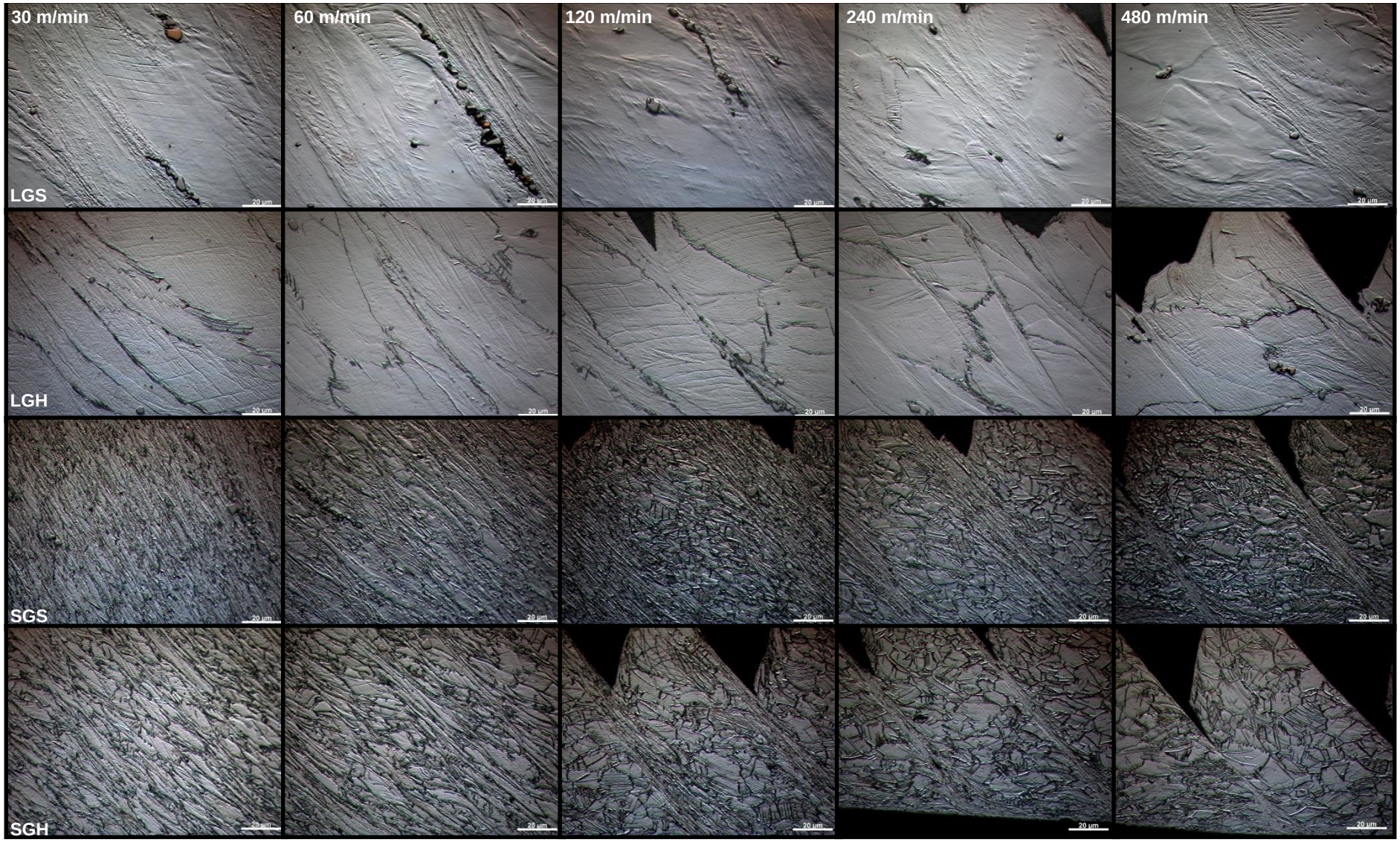

Figure 26: High magnification of chip microstructures. Rows are from top to bottom: Large grains not hardened, Large grains hardened, Small grains not hardened, Small grains hardened. Columns are from left to right: V_c = 30 m/min, 60 m/min, 120 m/min, 240 m/min and 480 m/min. Scale bars are 20 µm.

Some observations will be listed below together with figures highlighting the observations where they are not obvious in figure 24, figure 25 and figure 26.

1. The chips tend to get thinner when the cutting speed is increased.
2. In both small grained material conditions a transition from continuous chips to segmented chips occur somewhere between 60 and 120 m/min.
3. The width of the zone where localized shear takes place is reduced as the cutting speed is increased in the small grained materials (see figure 27).

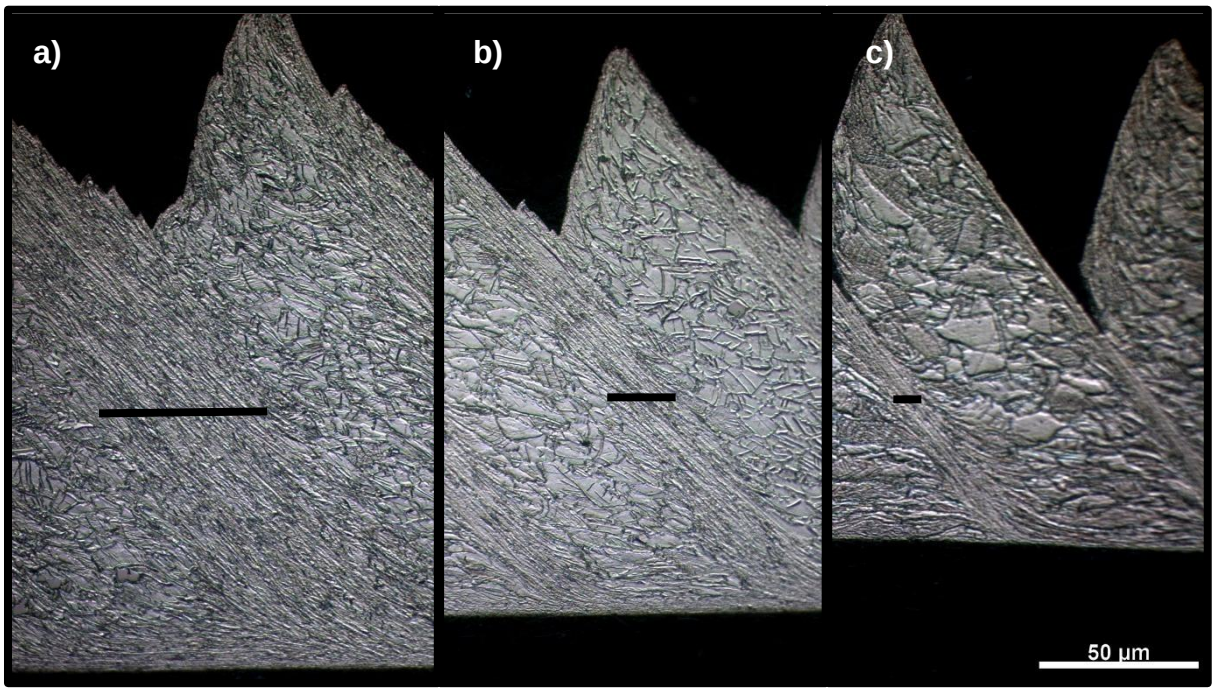

Figure 27: The width of the localized shear zone is decreased as cutting speed is increased. Small grained not hardened material with cutting speeds according to a) 120 m/min b) 240 m/min c) 480 m/min. Same scale in all three figures. The width of the zone is indicated by the lines.

4. The width of the localized shear zone is smaller in the hardened material than in the not hardened material (see figure 28).

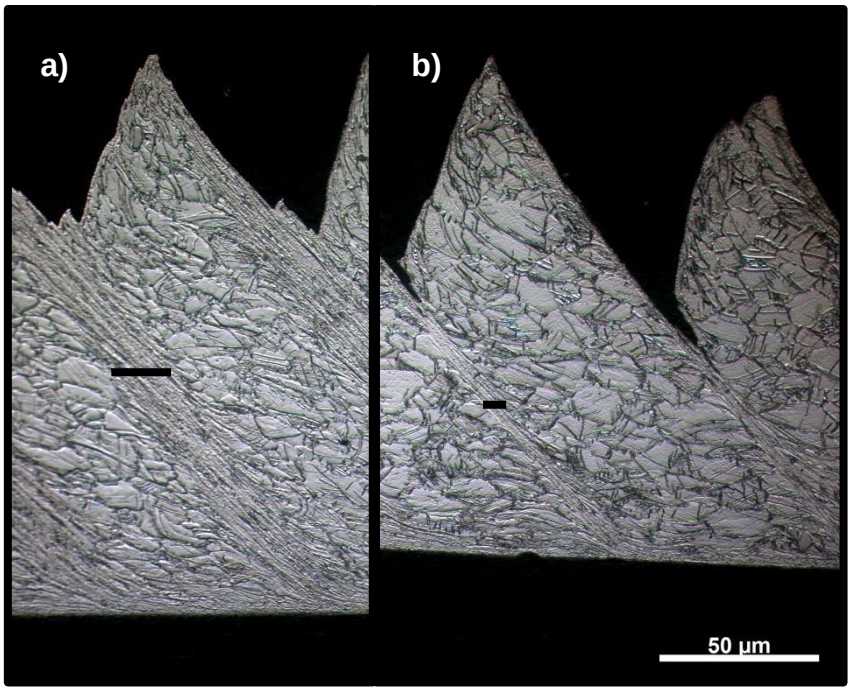

Figure 28: Difference in localized shear band with in different materials. a) Small grained not hardened material b) small grained hardened material. Cutting speed 240 m/min in both cases. Same scale in both figures. The width of the zone is indicated by the lines.

5. The area between two localized shear zones in the small grained materials tend to have more or less equiaxed grains meaning that almost no deformation has taken place there (see figure 29).

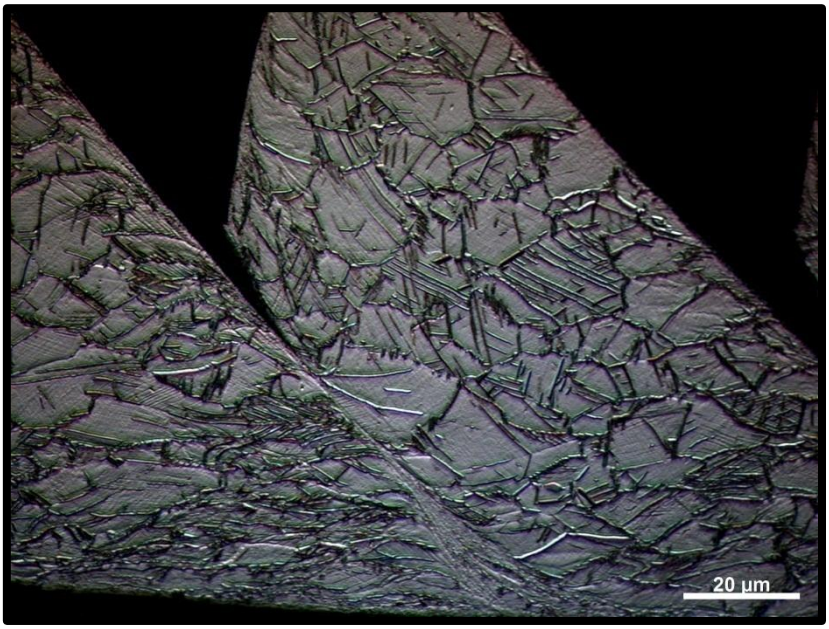

Figure 29: The area between the localized shear zones is more or less undeformed. Small grained material hardened, cutting speed 480 m/min.

6. The large grained, hardened material shows localized deformation within the grains (see figure 30).

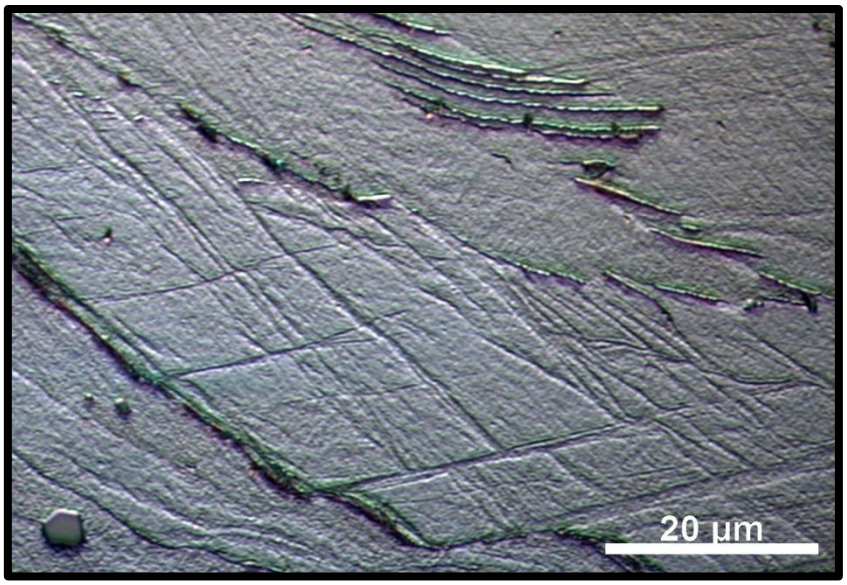

Figure 30: Localized shear in different directions within a grain. Large grained, hardened material, cutting speed 30 m/min.

7. The large grained materials show a serrated chip at all cutting speeds.
8. Carbides are often found within localized shear zones in the large grained not hardened material (see figure 31).

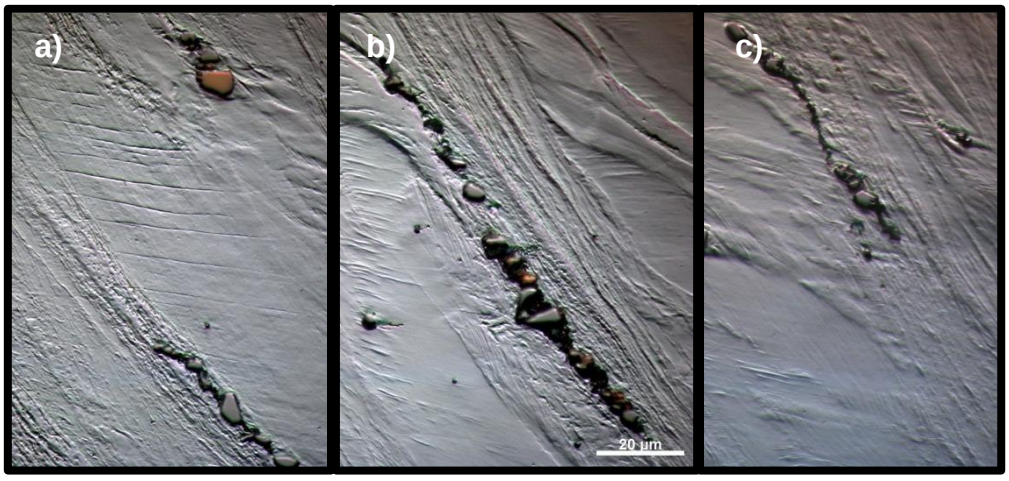

Figure 31: Carbides ordered in bands within localized shear zones in large grained not hardened material. Cutting speed is a) 30 m/min b) 60 m/min c) 120 m/min. Same scale in all figures.

9. The large grained, not hardened material seems to show an increased ordering of the serration into more equally spaced localizations at higher cutting speeds.
10. The deformation pattern in the small grained materials is much more organized than in the large grained materials.

6.2 Chip macrostructure

Figure 32 and figure 33 shows the serrated side of the chips as seen in a stereomicroscope.

An observation from the figures is that the segmentation in small grained materials at high speeds seems to go through the whole width of the chips whereas in the large grained materials no ordered segmentation can be seen.

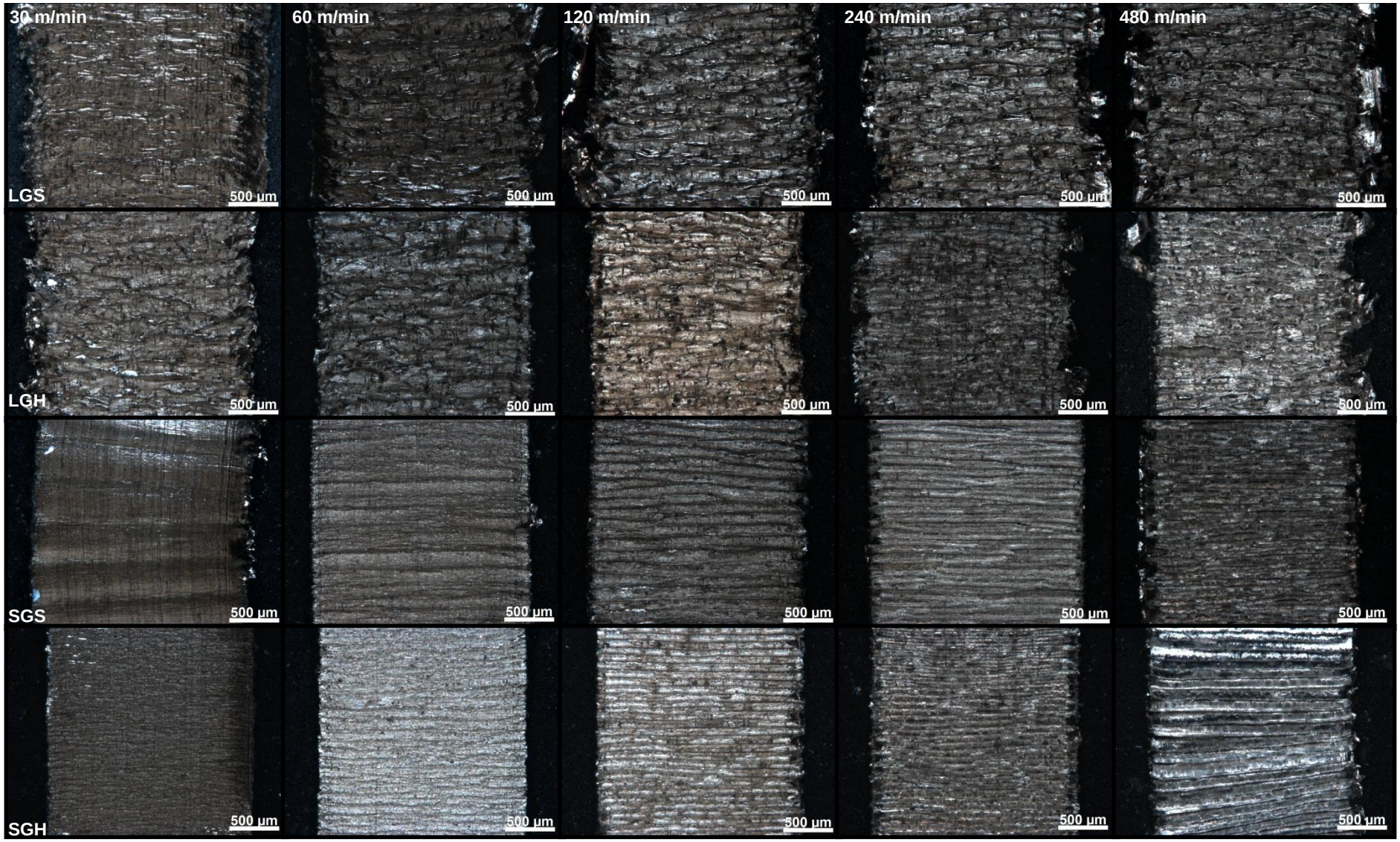

Figure 32 Low magnification of chip macro deformation pattern. Rows are from top to bottom: Large grains not hardened, Large grains hardened, Small grains not hardened, Small grains hardened. Columns are from left to right: V_c = 30 m/min, 60 m/min, 120 m/min, 240 m/min and 480 m/min. Scale bars are 500 µm.

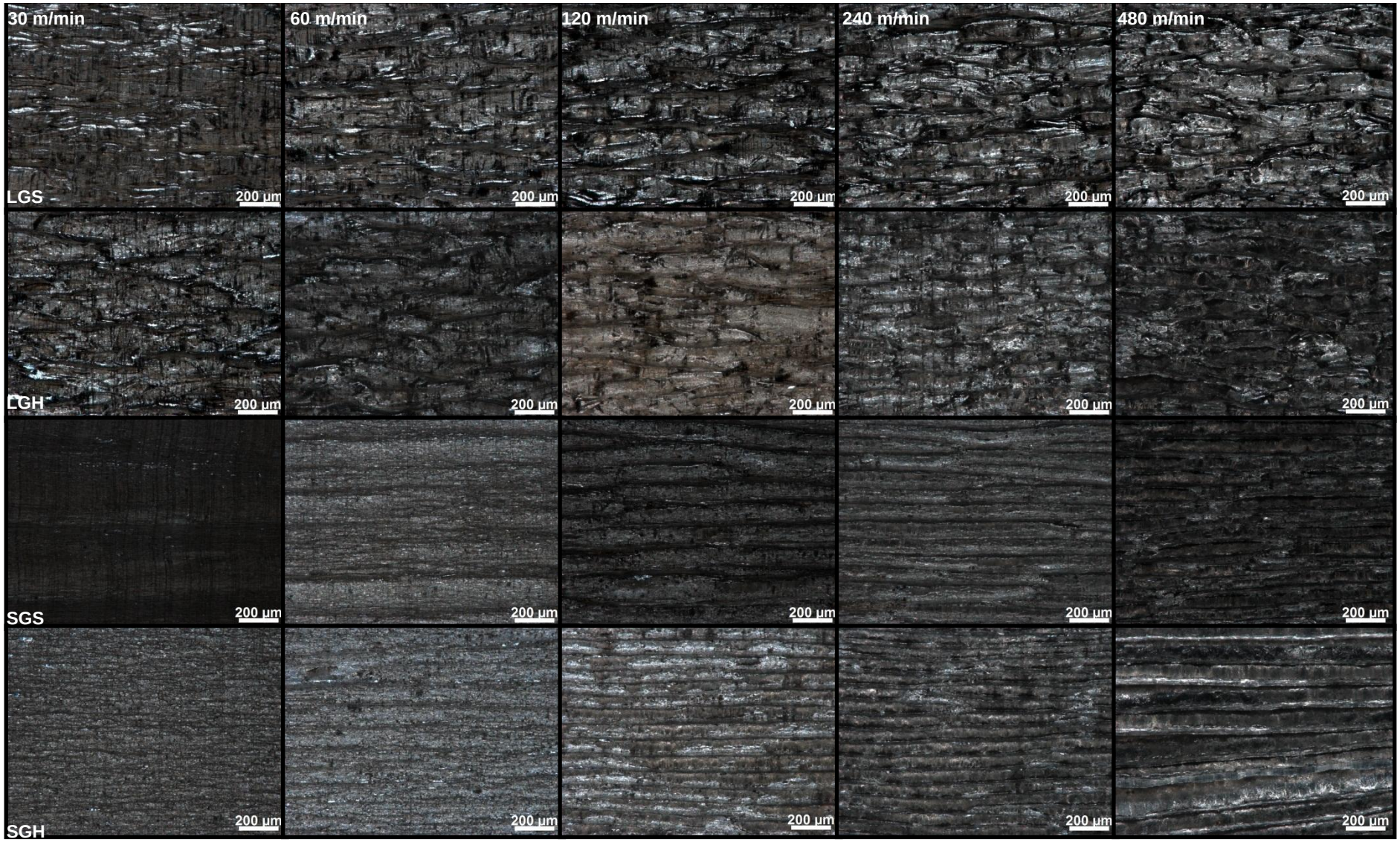

Figure 33 High magnification of chip macro deformation pattern. Rows are from top to bottom: Large grains not hardened, Large grains hardened, Small grains not hardened, Small grains hardened. Columns are from left to right: V_c = 30 m/min, 60 m/min, 120 m/min, 240 m/min and 480 m/min. Scale bars are 200 µm.

6.3 Chip dimensions

Chip dimensions will be presented below.

6.3.1 Segment width

The segment width is given in figure 34. The measurements show no relevant difference between either materials or cutting speeds.

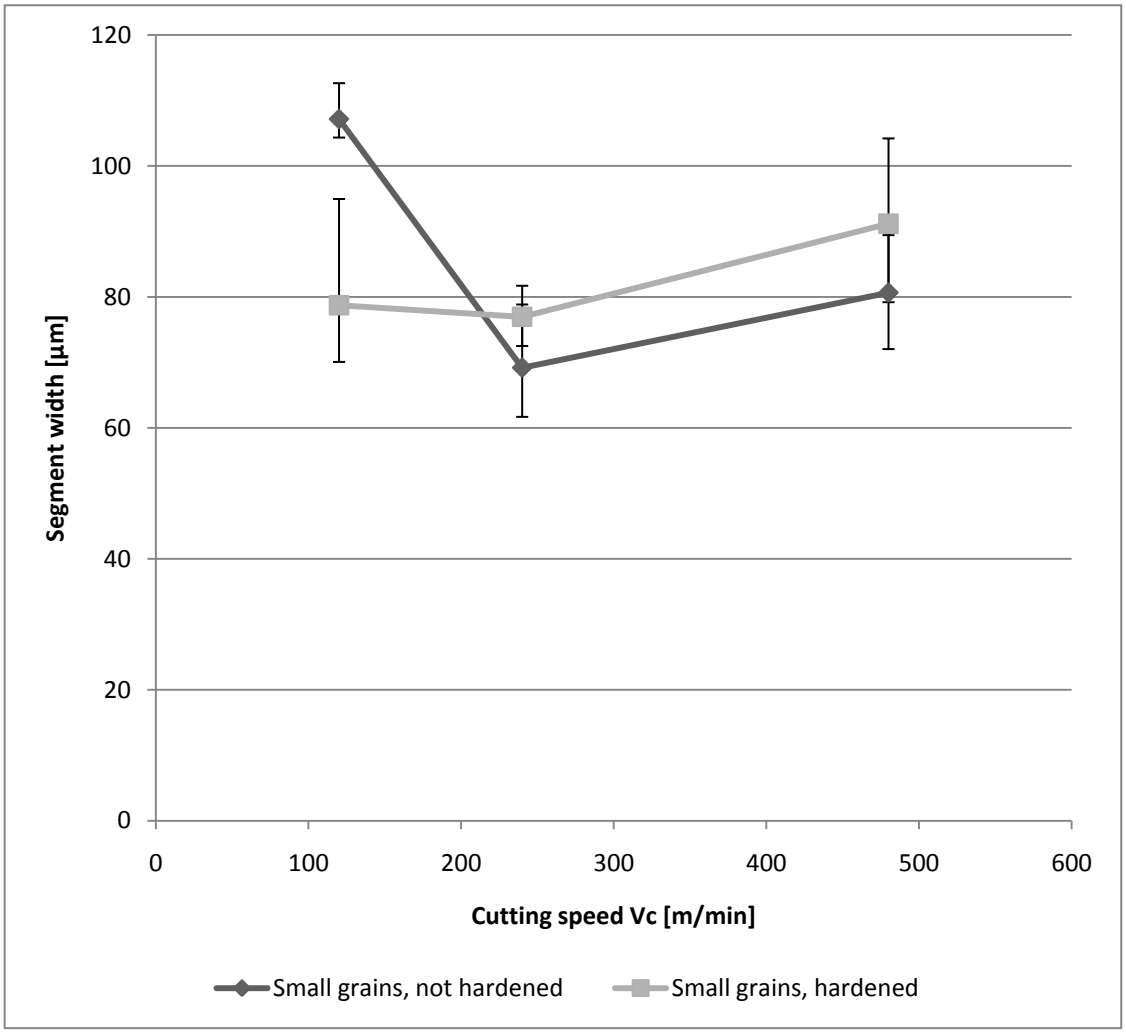

Figure 34: Segment width. Error bars show distance to highest/lowest value measured.

6.3.2 Localized shear zone width

Figure 35 shows the width of the localized shear zone. It is clear from the measurements that the width of the localized shear zone decreases with increased cutting speed. It is also clear that the width of the zone is larger for the not hardened material than for the hardened material.

It should be noted that the not hardened material shows a value approximately three times larger than the hardened material for all cutting speeds.

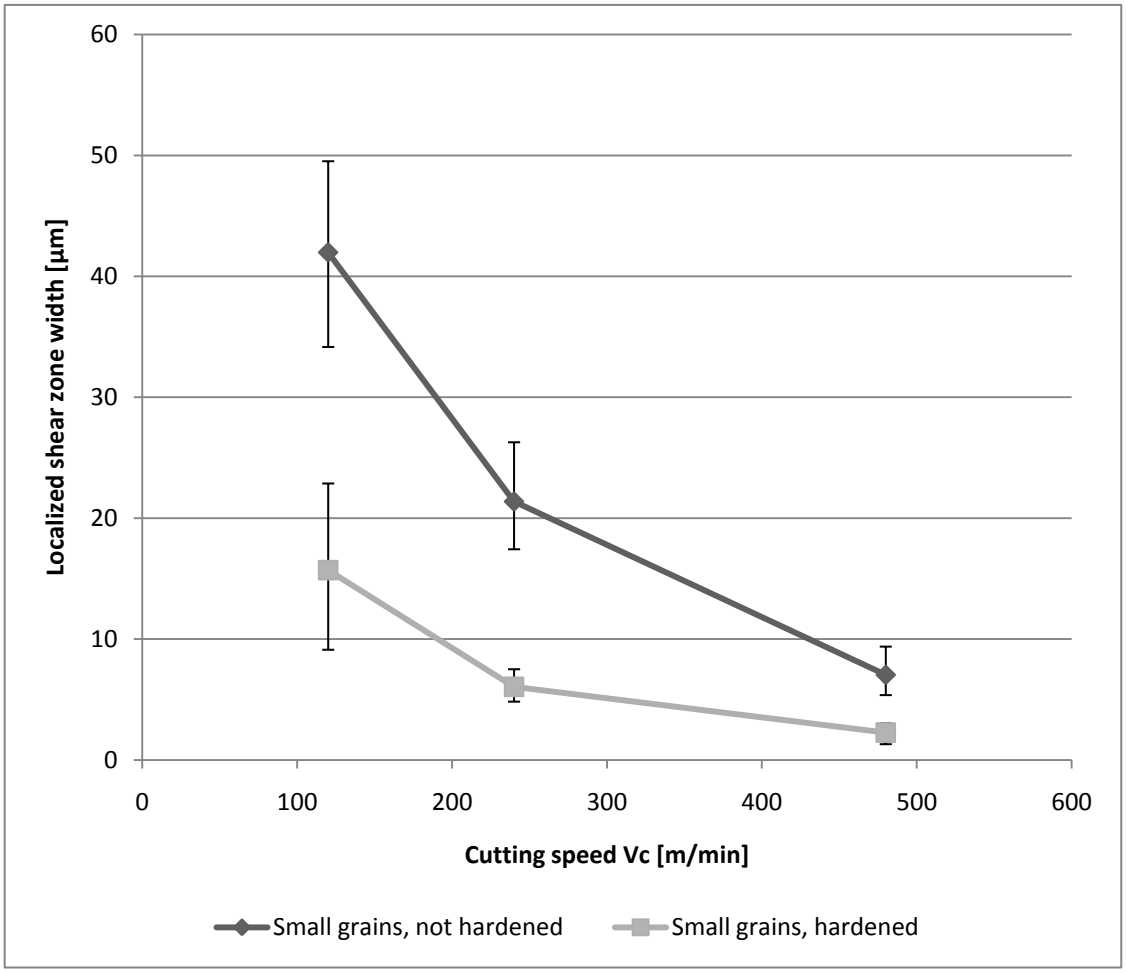

Figure 35: Localized shear zone width. Error bars show distance to highest/lowest value measured.

6.3.3 Chip thickness

Figure 36 shows chip thickness measurements. It should be noted that the chips produced at 30 and 60 m/min have a continuous form with little or no local variation in thickness while the chips produced at speeds from 120 to 480 m/min are segmented and show a hill and valley profile. The figure shows mean values of hill and valley measurements.

Observations from the measurements are that the chips get thinner as the cutting speed is increased and that the hardened material gives thinner chips.

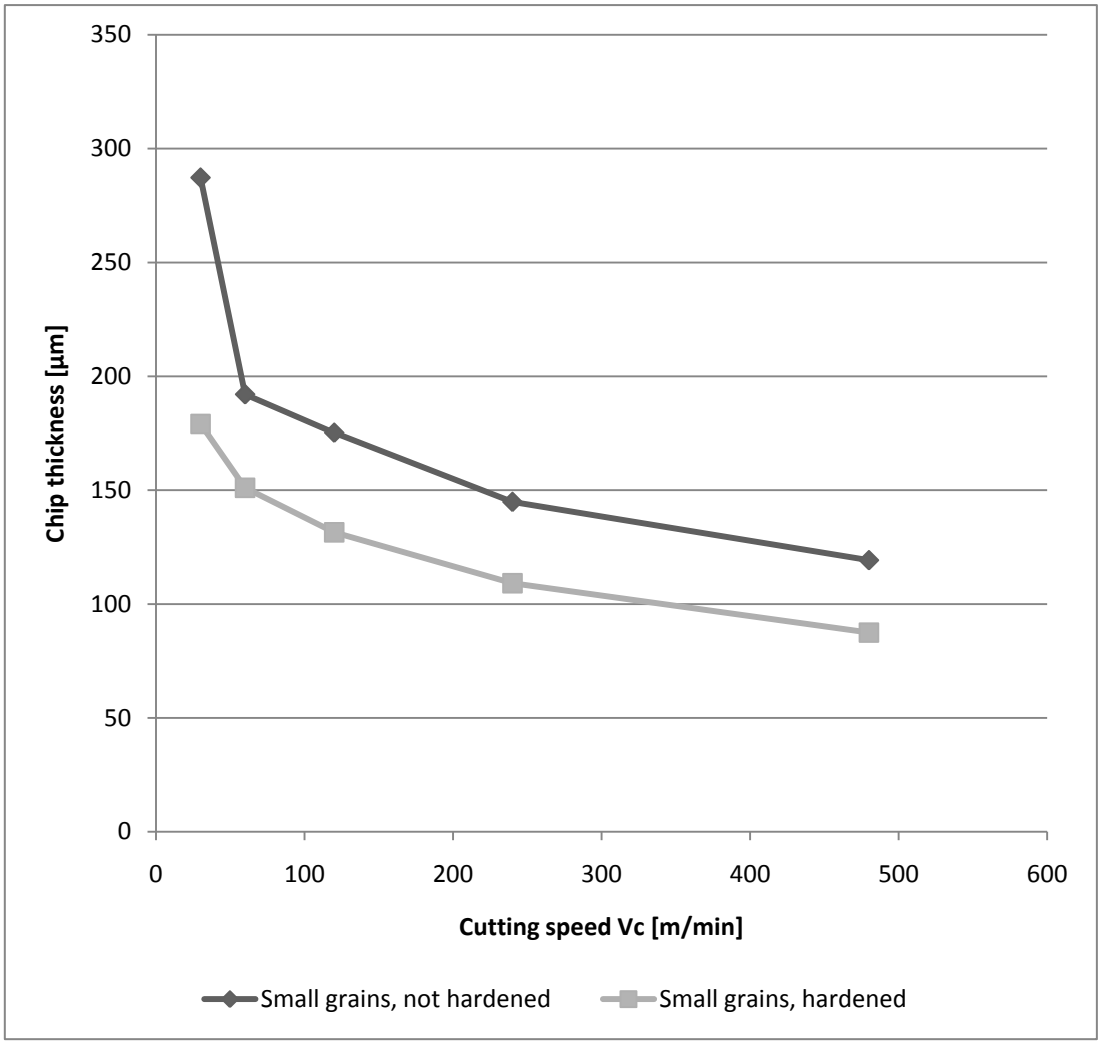

Figure 36: Chip thickness. Mean thickness of continuous chips in the case of V_c = 30 m/min and V_c = 60 m/min, mean of chip hills and valleys in the case of V_c = 120 m/min to V_c = 480 m/min. See 5.1.5 Chip dimension measurements for more details. No significant variation was found between the data points except for small grains not hardened at V_c =30 m/min where vibrations produced a chip with long range variations in chip thickness.

6.3.4 Chip width

Figure 37 shows measurements of chip width with the width of the flange (2000 µm) subtracted. This should be equal to chip widening. It should be noted that no actual measurements of the flange widths were taken and that the variation in flange width is uncertain. It should also be noted that the chips had irregular edges and that the width locally can be much larger than the measured width.

The measurements seem to imply that the widening is larger in the not hardened material than in the hardened but the above considerations should be kept in mind when doing such an analysis.

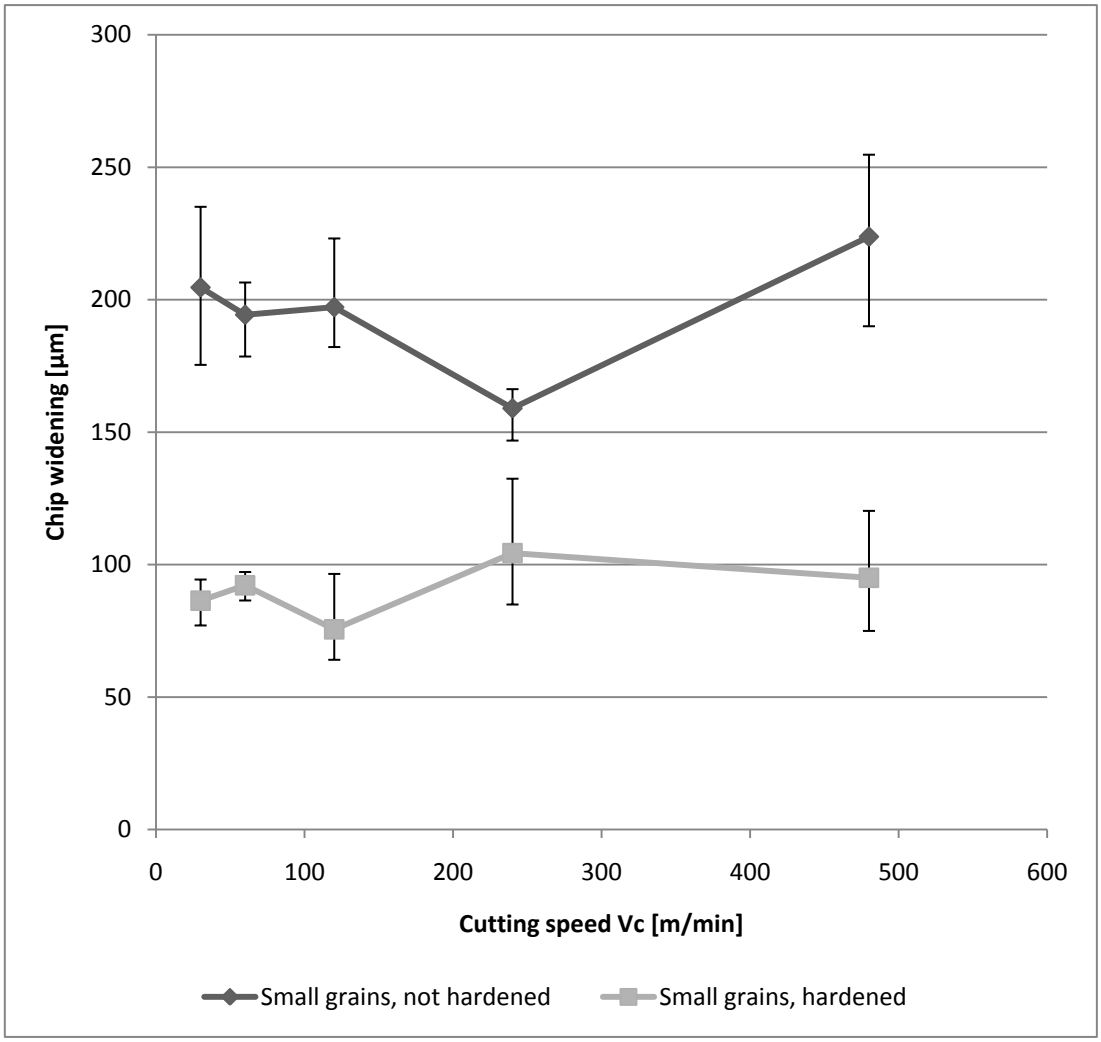

Figure 37: Chip widening. Error bars show distance to highest/lowest value measured.

6.4 Contact lengths

The chip - tool contact length can be seen in figure 38. At cutting speeds from 120 m/min and above two distinct zones were found on the inserts and the short darker zone can be seen in figure 39. The actual contact lengths measured can be found in appendix B.

The contact length is greatly reduced from 30 to 60 m/min in all materials except the large grained, hardened material. The decrease in contact length for higher cutting speeds is not as significant but even so a shorter contact length is measured as the cutting speed is increased.

The contact length shows a dependency on the state of the material, with higher contact lengths for the non-hardened material compared to the hardened for both grain sizes.

It can also be noted that a very rough estimate for the difference between the long and short contact length is 100 µm.

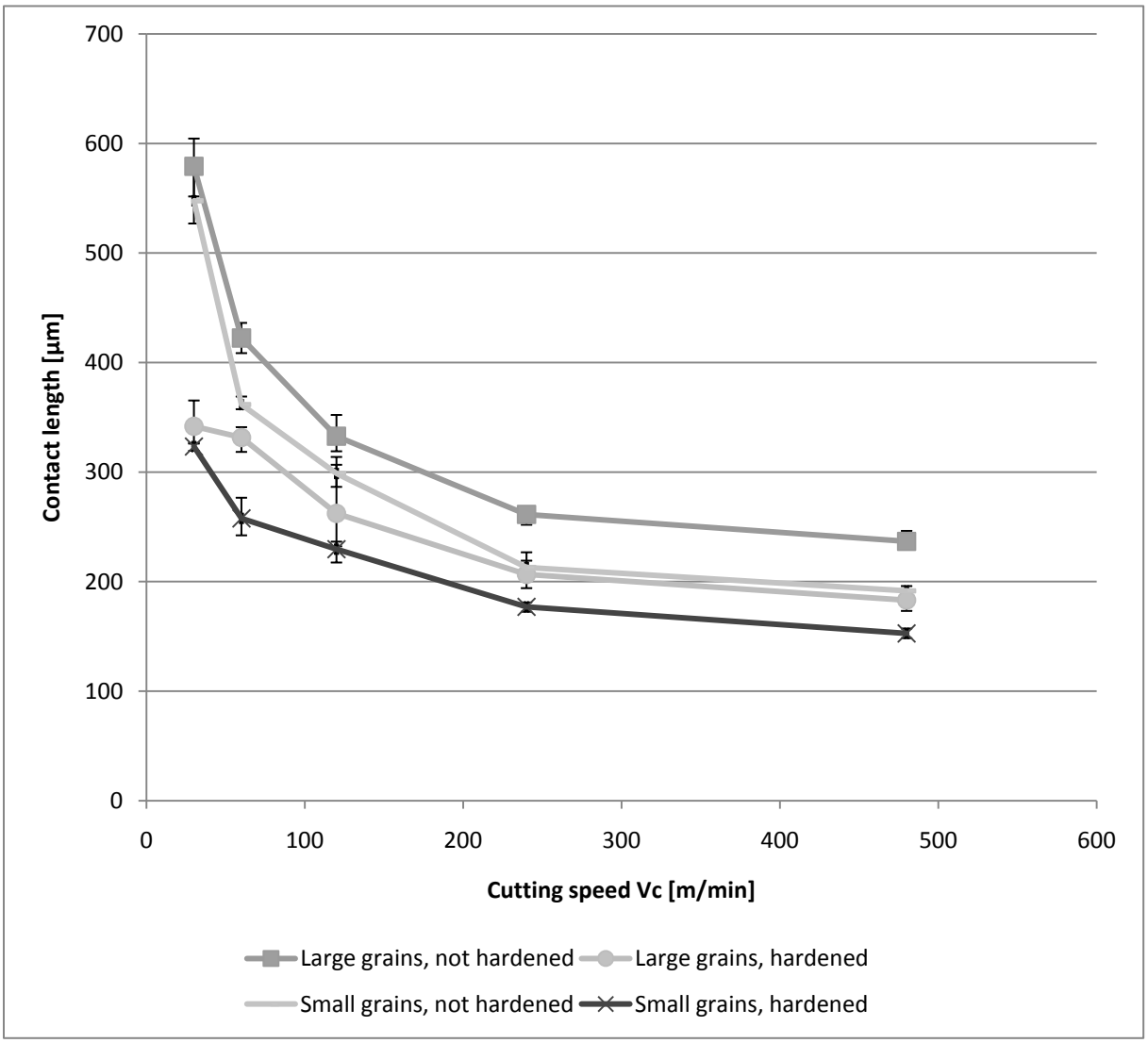

Figure 38: Total contact length. Error bars show the distance to the longest/shortest mean cutting length among the test runs.

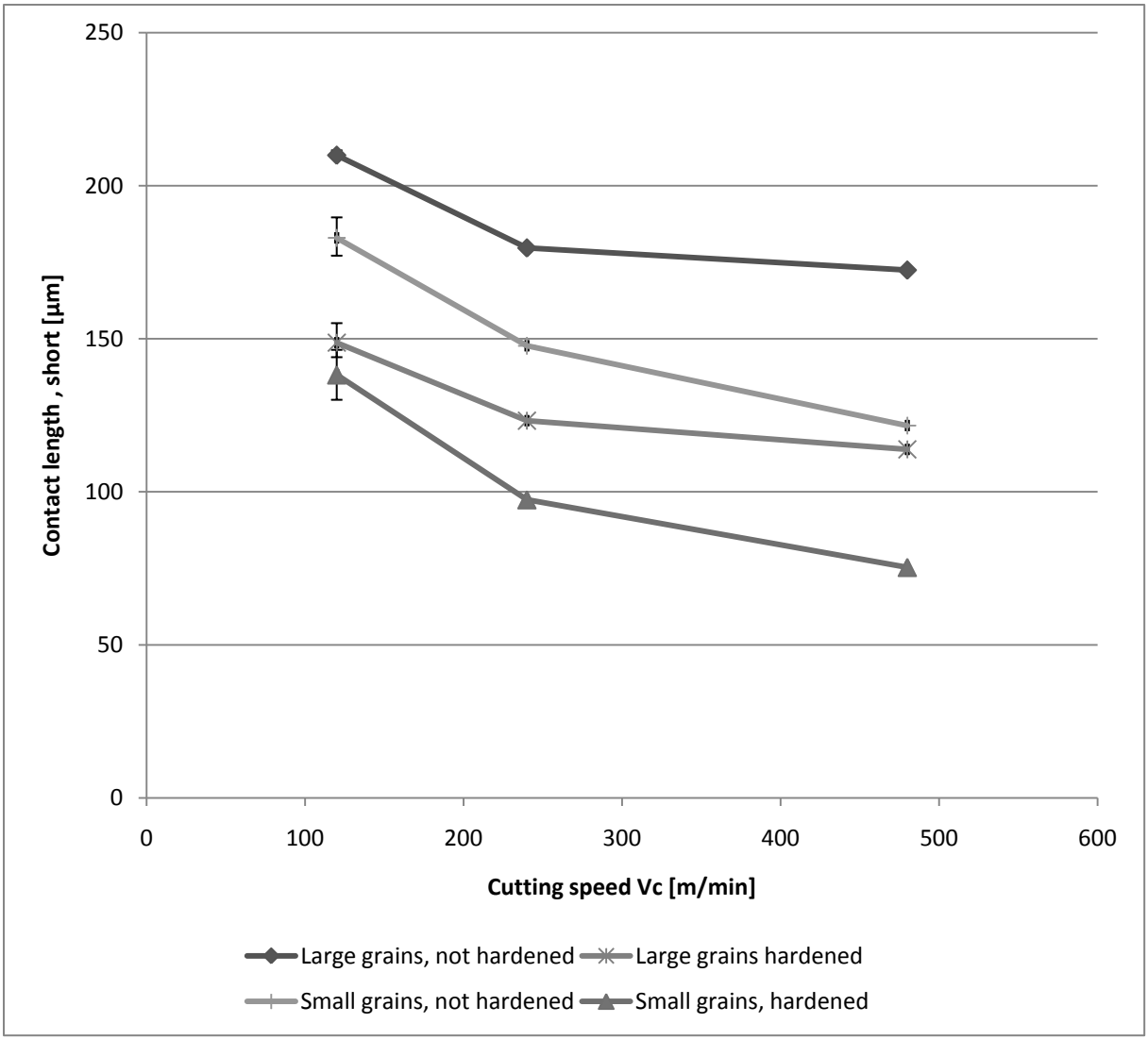

Figure 39: Short contact length. Error bars show the distance to the longest/shortest mean short cutting length among the test runs.

Figure 40 and figure 41 shows the segment width to contact length ratio for the longer and shorter contact lengths respectively. The aged material shows higher ratios for both contact lengths at the higher cutting speeds.

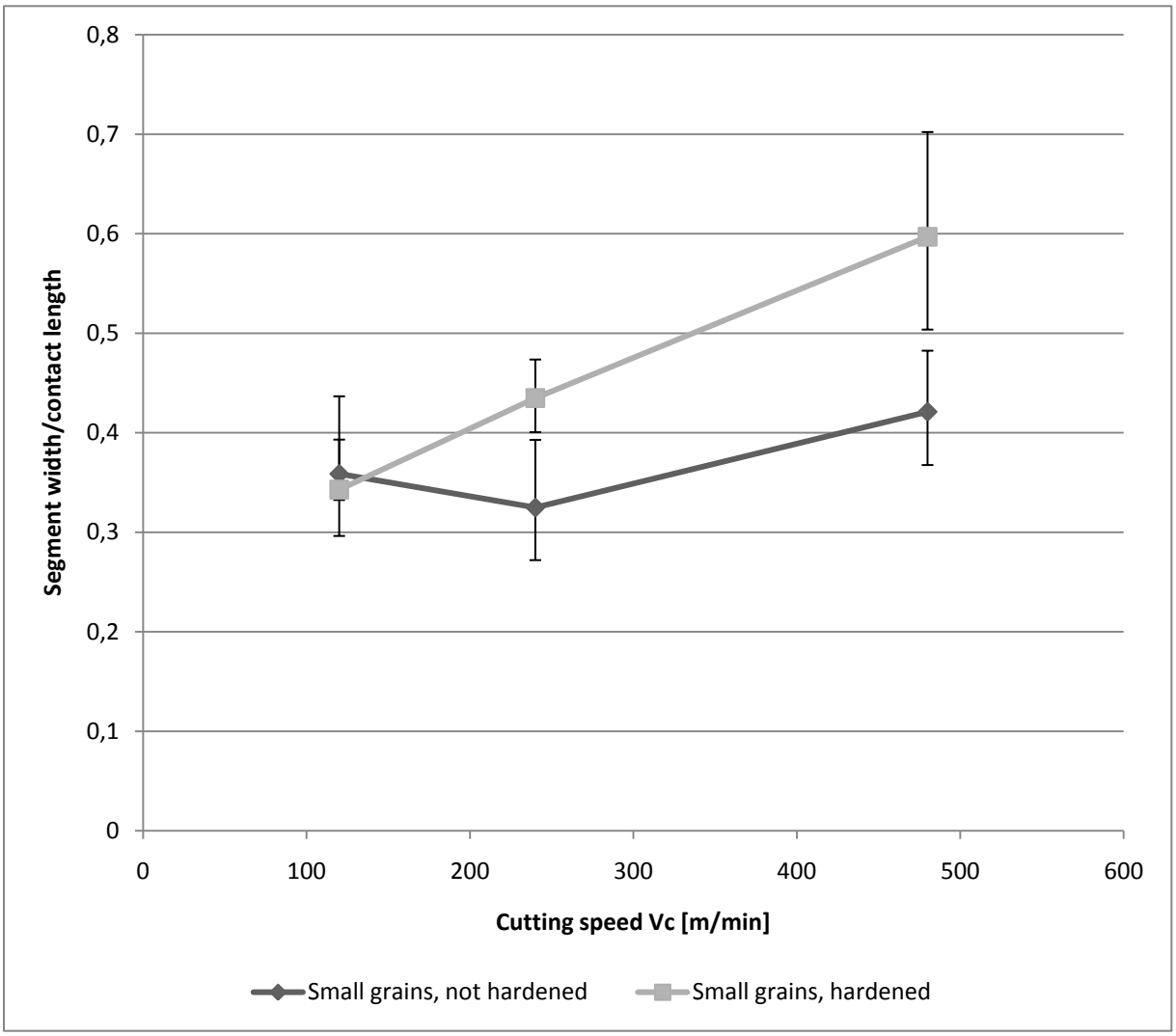

Figure 40: Ratio between segment width and contact length. Error bars show the maximum and minimum attainable ratios. Maximum is calculated as the largest measured segment width divided by the smallest measured contact length. Minimum is calculated as the smallest measured segment width divided by the largest measured contact length.

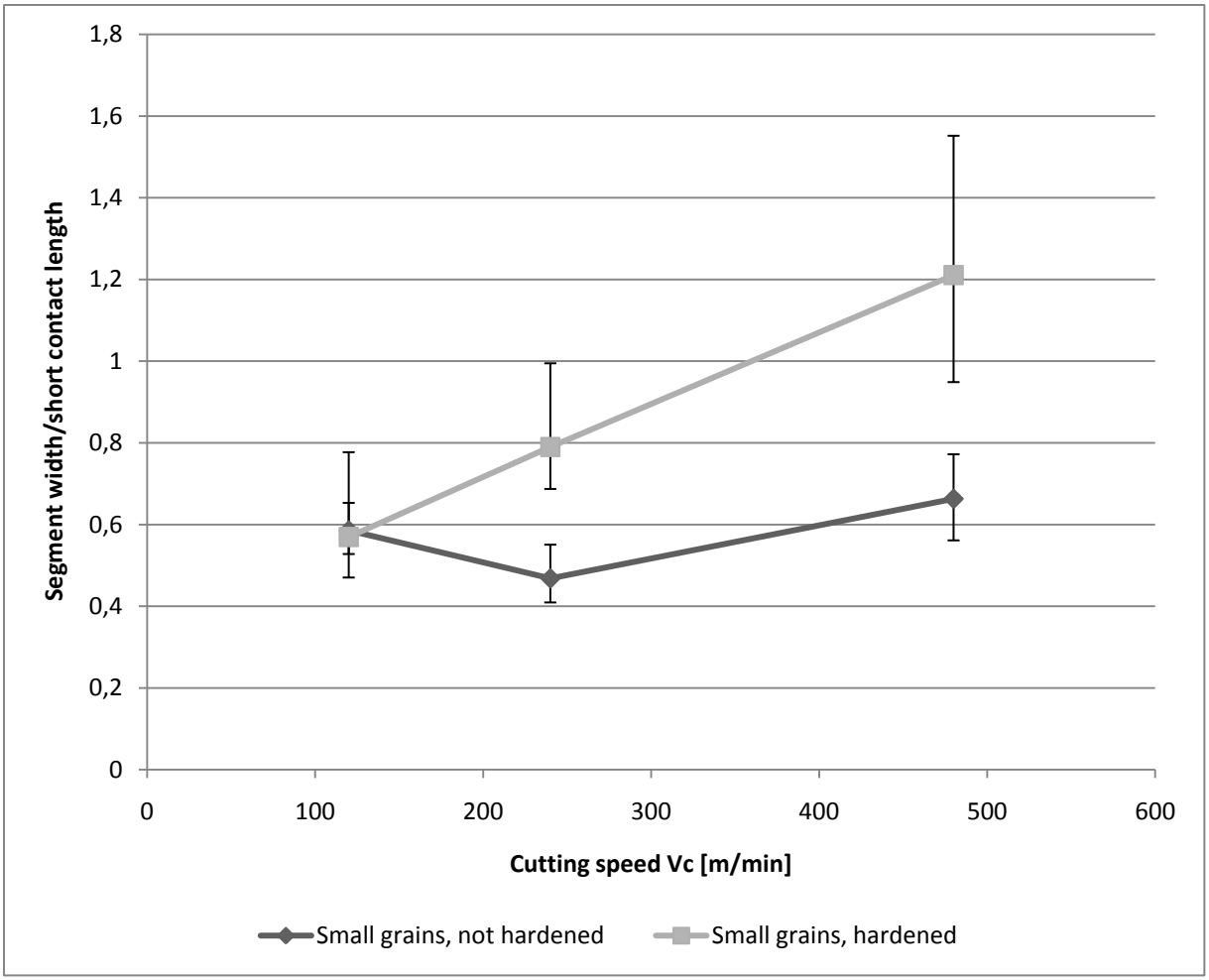

Figure 41: Ratio between segment width and short contact length. Error bars show the maximum and minimum attainable ratios. Maximum is calculated as the largest measured segment width divided by the smallest measured short contact length. Minimum is calculated as the smallest measured segment width divided by the largest measured short contact length.

6.5 Forces

The cutting force (main component) can be seen in figure 42 and the feed component can be seen in figure 43.

6.5.1 Cutting force (main component)

The main cutting force component shows a difference in behavior between hardened and not hardened materials where the not hardened materials have a much more rapid decrease in force at low speeds then leveling out while the hardened materials shows a more consistent decrease over the whole speed spectrum.

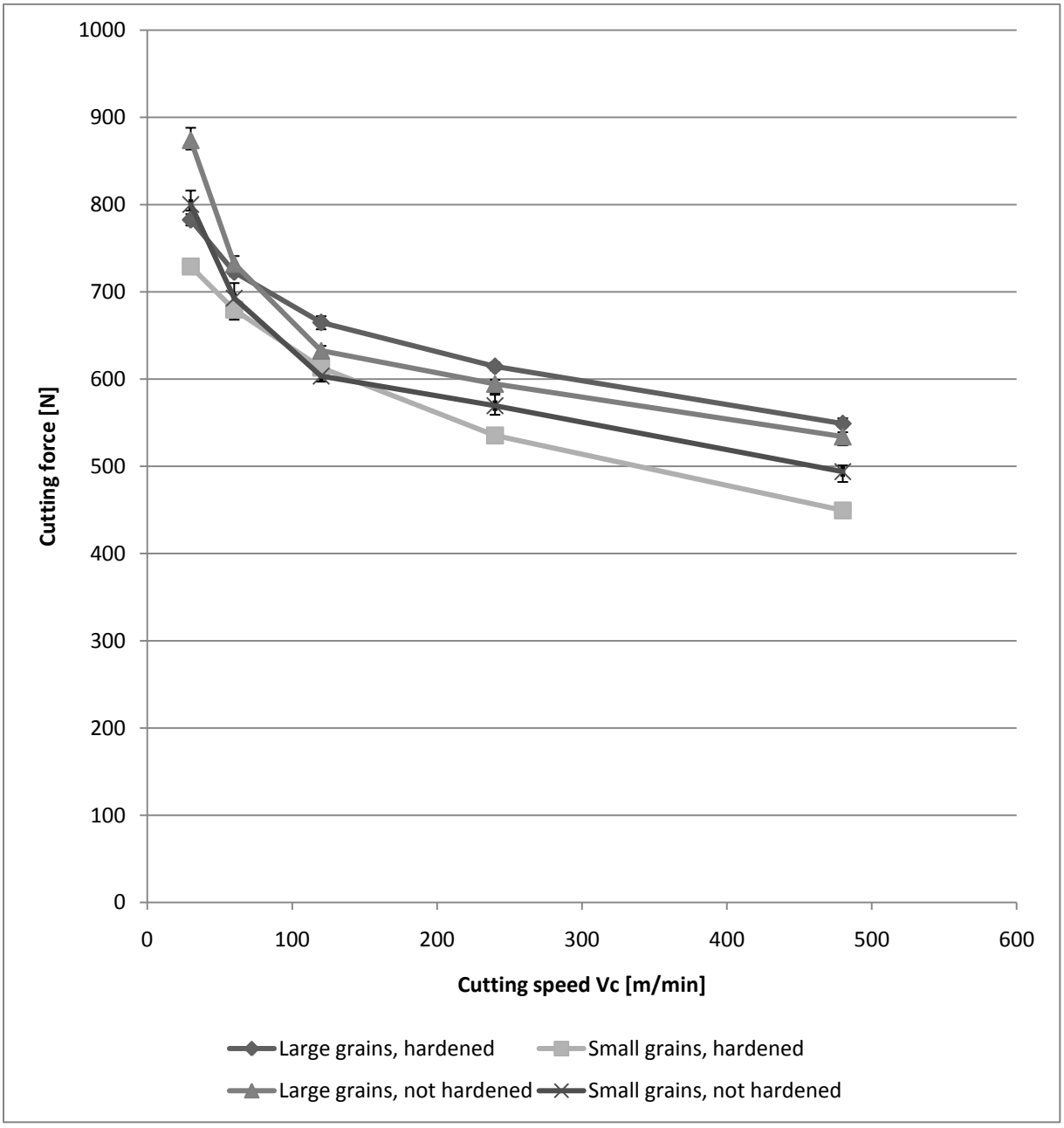

Figure 42: Cutting force (main component). Error bars show distance to highest/lowest value measured.

6.5.2 Feed force component

The feed force component shows larger variation but it is clear that the drop in force once again is largest for the not hardened materials when comparing low and high speeds.

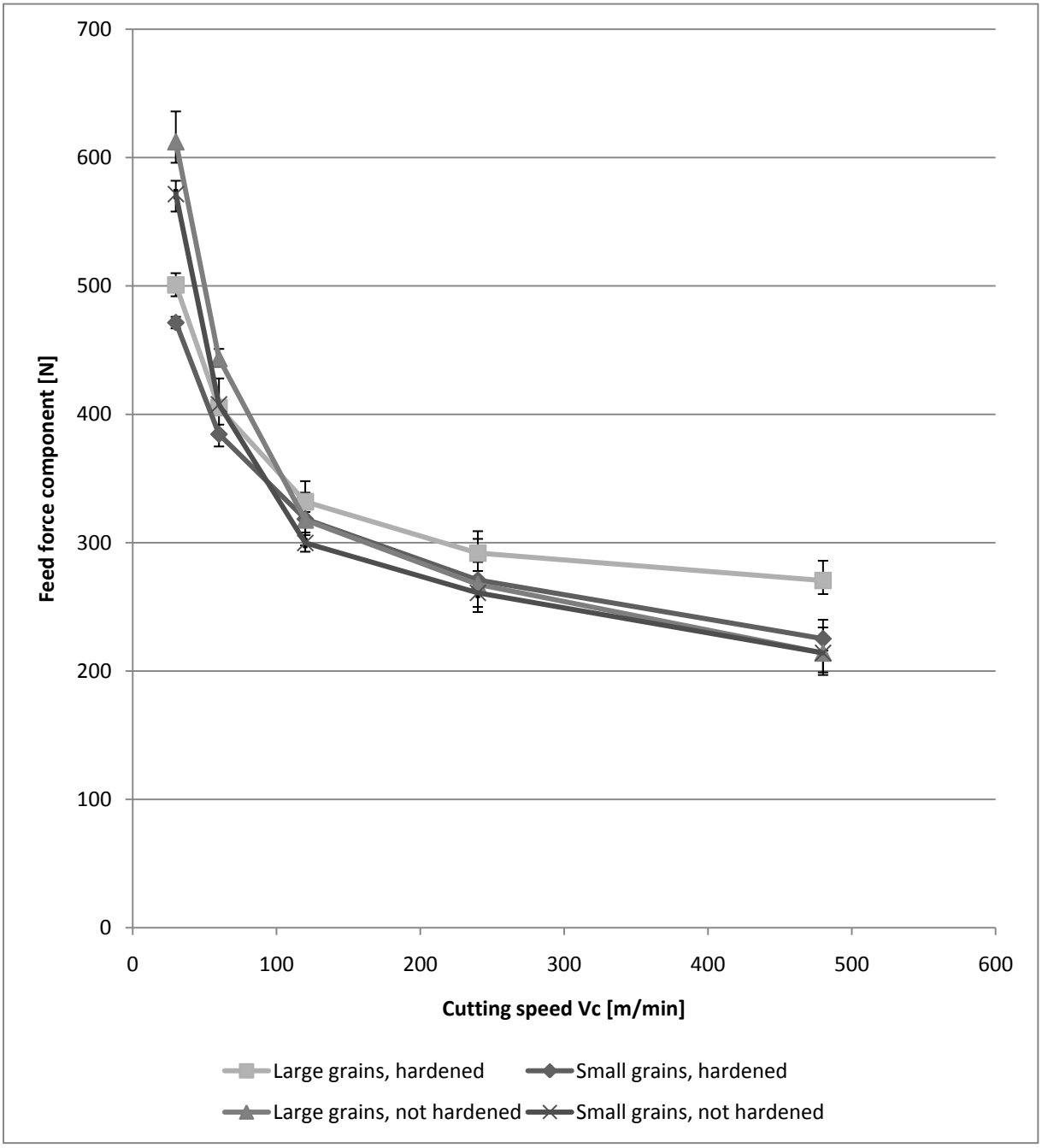

Figure 43: Feed component of the cutting force. Error bars show distance to highest/lowest value measured.

6.5.3 Ratio between components

Figure 44 shows the ratio between the cutting force component and the feed force component. The figure clearly shows that the materials behave differently depending on if they are hardened or not. The not hardened materials show a lower ratio at low cutting speeds meaning that the feed component is relatively larger than for the hardened materials, but a higher ratio at high cutting speed meaning the cutting force component is relatively larger than for the hardened materials.

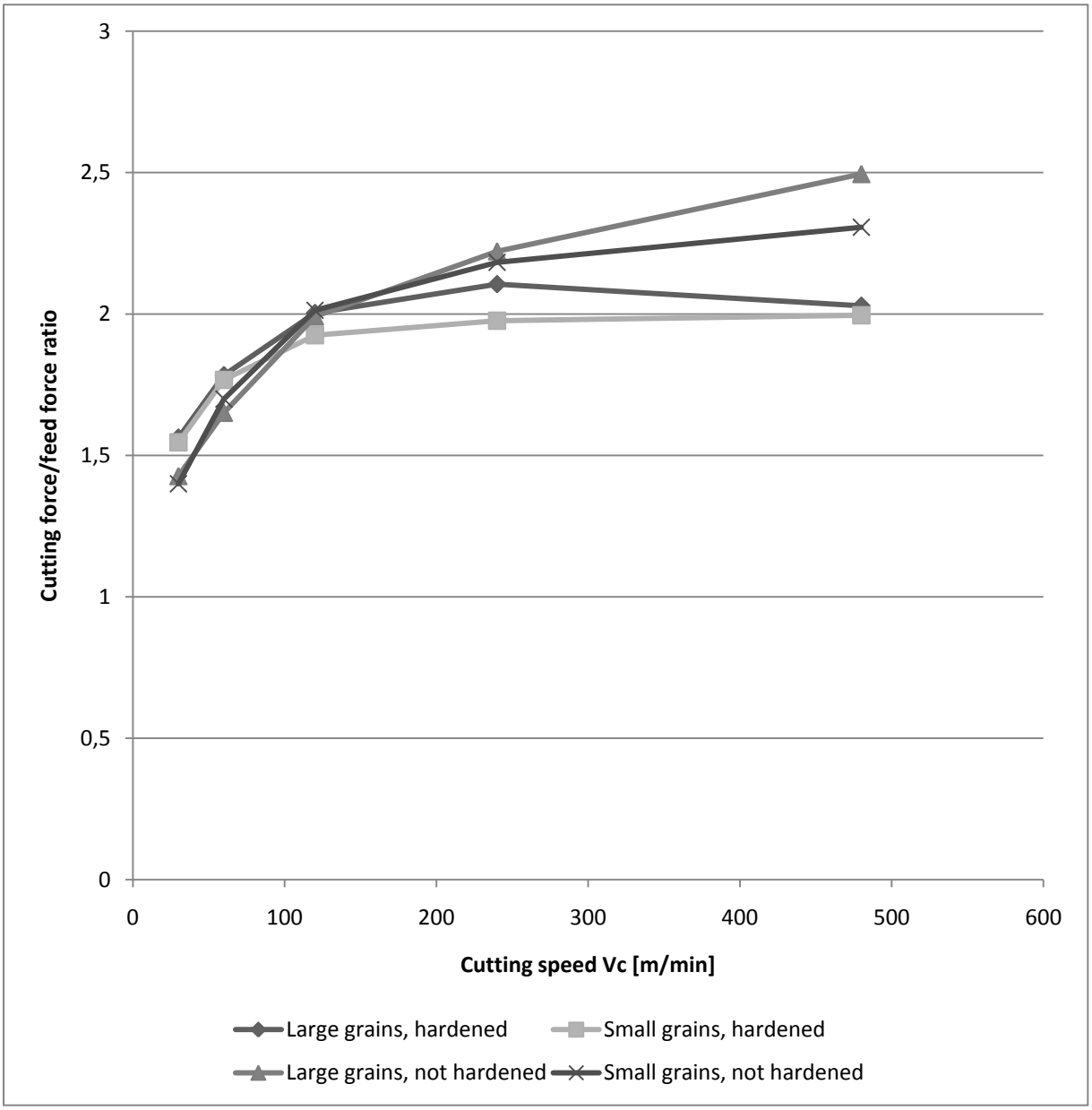

Figure 44: Cutting force/feed force ratio.

7 Discussion

Some questions raised by the results are the following:

- Why is there a change from continuous to segmented chips in the small grained materials?
- What is the reason for the difference in chip morphology between large and small grained materials?
- How can the cutting force decrease with increased cutting speed?
- How can the cutting force be the lowest for the material having the highest strength?

This section will try and discuss these questions, compare with results found in the literature on the subject and present explanations given by other authors.

Why is there a change from continuous to segmented chips in the small grained materials?

The change from continuous to segmented chips has been examined before in Inconel 718. One of these investigations was performed by Komanduri et al [26] who found that the chip morphology changed from a continuous one to one with localized shearing at speeds above 60 m/min. At speeds of about 91.5 m/min the chips had segments strongly joined together and at about 152.5 m/min the segments were completely isolated.

The same stages except for the fully isolated segments can be found in the small grained hardened material which is the material most similar to the material used by Komanduri. The cutting speed for which a change in morphology happens is not the same in the investigation done by Komanduri and the one found in this investigation as no segmentation can be found in the chips produced at 60 m/min and no isolated segments are produced even at a cutting speed of 480 m/min. This difference is believed to be due to the difference in cutting parameters between the investigations the main differences being a lower depth of cut (here 2 mm, Komanduri 2.5 mm) and a lower feed (0.1 mm/rev, Komanduri 0.2 mm/rev). That more localized chips are produced with an increase in feed is consistent with the results found by Hjärtstam [4].

In his 1981 paper [27] regarding the formation of segmented chips formed when machining titanium alloys, Komanduri et al proposes a model, based upon actual observations using a high speed camera for high cutting speeds (up to roughly 300 m/min) and observations inside a SEM (for low cutting speeds). This model is later applied to Inconel 718 [26].

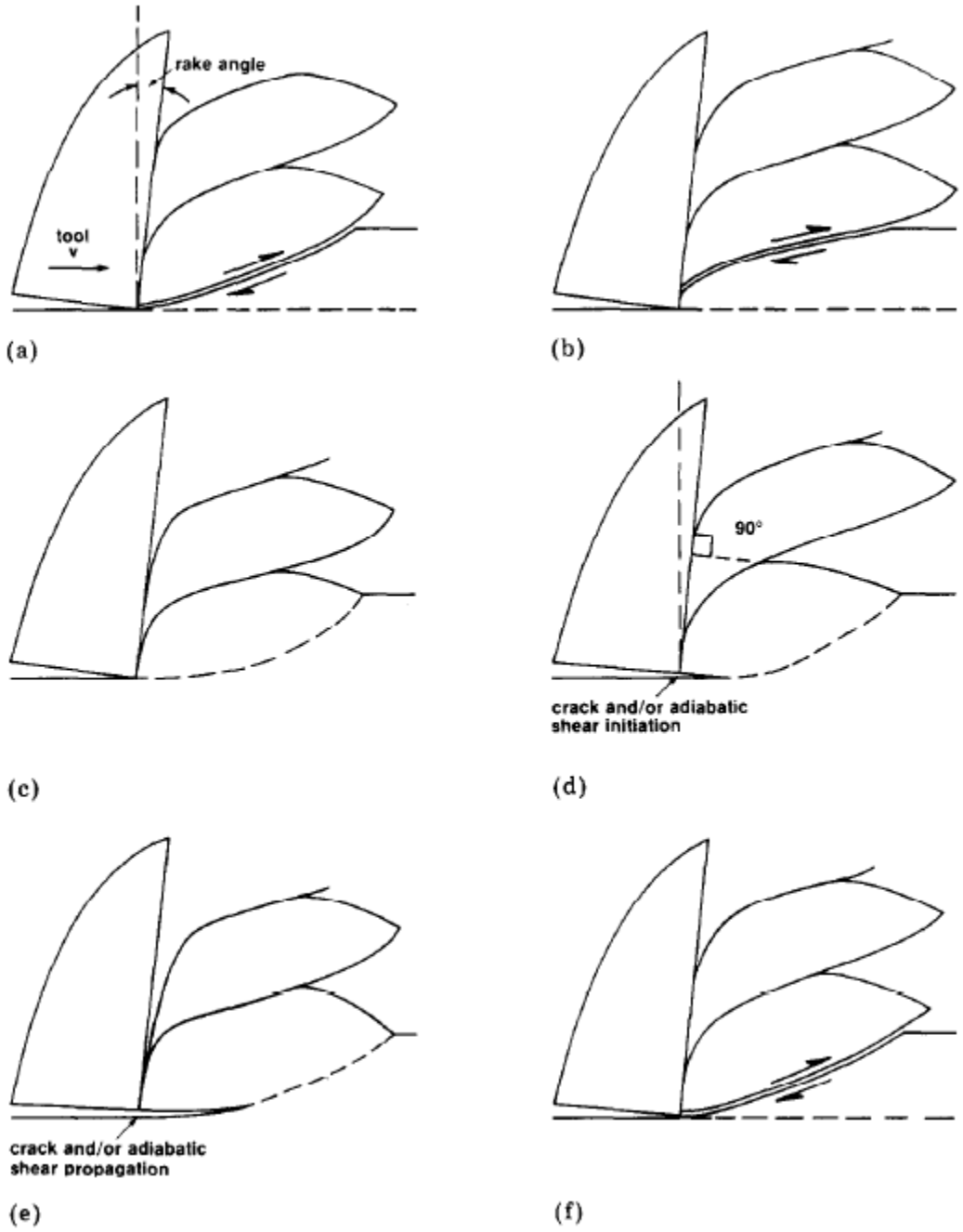

Figure 45: The different stages of the formation cycle ((a)-(f)) producing a shear localized (serrated) chip when machining titanium alloys. [27]

The process suggested by Komanduri et al can be seen in figure 45 starting from (a) and completing the cycle at (f). What happens is that the work material and the tool have a very narrow contact area at the tip of the tool. The compressive force from the adjacent work material then flattens this tip and causes the material to pile up or roll onto the tool (with almost no relative slipping motion against the tool) while pushing the previously formed segment upwards. The contact between the forming segment and the one formed just before, which is the zone in which the shear localization happened previously (see figure 45 (d) and (e)) then sees a lot of shear stress as the two segments "rub" against each other. This is followed by plastic instability (figure 45 (d)) and strain localization in

a band reaching from the tool tip to the free surface (figure 45 (e) dashed line) forming a segment and returning the cycle to its initial stage.

Using this model in the study of the chip formation when turning Inconel 718, Komanduri states that the contact between the segments of the chip is decreased and that the shear becomes more and more localized, which is consistent with our observations. Another interesting observation of our work was that once segmentation sets in, the segment width stays the same when the cutting speed is increased. Assuming that the scale bar in fig. 8 [26] is wrong (something which is strongly supported by the two following observations), and should be in the same scale as used in his fig. 9, measurements of his chips once again supports our observations in the case of decreasing average chip thickness (figure 36) and a more or less constant segment width with increasing cutting speed for the small grained, hardened material (figure 34).

Komanduri also states that "the contact length between the shear localized chip and tool is generally about one segment width". This could not be completely verified in our work, where segment width was compared to our two measured contact lengths; contact length (figure 40) and short contact length (figure 41). What can be said is that the results for the small grained, hardened material generally show better agreement compared to the non-hardened material with the same grain size.

A comparison of figure 40 and figure 41 also shows that the ratio between segment width and short contact length is closer to one (and therefore shows better agreement with Komanduri's statement). There is also a hint of a possible trend with increasing ratio for both contact length measurements with regard to cutting speed for the small grained, hardened material.

Another investigation of shear localized chips was performed by Sullivan et al [28]. In his investigation he studied quick-stop specimens from machining of a stainless steel showing shear localized chip formation. The chips produced in his investigation are similar to the ones produced in the not hardened small grained material in this investigation with wider zones of shear as opposed to the very thin bands found in the hardened material.

Sullivan's explanation of the phenomenon builds on the classic shear plane model and can be seen in figure 46. He argues that as a segment forms the shear plane angle is increased leading to a thinner chip ((a) to (c) in figure 46). As the chip gets thinner the chip velocity increases leading to higher deformation rates. He then argues that this deformation rate will make the material strain rate harden very quickly in the secondary shear zone as strain rates here can reach 10^4 s^{-1}, a rate at which most materials goes into a state which is associated with very rapid strain rate hardening. As the effect of strain rate hardening becomes dominating, the material can no longer be deformed in this way and the shear plane angle resets to a lower angle leading to a thicker chip again ((d) to (e) in figure 46). The whole cycle is then repeated giving the segmented chip morphology.

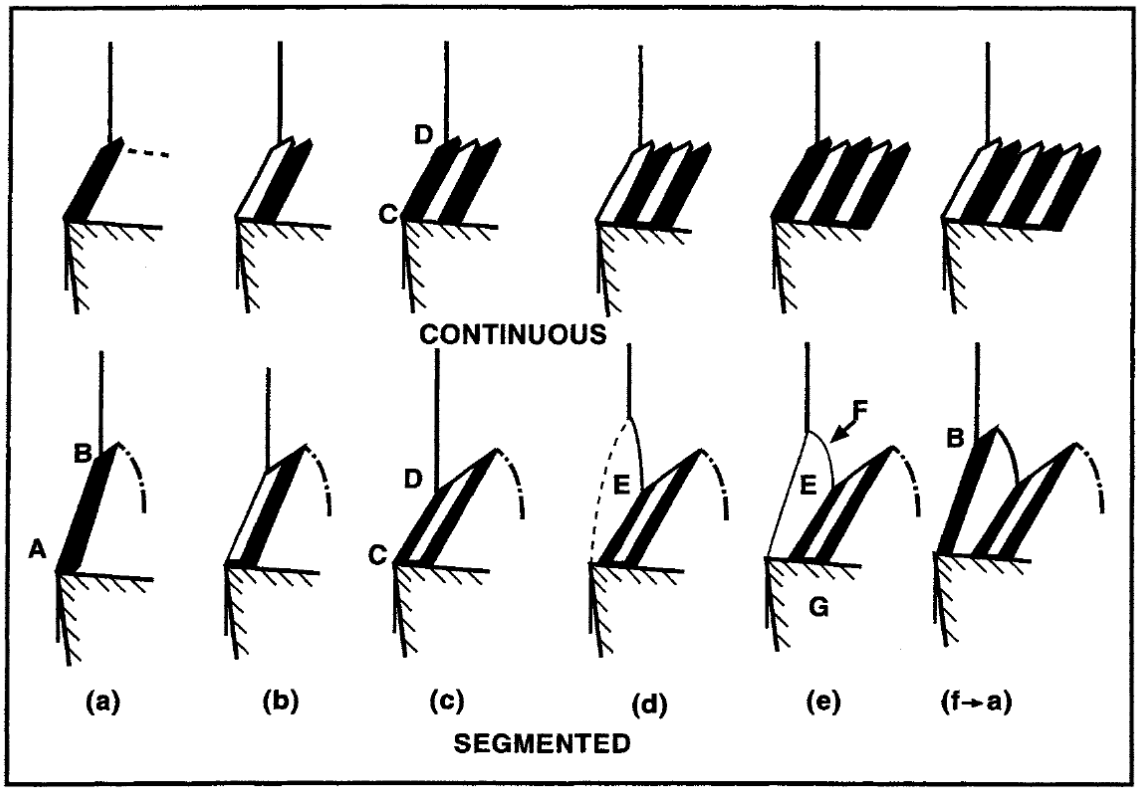

Figure 46: The top row describes continuous chip formation with only one shear plane angle while the second row describes segmented chip formation with a varying shear plane angle. [11]

A problem with the above mentioned model, when applying it to our results, is the fact that our investigation shows thinner chips at higher speeds as well as more localized deformation. This should lead to even higher strain rates meaning that the process should go faster. However our results show no difference in segment width and larger differences in chip peak to bottom distance when the cutting speed is increased. Even so, it is a fact that materials have a very distinct response to very high strain rates and it could very well be so that part of the explanation to segmented chip formation can be explained by this phenomenon.

In a recent review by Rittel [29] concerning shear localization, the idea that the embryo of shear bands could be regions of intense grain refinement due to dynamic recrystallization (DRX) is presented.

Rittel argues that the common understanding that shear localization at high strain rates is an effect of thermal instability might not be adequate to describe and account for all mechanisms active in the process of adiabatic shear banding (ASB).

Instead Rittel proposes that the dynamically stored energy of cold work is a key factor and that since this property depends on the material microstructure it is sound to investigate possible microstructural evolution connected to shear localization. This is backed up by experimental evidence for several different materials showing that the significant temperature rise happens at the onset of macroscopic localization and is preceded by DRX.

DRX is an athermal process, activated by the stored mechanical energy in the material and results in the formation of dislocation free nanograins which produce a local destabilization of the material, but the exact dynamics of this is not well understood.

In our work, no equipment able to confirm the results of Rittel was used. However, his results are both recent (2009) and provide a different view on how the plastic instability in the material is generated as well as offers a link between the microstructure of the material and the deformation mechanisms and is as such relevant in this context.

What is the reason for the difference in chip morphology between large and small grained materials?

That there is a difference in chip morphology related to grain size was shown by Olovsjö [2] at a cutting speed of 30 m/min. He explained this by the fact that as so few grains are deformed at once, the anisotropic nature of the crystal gives a variation in the deformation behavior. If the grain being deformed is oriented in a favorable way for deformation this will lead to a more deformed grain giving a “hill” in the chip while other grains not so favorably oriented will produce lower portions of the chip.

The results found in this investigation can be understood on the same principles. From the macroscopic investigation of the chips it is also evident that the serration seen in the large grained materials is not a segmentation in the same sense as it is in the small grained materials as there are no organized shear zones across the full chip width. It is probable that this difference between the materials is also due to the anisotropy found when so few grains are cut at once.

Another interesting observation in the large grained materials is the localized shear found within the grains (see figure 30). This deformation mode is only observed in large grained hardened material. The localized shear is not only in the primary deformation direction but also in a direction nearly orthogonal to the primary. It is often concentrated to certain grains while not found at all in others. That it is seen only in hardened material implies that the presence of gamma’’ precipitates play an important role in the formation of these shear bands. This can perhaps be understood as the material should have a higher tendency to deform in alternative modes to slip as the material is very strong but also as it should respond more markedly to heat as the dissolution of gamma’’ precipitates leads to a very abrupt loss of strength. In the non-hardened material no abrupt loss of strength is to be expected and the overall strength of the material is also lower and the material can deform in a more even way. It should however be noted that these small, short localized shear bands are very hard to find as they are extremely sensitive to the etching as well as a well calibrated microscope. This means that further characterization of these bands with regards to width, distance in between and density in the grains are very hard to do.

How can the cutting force decrease with increased cutting speeds?

That forces decrease with increasing cutting speed is a general trend in machining. This effect is often explained by thermal softening from increased shearing and shorter contact lengths [11]. Shorter contact lengths at higher cutting speeds have been measured in this work and are part of the explanation to the decreased cutting forces. The influence of the contact length on the cutting forces comes from adhesion and friction working between the tool and the work piece. The contact length that can be seen on the rake face of the insert is a built up layer left behind from the adhesion of material from the work piece on the tool.

The thermal softening explanation is complicated by strain hardening effects and the presence of localized shear. From the results it can be seen that the localized shear zone width decreases with increasing speed irrespective of material, meaning that less energy is required to deform a given volume of material. If this is because of the total amount of deformation (strain) is lower (more concentrated) or that the energy required to deform the material decreases or a combination of the two is hard to draw any conclusions about from the results of this work alone.

What can be said is that the material is known to severely strain harden, that it is strain rate dependent [30] and that higher cutting speeds should produce higher strain rates (but this is dependent on the angle of shearing if using the shear plane model). These factors have to be considered keeping the ideas of Zener and Hollomon [23] regarding the two counteracting effects of strain hardening and thermal softening in mind.

To summarize, the measured forces both decrease with increasing cutting speed, which is also partly explained by the contact length measurements. The other part can be explained from the fact that our measurements shows decreasing localized shear zone widths with increasing cutting speeds, something which signifies that less energy is required to deform the material, which directly translates to a lower force.

How can the cutting force be the lowest for the material having the highest strength?

In a study by DeMange et al [30] concerning ballistic penetration (very high strain rates) of Inconel 718 in both annealed (not-hardened) and hardened state it was shown that the annealed material had superior penetration resistance. This was attributed to the fact that the annealed material distributed the impact energy over a larger area and diffusing the macroscopic shear zone over a wider area (over several grains). The aged (hardened) material on the other hand exhibited a much more localized deformation zone.

Generally, shear localization is higher for materials showing minimal strain hardening and high strength. This was also observed in the Split-Hopkinson pressure bar top hat shear tests performed for both materials by the authors, where “significant differences in mechanical behavior for the two states” were observed. In the annealed material low flow stress levels combined with substantial work hardening was seen during tests reaching strain rates up to 10^3/s. The aged material showed yield stresses which were about four times higher than for the annealed material, but low degrees of strain hardening both which favor shear localization. The consequences of this were that the aged material readily formed shear bands and that the impact energy was dissipated through localization and subsequent crack propagation resulting in catastrophic failure.

This correlates well with what was observed during this work, with the shear band width and cutting forces being higher for the small grain, not aged material at the higher cutting speeds (see figure 28). It may also provide a clue to how segmented chips ultimately become discontinuous as more and more of the energy is used in crack propagation as the cutting speed (resulting in higher strain rates) is raised (see figure 24 and figure 25).

8 Conclusions

Some important results from this work are summarized below.

General conclusions

- Large grained materials give serrated chips at all cutting speeds.
- Large grained materials show more irregular deformation than small grained materials.
- Small grained material gives continuous chips at low cutting speeds (30 and 60 m/min) and segmented chips at high cutting speeds (120 to 480 m/min).
- A higher cutting speed gives lower cutting forces.

Further conclusions for small grained materials

- Hardened material show more localized shear than not hardened material.
- Cutting forces are lower for hardened materials than for not hardened materials.
- A higher cutting speed gives almost no difference in segment width.
- A higher cutting speed gives more localized shear, thinner shear zones, between the segments.

9 Future work

The following list contains some ideas and suggestions for investigations that would shed more light on the topics discussed in this work.

- An investigation of higher cutting speeds, including speeds at which the chips become discontinuous.
- Extended study of speeds around 120 m/min to evaluate more precisely when segmentation sets in for the small grained materials.
- Higher sampling frequency for the force measurements to record the influence of segmentation.
- Quick-stop experiments to gain more precise insight in how the deformation takes place.
- Development of measurement methods and a more thorough statistical investigation should be performed, especially for segment width and chip widening measurements.
- Development of a good method to estimate the amount of deformed material in the chips as well as a way to better characterize the deformation of large grained materials.
- Temperature measurements and subsequent TEM investigation in order to further characterize the shear bands.
- EBSD analysis to gain knowledge about crystallographic orientation in the large grained material and its effect on the deformation mechanisms active.
- An extension of this work to include more materials.

10 Acknowledgements

This work could not have been done without the support, encouragement and guidance given to us from all the people involved in the project both at Chalmers and at Volvo Aero. We are grateful to all that have been involved but would like to thank some individually.

First we would like to thank adjunct professor Göran Sjöberg, representing both Chalmers and Volvo Aero, for giving us the opportunity to do this work at all. Your guidance and involvement along the way was key to the successful completion of this work!

Equally big thanks goes to Stefan Cedergren, our supervisor also representing both Chalmers and Volvo Aero, who has worked with us for almost half a year in all parts of the project giving us invaluable guidance as well as putting in a lot of work into the project itself. That you did this while maintaining a humorous and inviting attitude made the work a lot easier to do!

We would also like to thank Sven Ekered at Chalmers department for Product and production development at campus Lindholmen for his assistance with the turning experiments. Thank you for always having a welcoming and problem solving attitude!

Valuable guidance was given by Stefan Olovsjö and Joakim Johansson at Chalmers and Leif Skoog and Anders Oskarsson at Volvo Aero regarding sample preparation and microscopy techniques. You all greatly contributed to making the results of this work better than they had otherwise been! An extra thank you goes out to Stefan Olovsjö for allowing us to use the material from his earlier work. It saved us a lot of time.

As mentioned before many more were involved both at Chalmers and Volvo Aero and we thank all of you for your contributions and kindness!

11 References

1. **Krook, Maria.** *Microstructural Factors Influencing the Machinability of Nickel-Based Superalloys.* Department of Materials and Manufacturing Technology. Göteborg : Chalmers Reproservice, 2005.

2. **Olovsjö, Stefan.** *On the Effect of Grain Size and Hardness on the Machinability of Superalloys and Chip Deformation.* Göteborg : Chalmers Reproservice, 2009.

3. **Puyoo, Geraldiné.** *Machinability of Nickel-based Superalloys.* Department of Materials and Manufacturing Technology. Göteborg : Chalmers University of Technology, 2008.

4. **Hjärtstam, Peter J.** *Material Deformation Mechanisms Involved During Machining of Superalloys.* Department of Materials and Manufacturing Technology. Göteborg : Chalmers reproservice, 2009.

5. *The Development of the Junkers Jumo 004B - The World's First Production Turbojet.* **Mher-Homji, C. B.** October 1997, Journal of Engineering for Gas Turbines and Power, Vol. 119, pp. 783-789.

6. **Donachie, Matthew J. and Donachie, Stephen J.** *Superalloys : A Technical Guide.* Materials Park : ASM International, 2002.

7. *Nimonic Alloys - Their Application To Aircraft Gas Turbines.* September 23, 1948, Flight, pp. 383-385.

8. **Sims, Chester T., Stoloff, Norman S. and Hagel, William C.** *Superalloys II.* New York : John Wiley & Sons, 1987.

9. Special Metals. [Online] [Cited: May 24, 2010.] http://www.specialmetals.com/documents/Inconel%20alloy%20718.pdf.

10. **Reed, Roger C.** *The Superalloys Fundamentals and Applications.* New York : Cambridge University Press, 2006.

11. **Trent, Edward M. and Wright, Paul K.** *Metal Cutting.* 4th. Boston : Butterworth-Heinemann, 2000.

12. **Juneja, B. L., Sekhon, G. S. and Seth, Nitin.** *Fundamentas of Metal Cutting and Machine Tools.* 2nd. New Delhi : New Age International (P) Ltd., 2003. pp. 3-4.

13. **Sandvik Coromant AB.** Technical Guide. [Online] 2010. http://www2.coromant.sandvik.com/coromant/downloads/tech_guide/ENG/Technical_guide2010.zip.

14. *Chapter 4: Turning Tools and Operations.* **Schneider, George Jr.** s.l. : Penton Media, Inc., 2010, American Machinist, Vol. 154. ISSN 1041-7958.

15. **Childs, Thomas, et al.** *Metal Machining - Theory and Applications.* London : Arnold, 2000.

16. *A review of developments towards dry and high speed machining of Inconel 718 alloy.* **Dudzinski, D., et al.** 2004, International Journal of Machine Tools & Manufacture, Vol. 44, pp. 439-456.

17. *Performance of cutting fluids during face milling of steels.* **Vieira, J.M., Machado, A.R. and Ezugwu, E.O.** 2001, Journal of Materials Processing Technology, Vol. 16, pp. 244-251.

18. **Hawk, Jeffrey A., et al.** Abrasive Wear Failures. *ASM Handbooks Online.* s.l. : ASM International, 2003, Vol. 11. http://www.asmmaterials.info.

19. **Oberg, E, et al.** *Machinery's Handbook.* New York : Industrial Press, 2000.

20. **Santhanam, A. T.; Tierney, P.** Cemented Carbides. *ASM Handbooks Online.* s.l. : ASM International, 2002, Vol. 16. http://www.asmmaterials.info.

21. *On the inadequacy of the single-shear plane model of chip formation.* **Astakhov, Viktor P.** 47, 2005, International Journal of Mechanical Sciences, pp. 1649-1672.

22. **Callister, William D.** *Materials Science and Engineering an Introduction.* 7. New York : John Wiley & Sons, Inc, 2007.

23. **Zener, C. and Hollomon, J. H.** 1944, Journal of Applied Physics, Vol. 15.

24. **Meyers, Marc André.** *Dynamic Behaviour of Materials.* New York : John Wiley & Sons, Inc, 1994.

25. *Shear Localization: A Historical Overview.* **Walley, S.M.** 11, u.o. : Springer Boston, 2007, Metallurgical and Materials Transactions A, Vol. 38, ss. 2629-2654.

26. *On Shear Instability in Maching a Nickel-Iron Base Superalloy.* **Komanduri, R. and Schroeder, T. A,.** May 1986, Journal of Engineering for Industry, Vol. 108, pp. 93-100.

27. *New observations on the mechanism of chip formation when machining titanium alloys.* **Komanduri, R. and Turkovich, B. F.** 69, 1981, Wear, pp. 179-188.

28. *Metallurgical appraisal of instabilities arising in machining.* **Sullivan, K. F., Wright, P. K. och Smith, P. D.** June 1978, Metals Technology, Vol. 5, ss. 181-189.

29. *A different viewpoint on adiabatic shear localization.* **Rittel, D.** 2009, Journal of Physics D: Applied Physics, Vol. 42.

30. *Effects of material microstructure on blunt projectile penetration of a nickel-based super alloy.* **DeMange, Jeffrey J., Prakash, Vikas and Pereira, J. Michael.** 2009, International Journal of Impact Engineering, pp. 1027-1043.

Appendix A: Chip microstructures

This appendix contains a complete collection of all microstructures in all materials and speeds. Every page includes all four materials at one cutting speed and one magnification. For every cutting speed three magnifications are available and presented on three consecutive pages.

Abbreviations used in the figures are as following:

LGS	Large grained, not hardened material
LGH	Large grained, hardened material
SGS	Small grained, not hardened material
SGH	Small grained, hardened material
30 m/min	Cutting speed 30 m/min
60 m/min	Cutting speed 60 m/min
120 m/min	Cutting speed 120 m/min
240 m/min	Cutting speed 240 m/min
480 m/min	Cutting speed 480 m/min

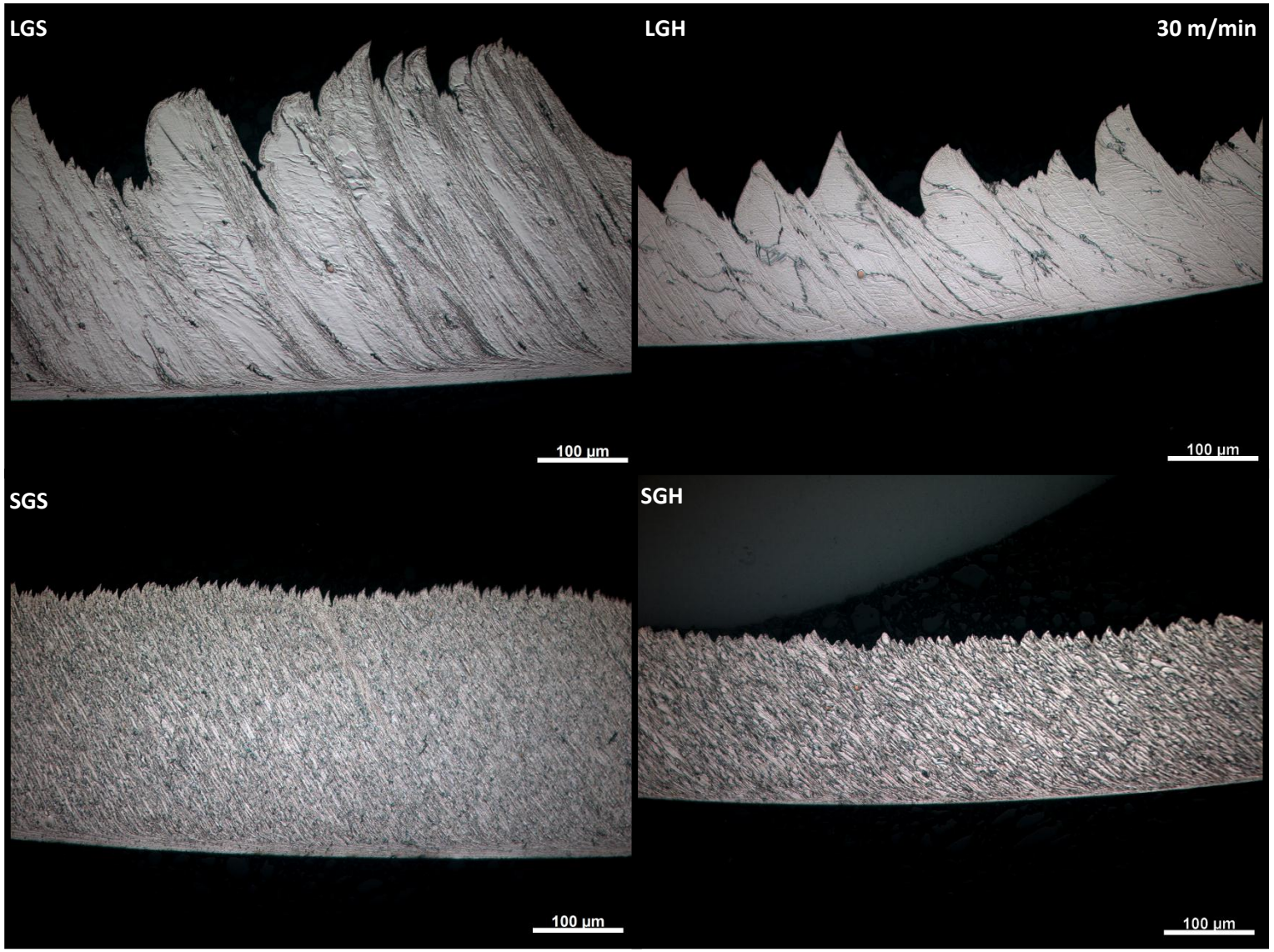

Figure 1 Low magnification of chip microstructures. Cutting speed is 30 m/min. First row is large grains not hardened, large grains hardened. Second row is small grains not hardened, small grains hardened. Scale bars are 100 µm.

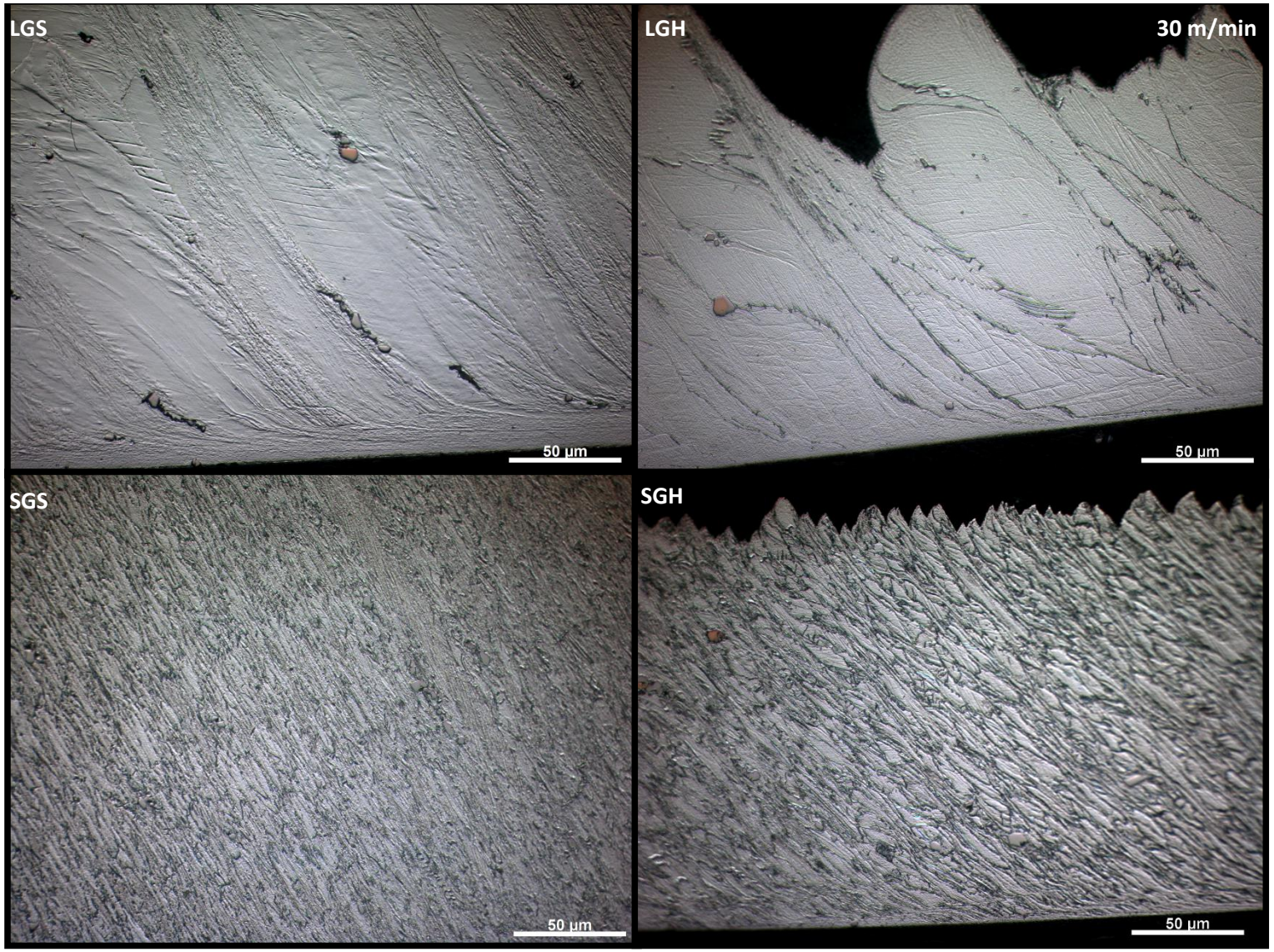

Figure 2 Medium magnification of chip microstructures. Cutting speed is 30 m/min. First row is large grains not hardened, large grains hardened. Second row is small grains not hardened, small grains hardened. Scale bars are 50 µm.

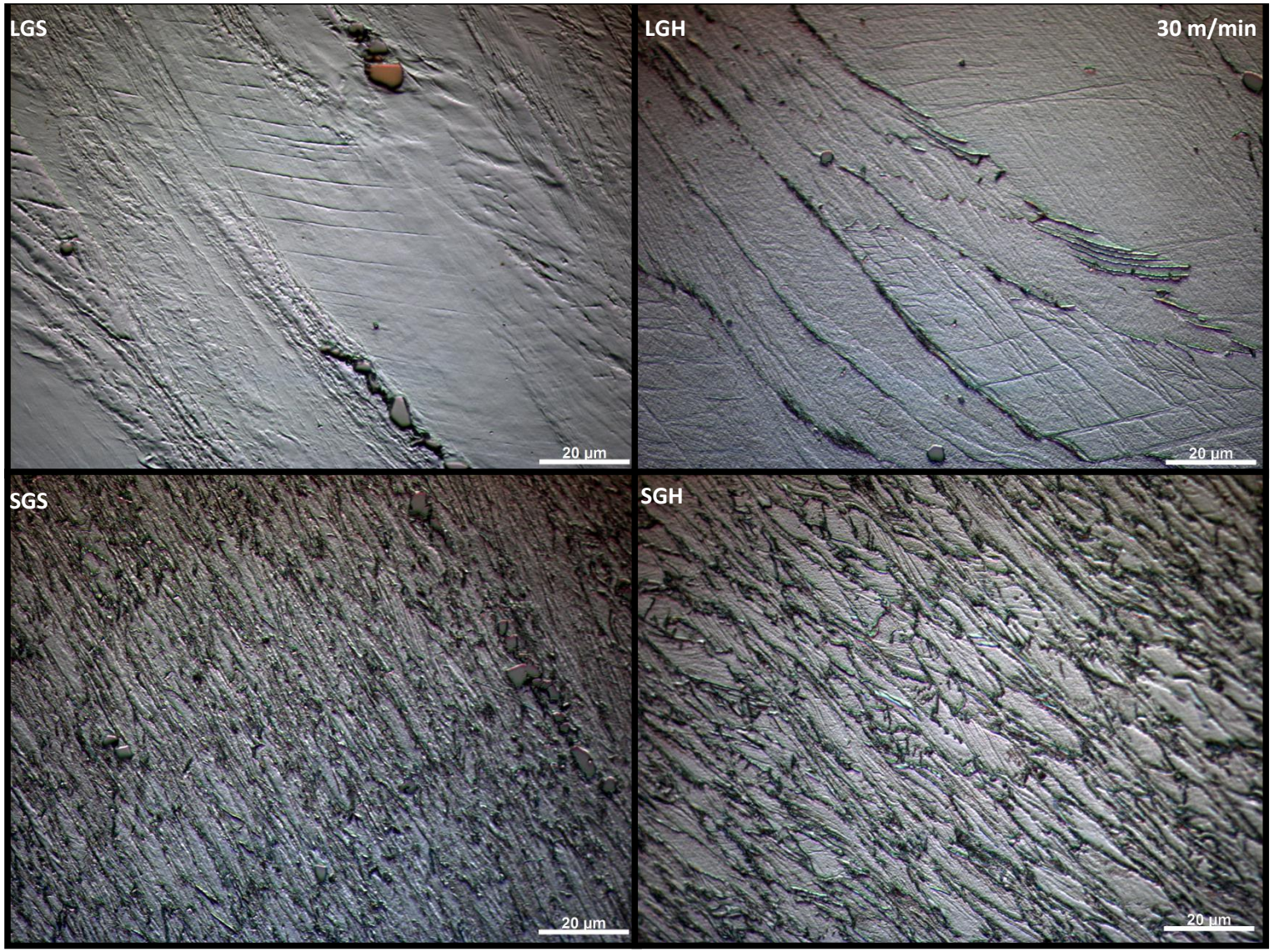

Figure 3 High magnification of chip microstructures. Cutting speed is 30 m/min. First row is large grains not hardened, large grains hardened. Second row is small grains not hardened, small grains hardened. Scale bars are 20 µm.

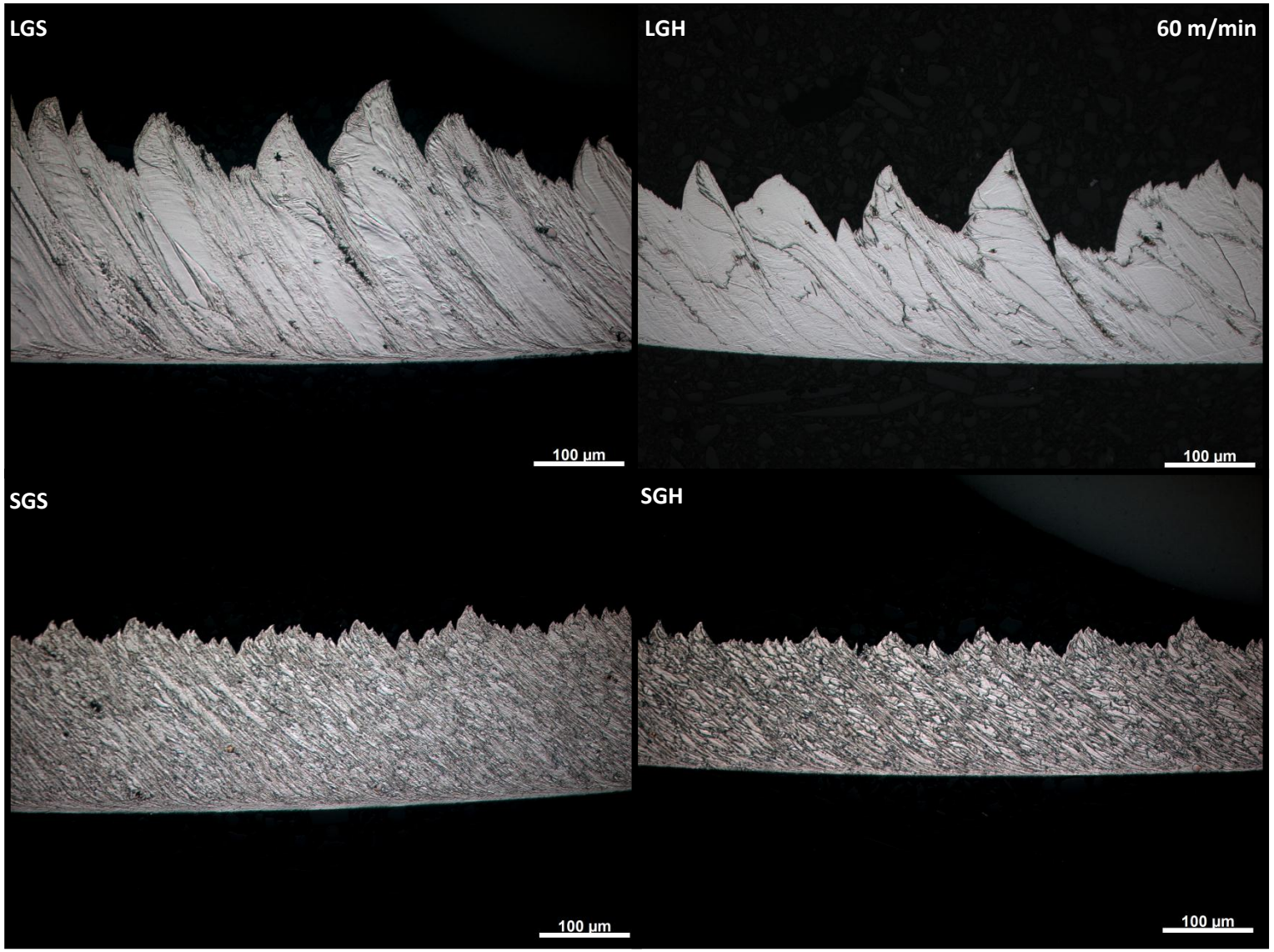

Figure 4 Low magnification of chip microstructures. Cutting speed is 60 m/min. First row is large grains not hardened, large grains hardened. Second row is small grains not hardened, small grains hardened. Scale bars are 100 µm.

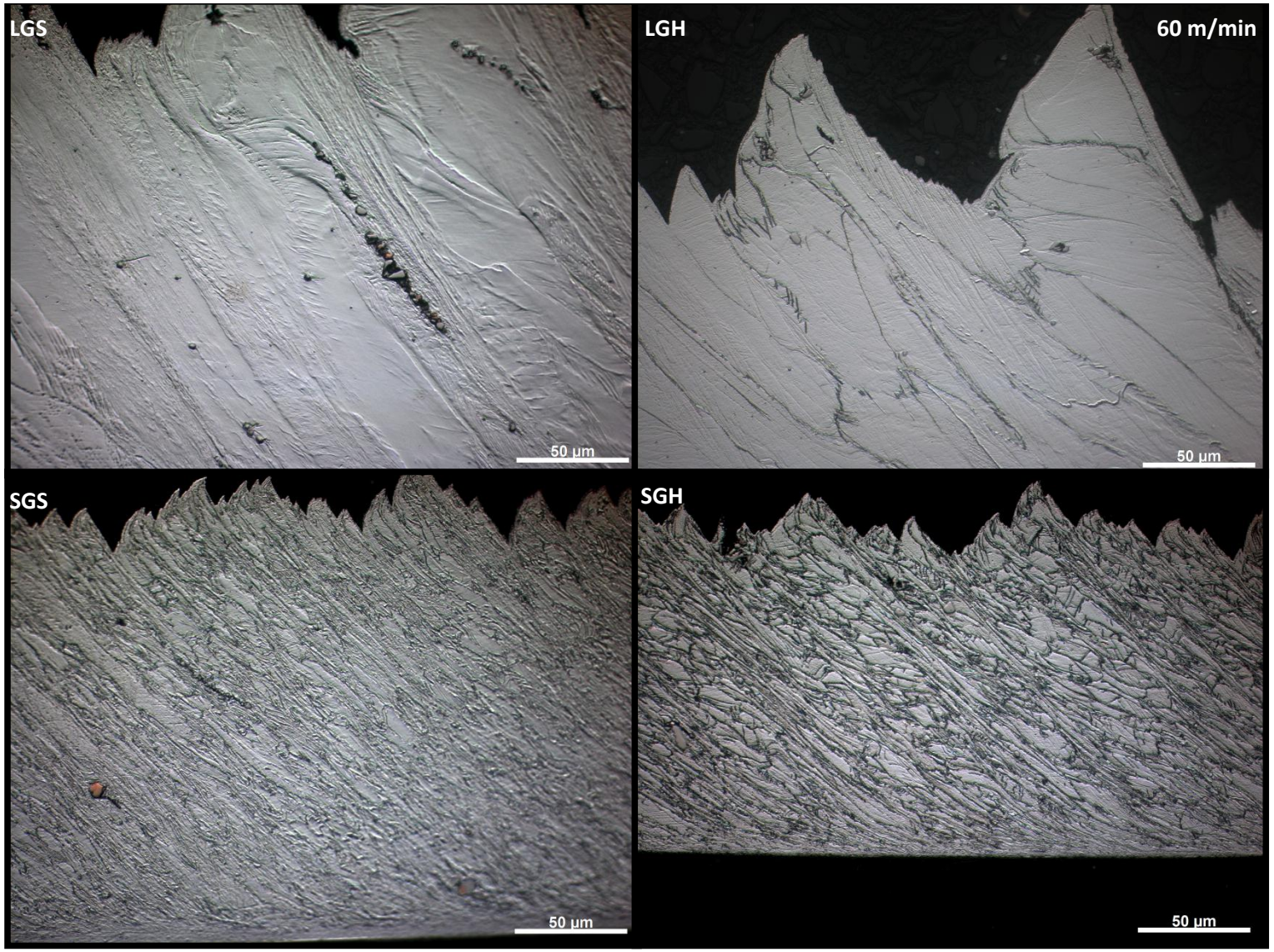

Figure 5 Medium magnification of chip microstructures. Cutting speed is 60 m/min. First row is large grains not hardened, large grains hardened. Second row is small grains not hardened, small grains hardened. Scale bars are 50 µm.

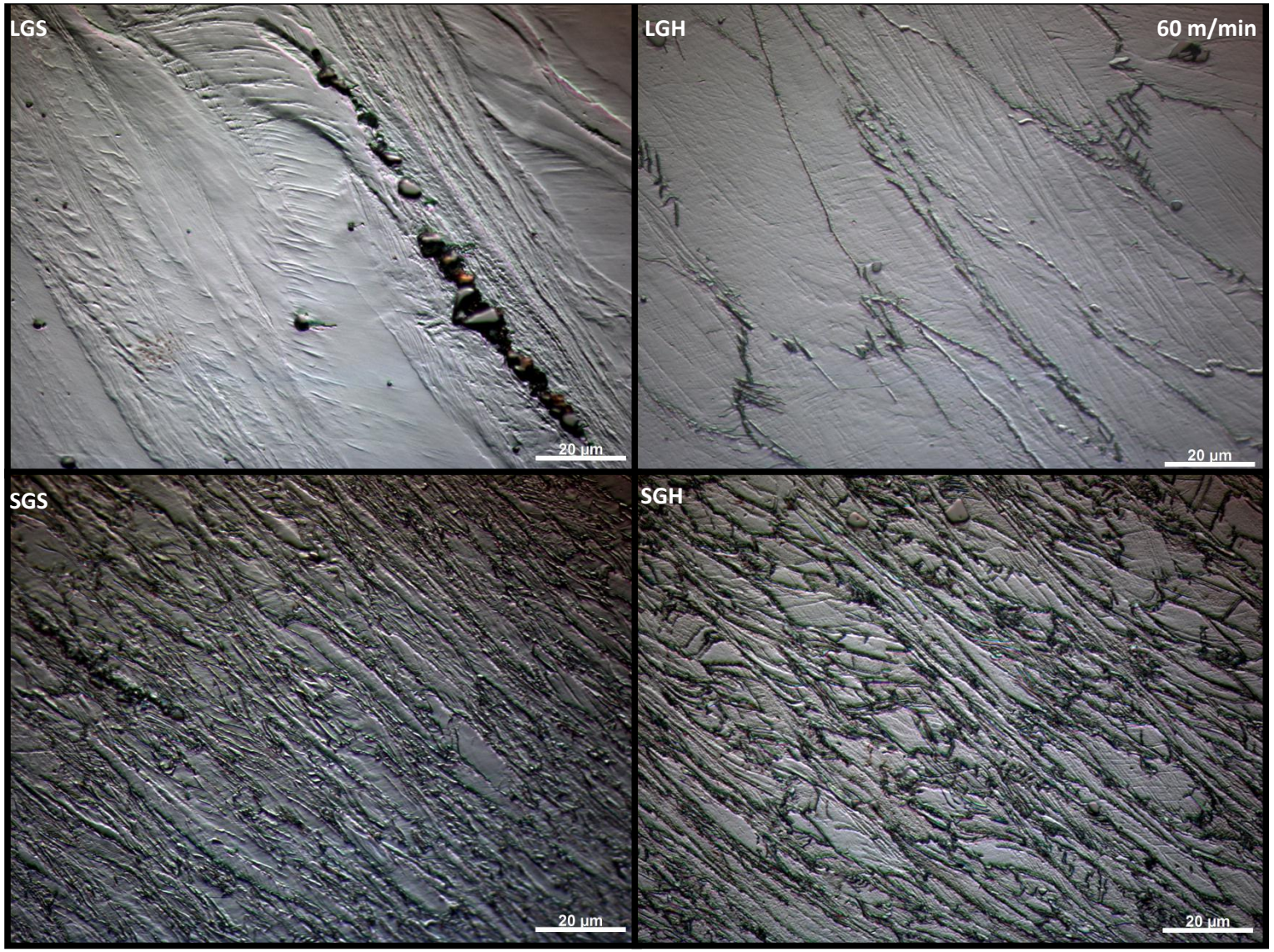

Figure 6 High magnification of chip microstructures. Cutting speed is 60 m/min. First row is large grains not hardened, large grains hardened. Second row is small grains not hardened, small grains hardened. Scale bars are 20 µm.

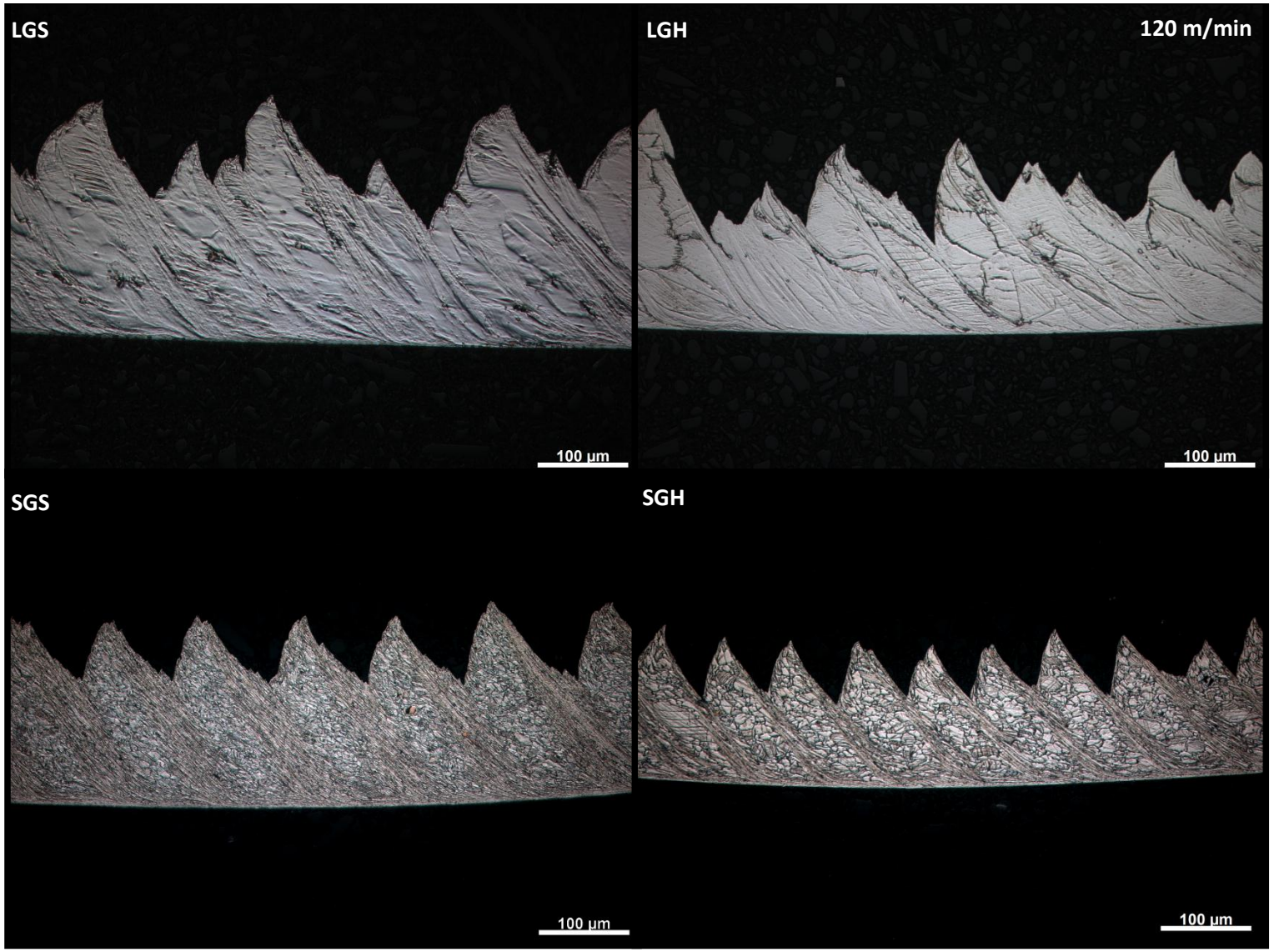

Figure 7 Low magnification of chip microstructures. Cutting speed is 120 m/min. First row is large grains not hardened, large grains hardened. Second row is small grains not hardened, small grains hardened. Scale bars are 100 µm.

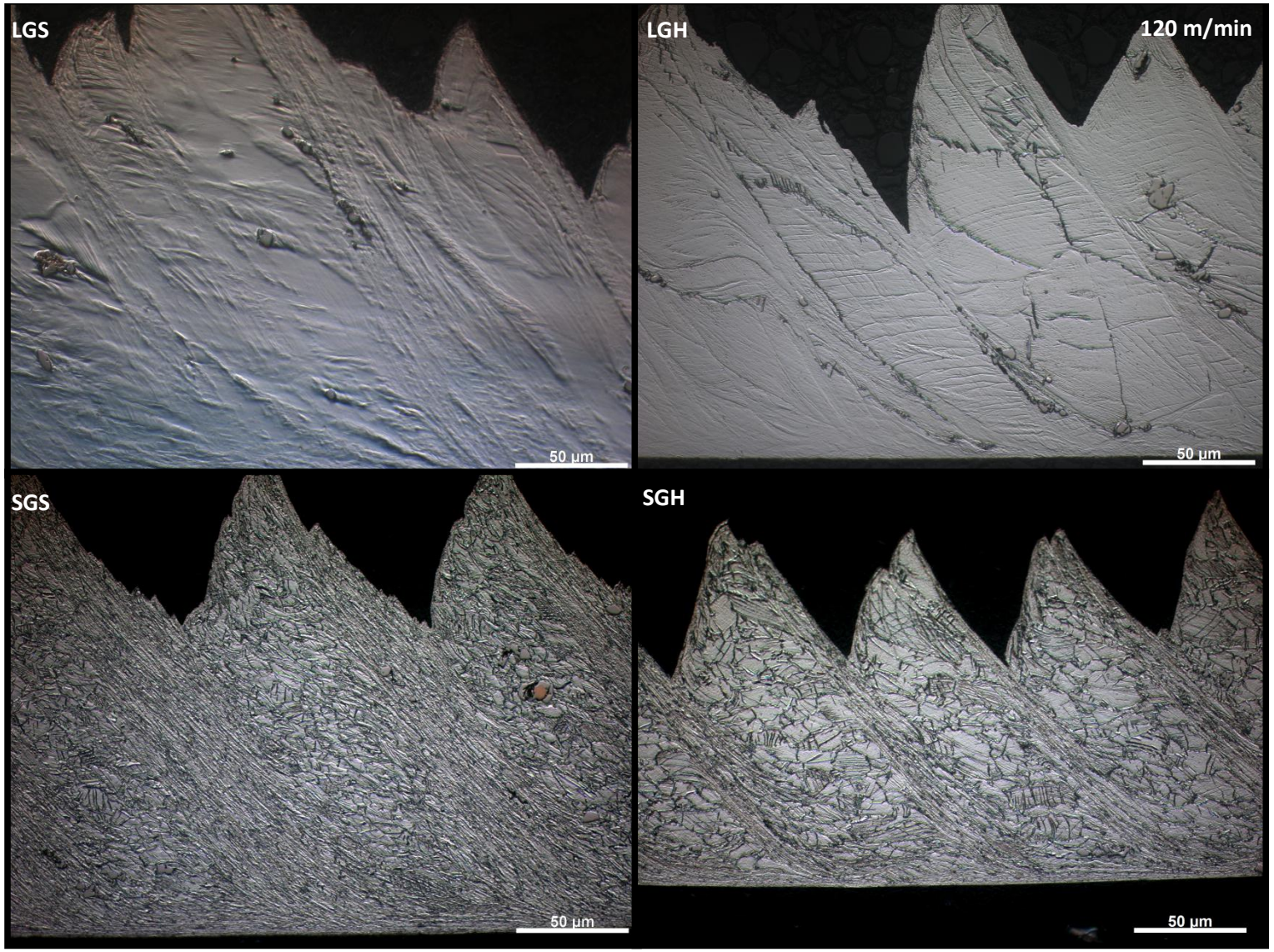

Figure 8 Medium magnification of chip microstructures. Cutting speed is 120 m/min. First row is large grains not hardened, large grains hardened. Second row is small grains not hardened, small grains hardened. Scale bars are 50 µm.

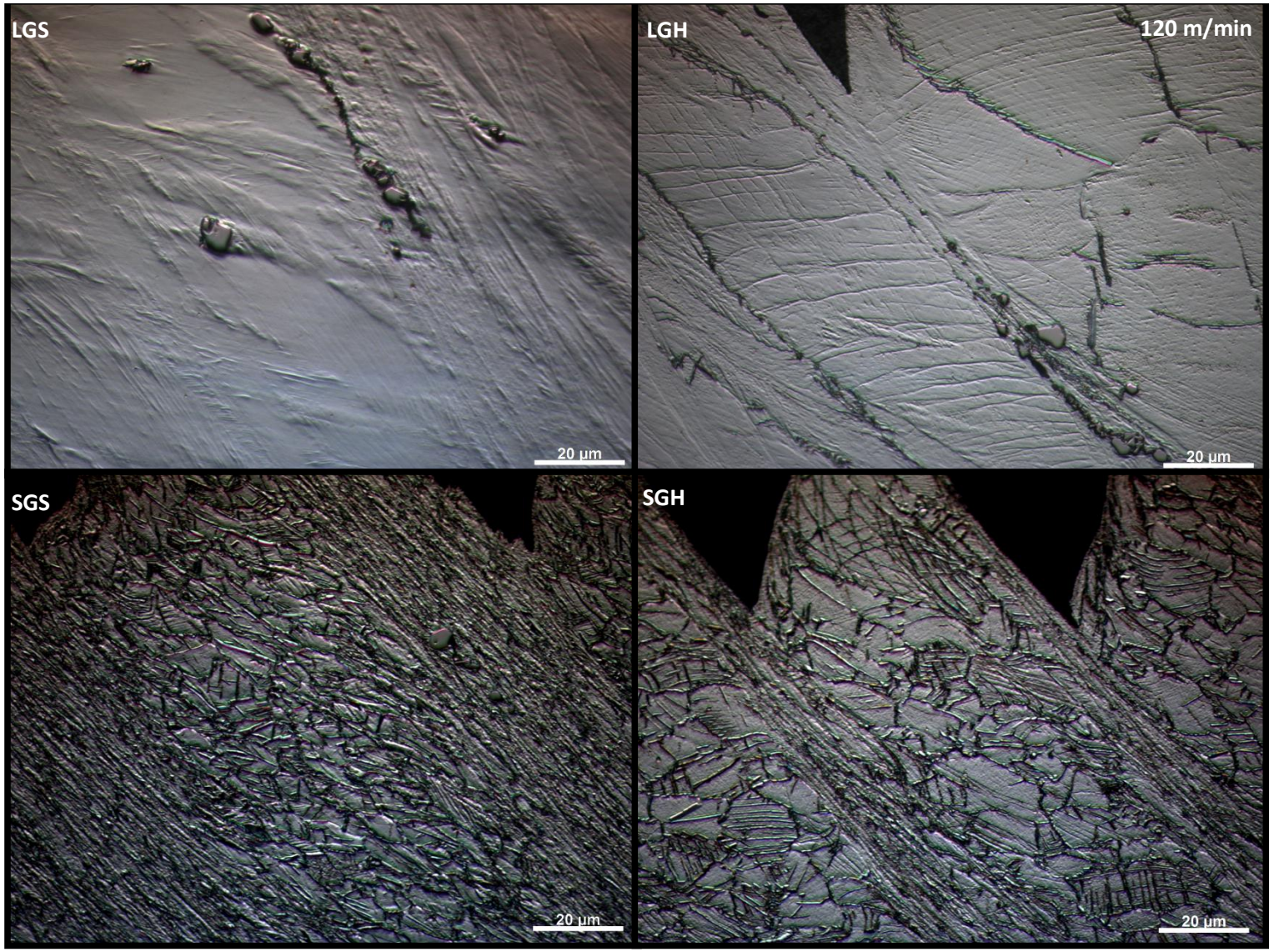

Figure 9 High magnification of chip microstructures. Cutting speed is 120 m/min. First row is large grains not hardened, large grains hardened. Second row is small grains not hardened, small grains hardened. Scale bars are 20 µm.

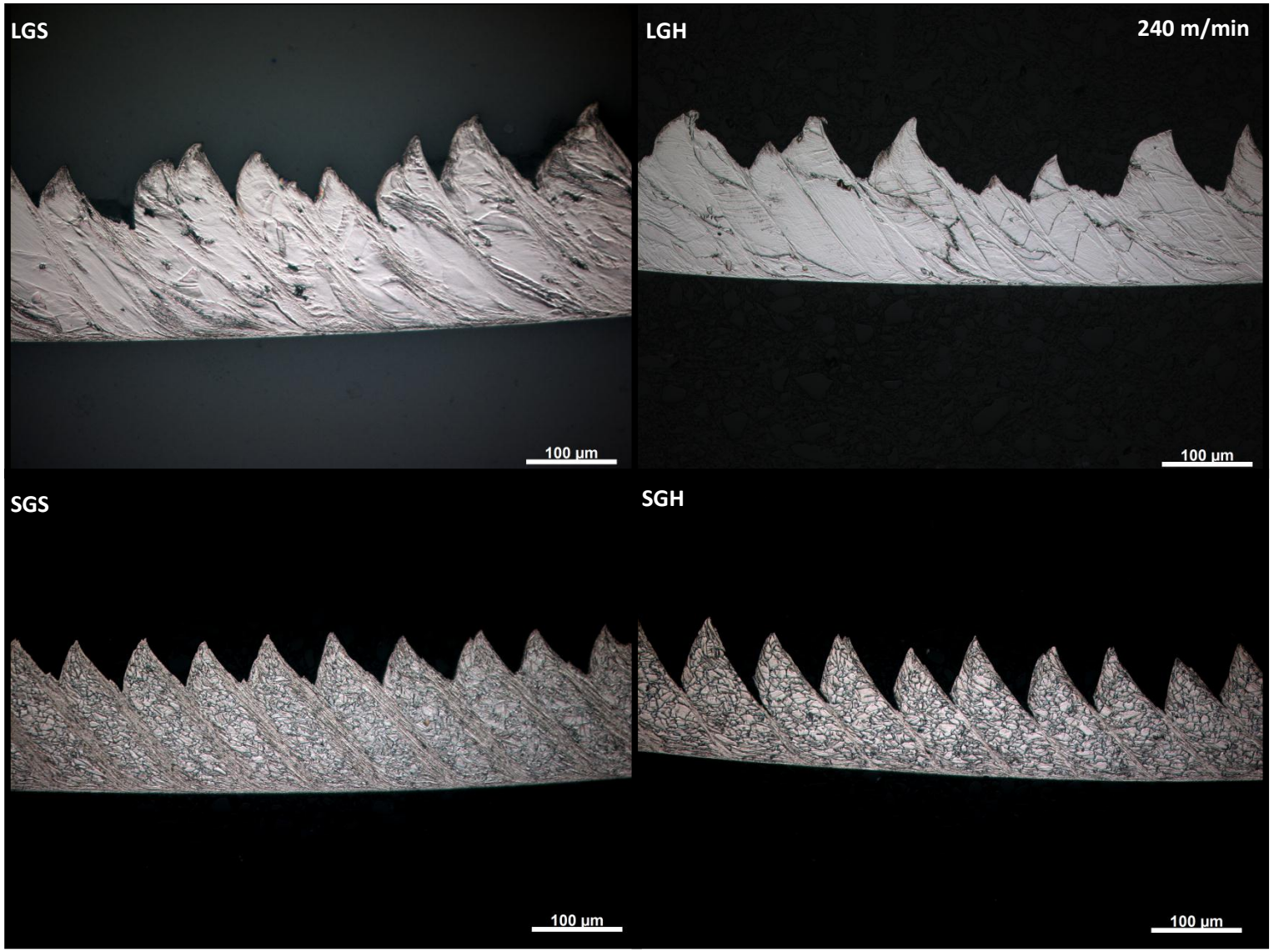

Figure 10 Low magnification of chip microstructures. Cutting speed is 240 m/min. First row is large grains not hardened, large grains hardened. Second row is small grains not hardened, small grains hardened. Scale bars are 100 µm.

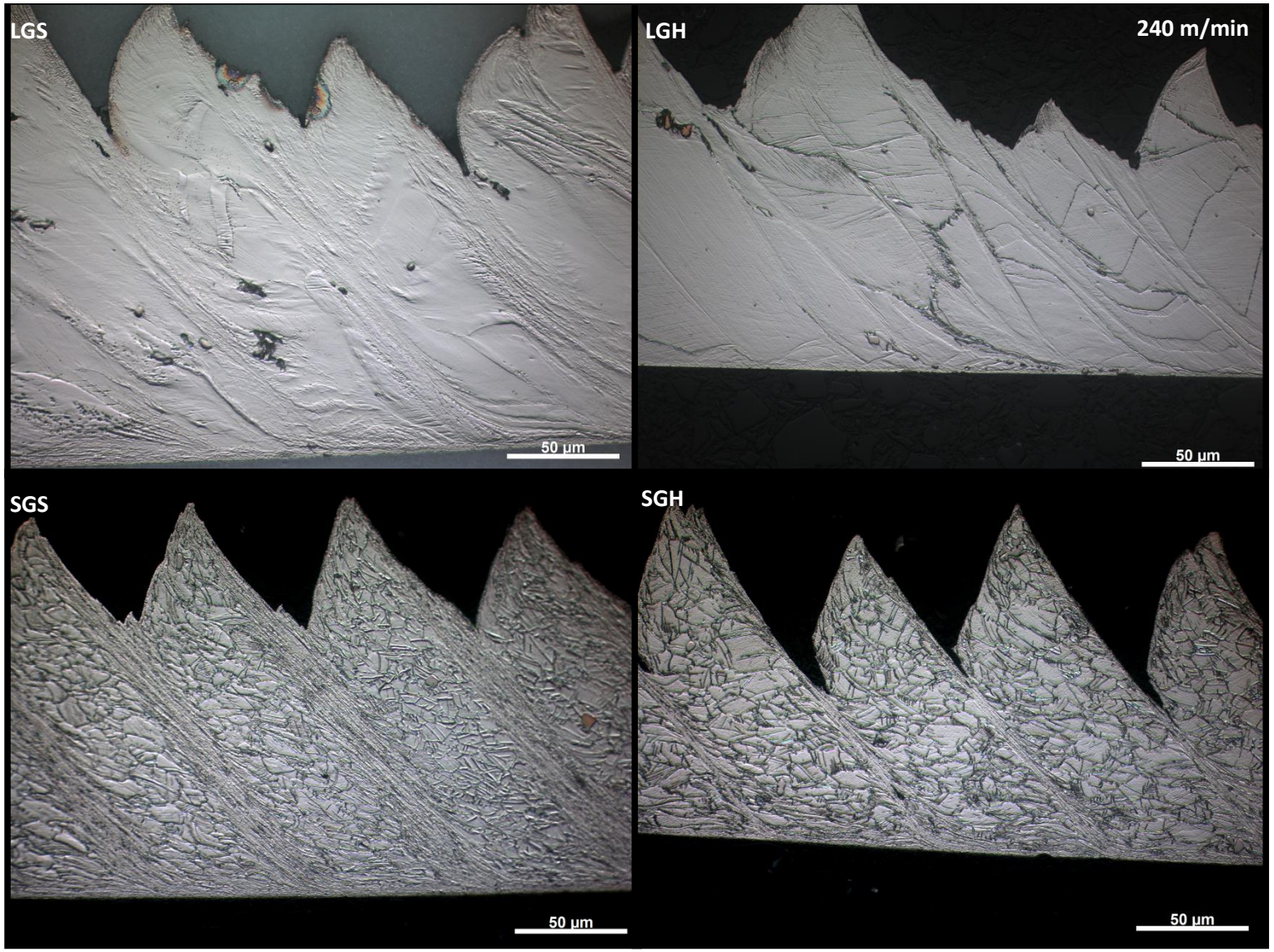

Figure 11 Medium magnification of chip microstructures. Cutting speed is 240 m/min. First row is large grains not hardened, large grains hardened. Second row is small grains not hardened, small grains hardened. Scale bars are 50 µm.

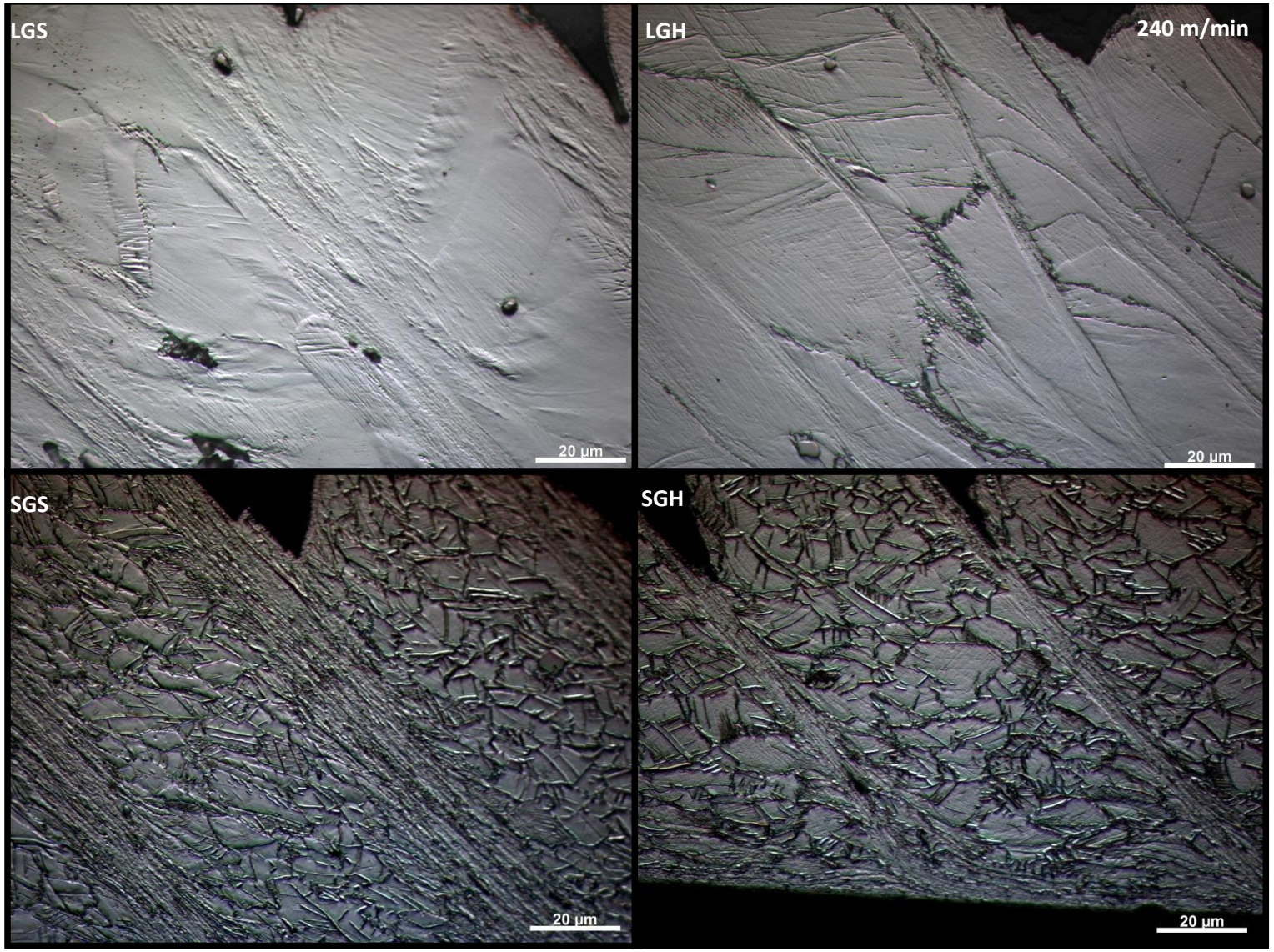

Figure 12 High magnification of chip microstructures. Cutting speed is 240 m/min. First row is large grains not hardened, large grains hardened. Second row is small grains not hardened, small grains hardened. Scale bars are 20 µm.

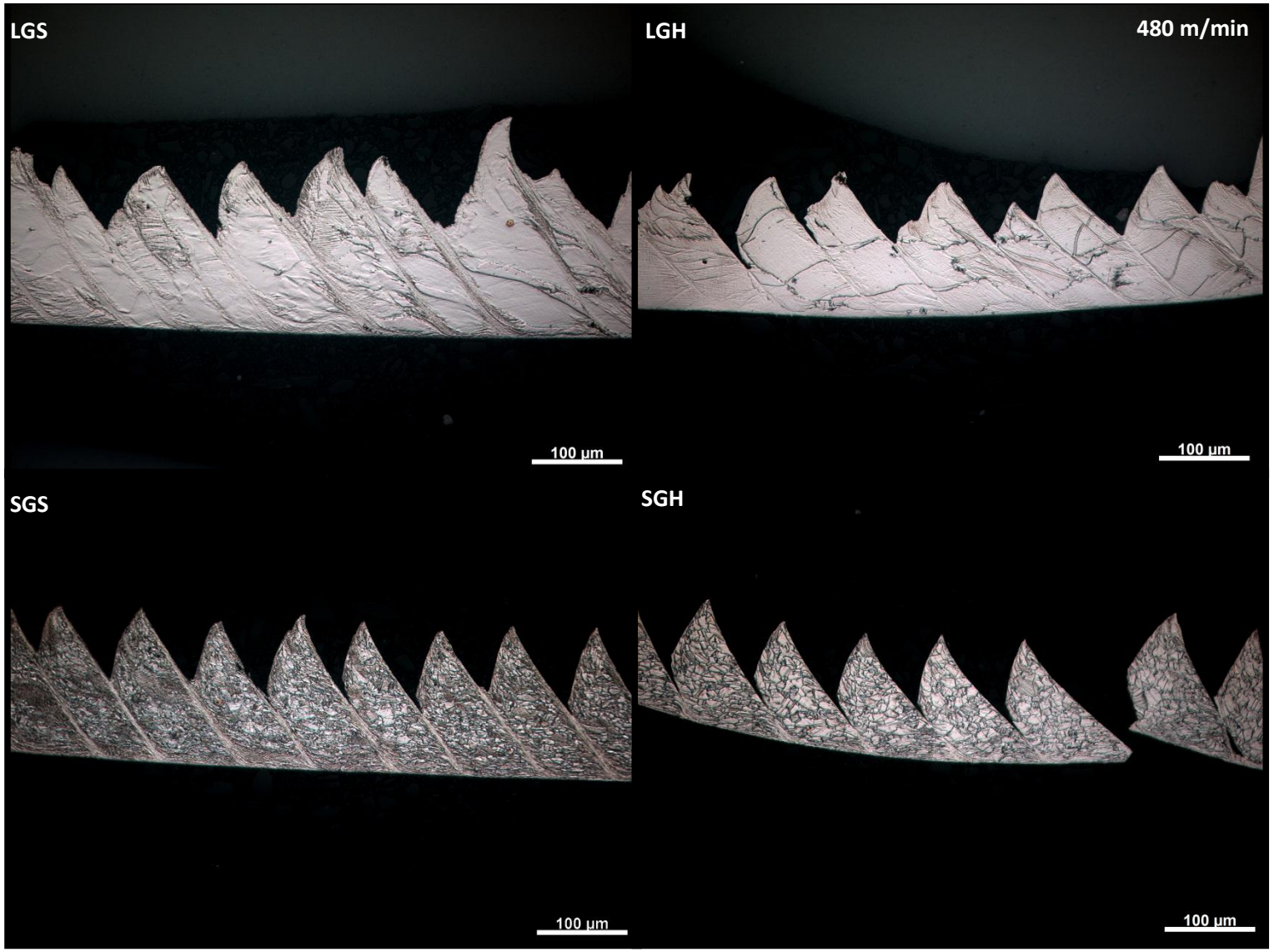

Figure 13 Low magnification of chip microstructures. Cutting speed is 480 m/min. First row is large grains not hardened, large grains hardened. Second row is small grains not hardened, small grains hardened. Scale bars are 100 µm.

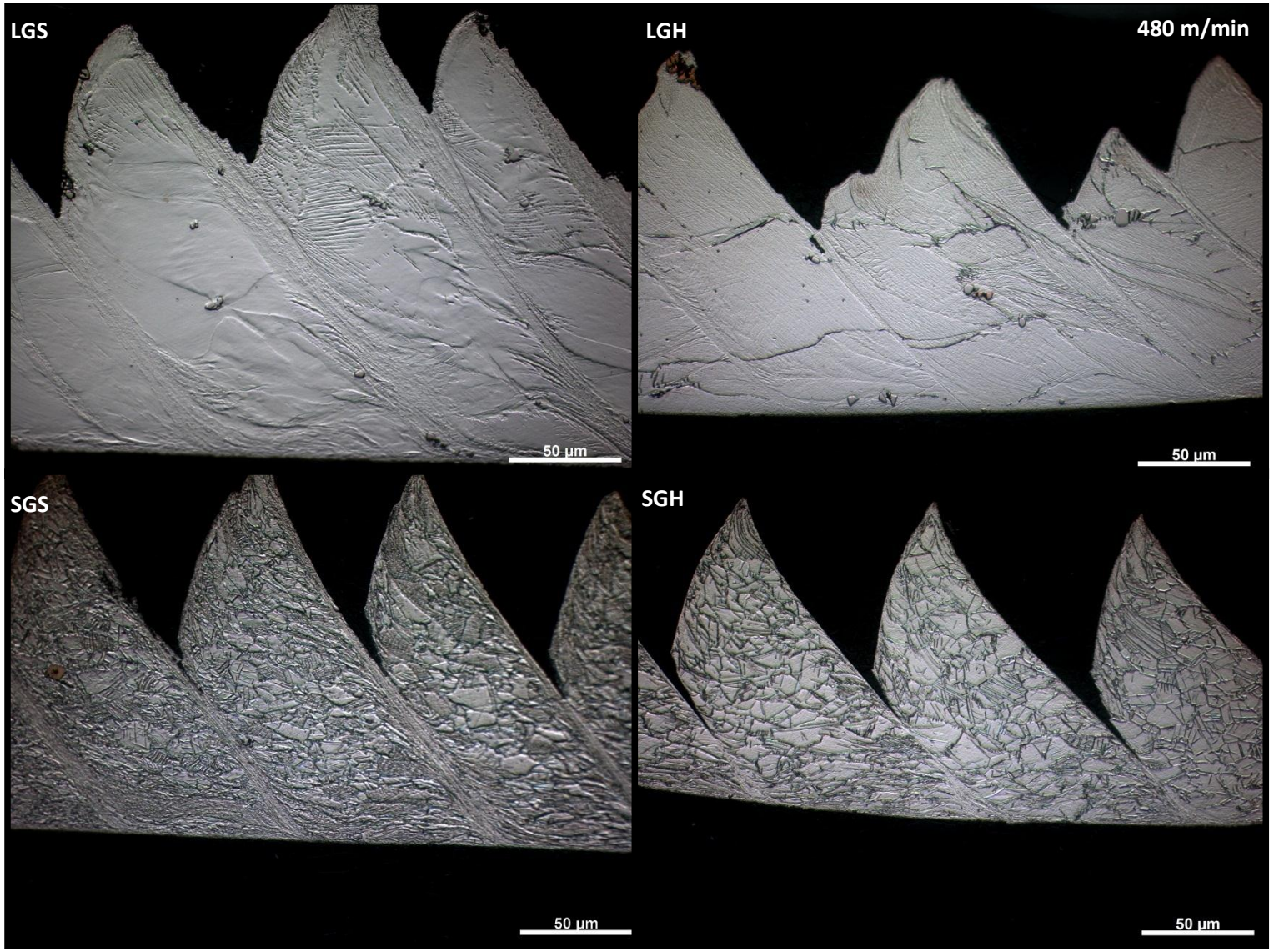

Figure 14 Medium magnification of chip microstructures. Cutting speed is 480 m/min. First row is large grains not hardened, large grains hardened. Second row is small grains not hardened, small grains hardened. Scale bars are 50 µm.

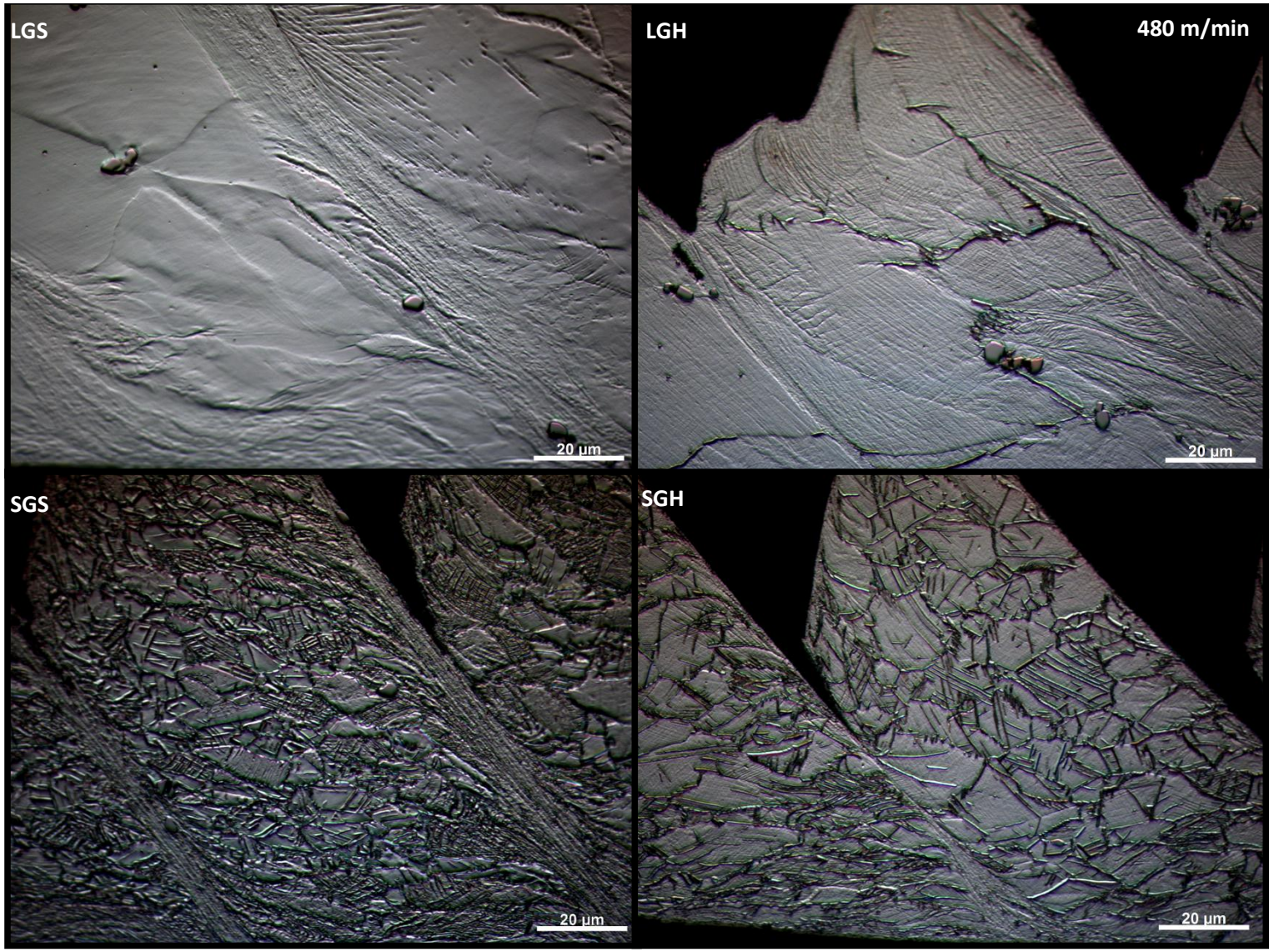

Figure 15 High magnification of chip microstructures. Cutting speed is 480 m/min. First row is large grains not hardened, large grains hardened. Second row is small grains not hardened, small grains hardened. Scale bars are 20 µm.

Appendix B: Contact lengths

This appendix contains images taken with a stereomicroscope of the rake face of all inserts used in the experiments showing the contact length. The organization is that the four different material states used are on their own pages (Large grains not hardened, large grains hardened, small grains not hardened, small grains hardened), the cutting speed is increased from top to bottom of the page (30 m/min at the top and 480 m/min at the bottom) and the three different runs done with the same material and speed are in the rows.

Abbreviations used in the figures are as following:

R1	Test run 1
R2	Test run 2
R3	Test run 3
30 m/min	Cutting speed 30 m/min
60 m/min	Cutting speed 60 m/min
120 m/min	Cutting speed 120 m/min
240 m/min	Cutting speed 240 m/min
480 m/min	Cutting speed 480 m/min

Large grains, not hardened

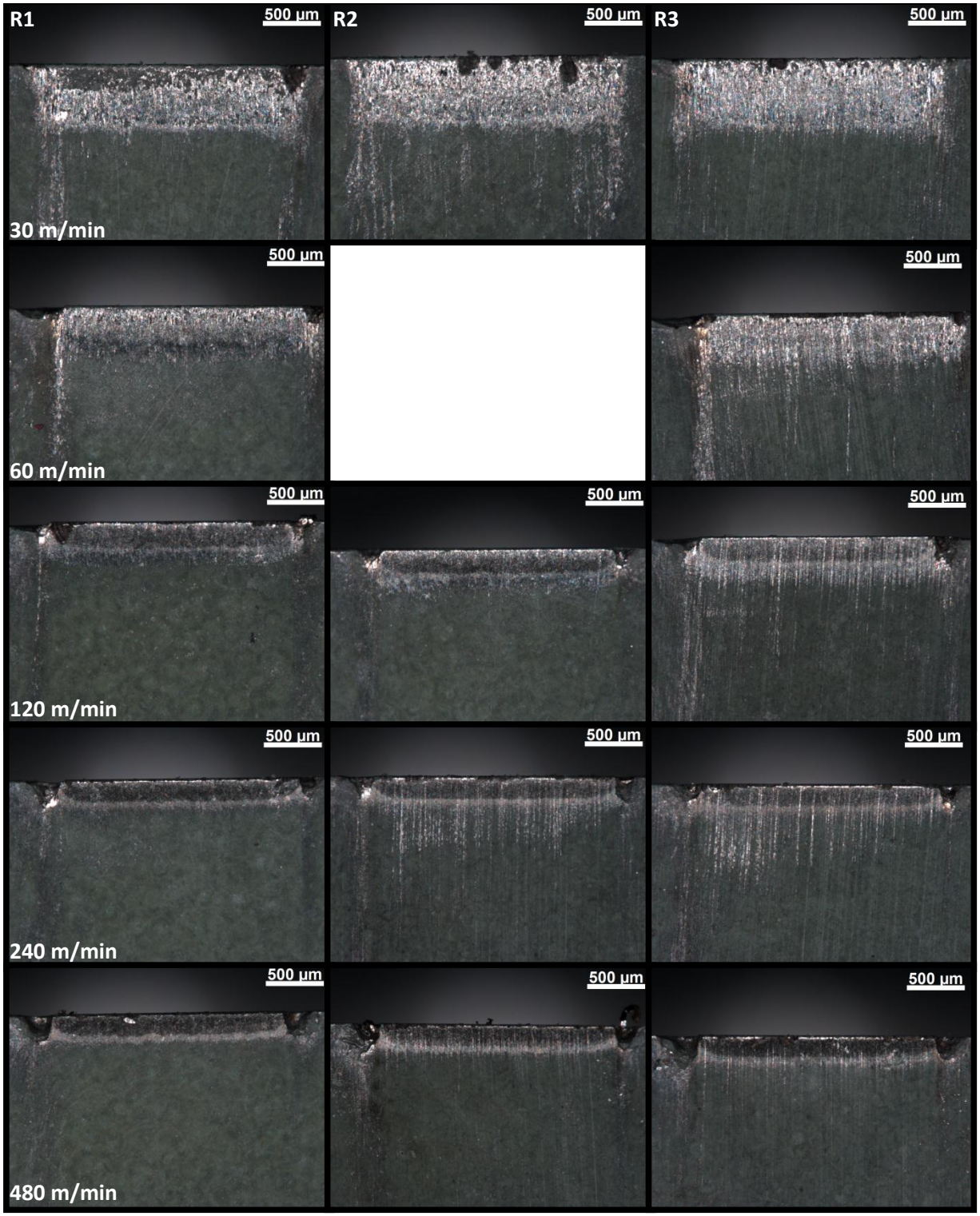

Figure 16 Rake face of inserts used for cutting large grains in the not hardened state. Speed is increased in the rows with the first row being 30 m/min second 60 m/min, third 120 m/min, fourth 240 m/min and the last 480 m/min. The columns contain the different tests performed in the same material state and the same speed. Scale bars are 500µm. The second run in 60 m/min is missing due to problems with the experiment.

Large grains, hardened

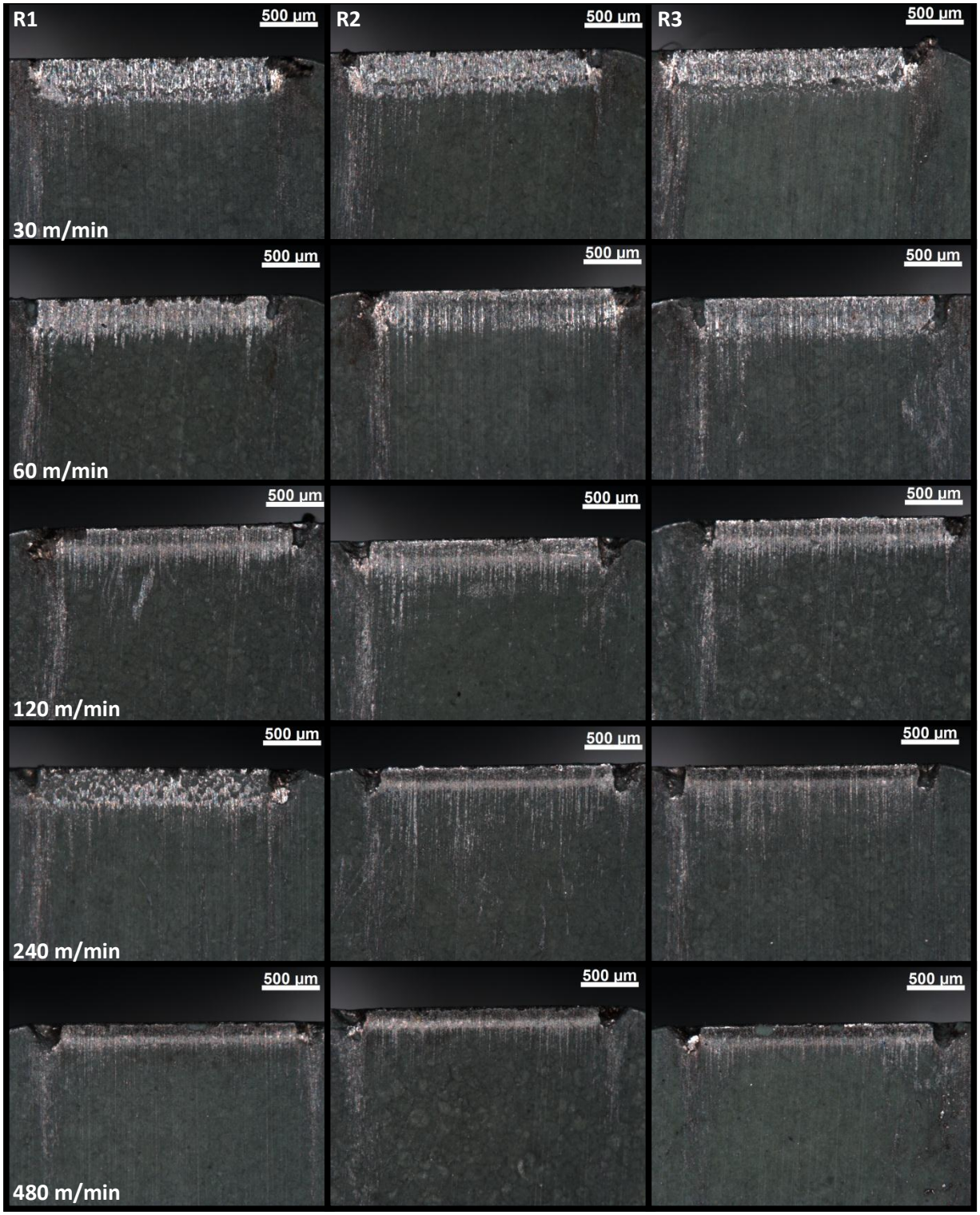

Figure 17 Rake face of inserts used for cutting large grains in the hardened state. Speed is increased in the rows with the first row being 30 m/min second 60 m/min, third 120 m/min, fourth 240 m/min and the last 480 m/min. The columns contain the different tests performed in the same material state and the same speed. Scale bars are 500µm.

Small grains, not hardened

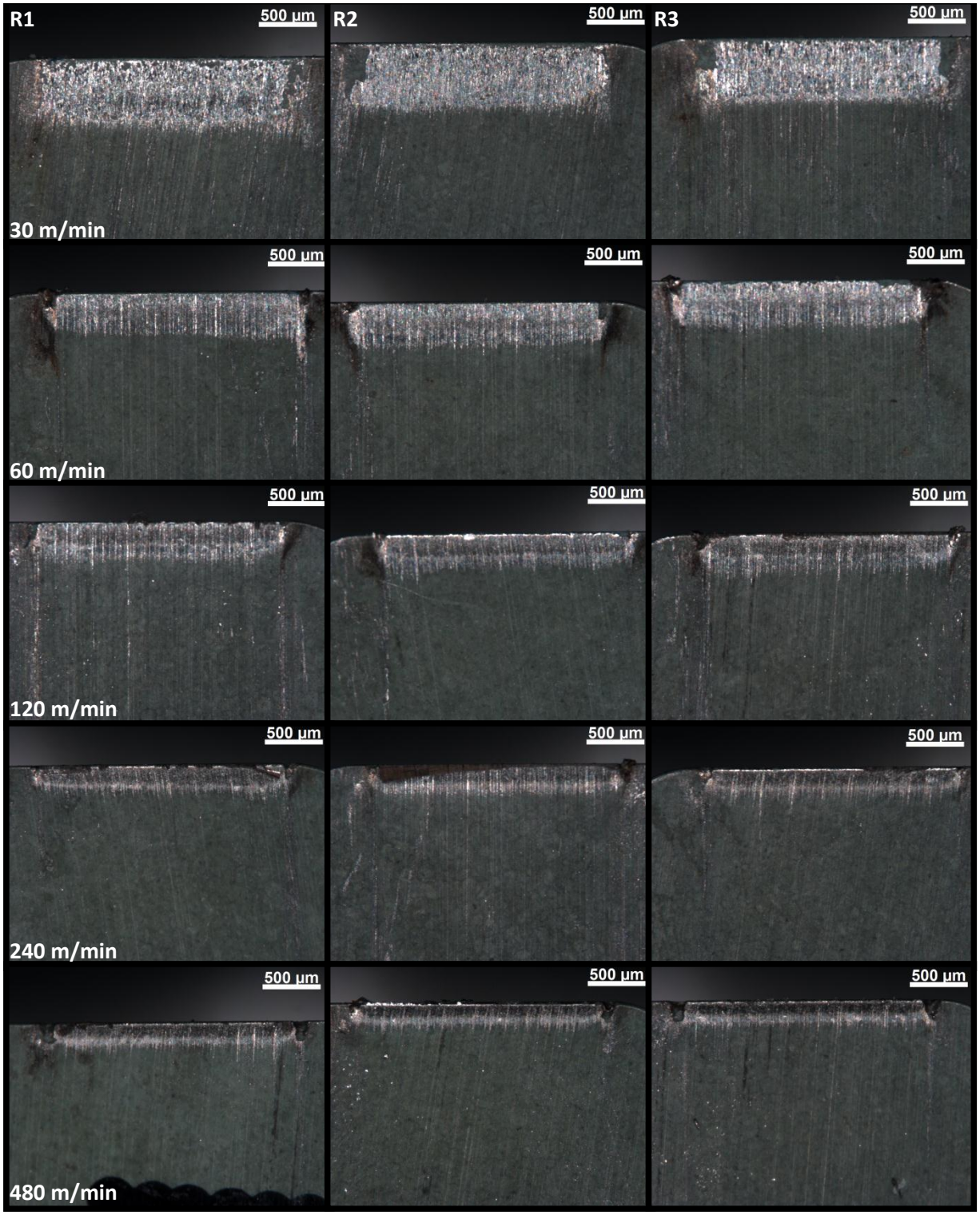

Figure 18 Rake face of inserts used for cutting small grains in the not hardened state. Speed is increased in the rows with the first row being 30 m/min second 60 m/min, third 120 m/min, fourth 240 m/min and the last 480 m/min. The columns contain the different tests performed in the same material state and the same speed. Scale bars are 500µm.

Small grains, hardened

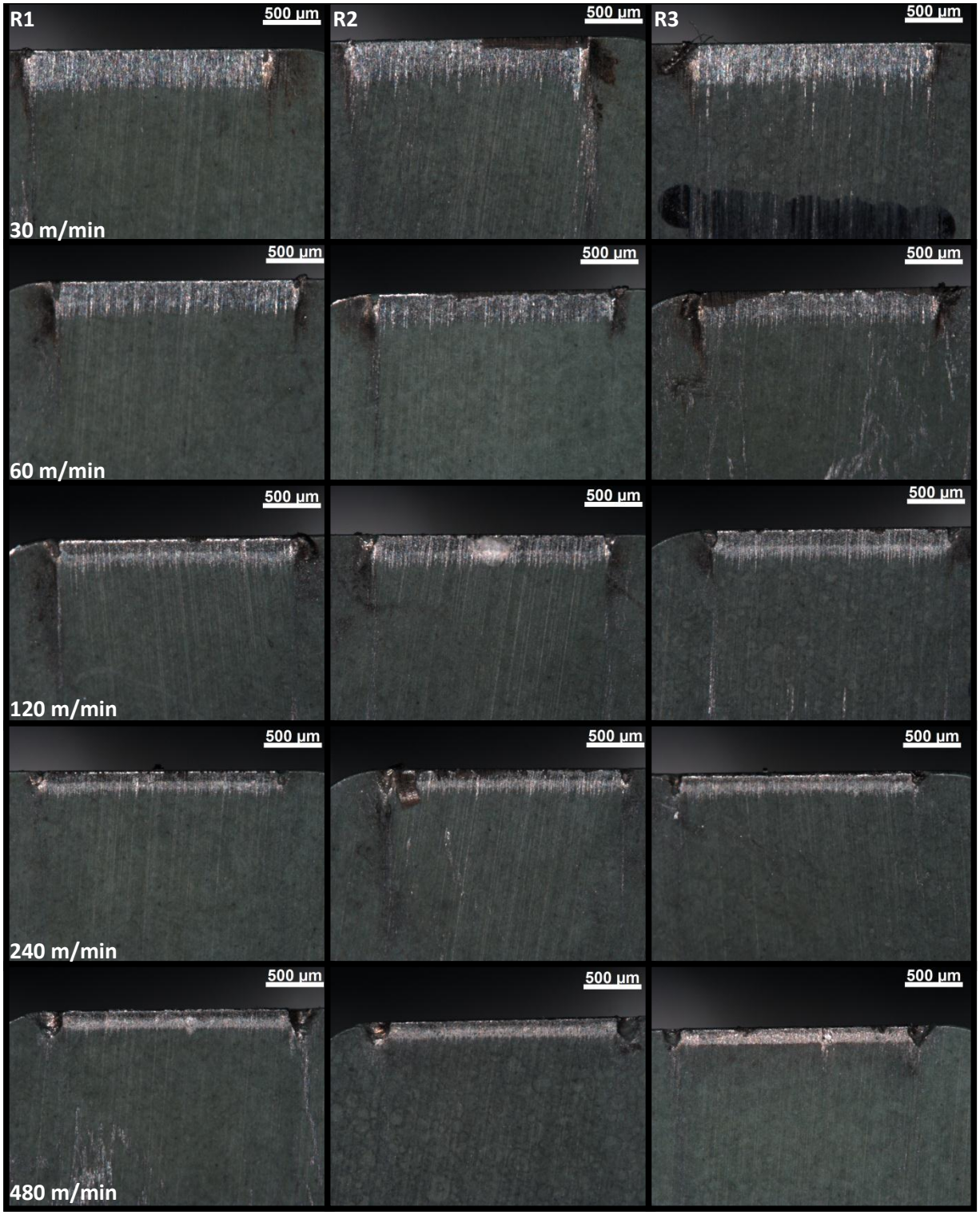

Figure 19 Rake face of inserts used for cutting small grains in the hardened state. Speed is increased in the rows with the first row being 30 m/min second 60 m/min, third 120 m/min, fourth 240 m/min and the last 480 m/min. The columns contain the different tests performed in the same material state and the same speed. Scale bars are 500µm.